
 BULLETIN DE L'ASSOCIATION MINÉRALOGIQUE DU CANADA

THE CANADIAN MINERALOGIST

 JOURNAL OF THE MINERALOGICAL ASSOCIATION OF CANADA

Volume 36

February 1998

Part 1

The Canadian Mineralogist
Vol. 36, pp. 1-47 (1998)

GEOLOGICAL SETTING AND PETROGENESIS OF SYMMETRICALLY ZONED, MIAROLITIC GRANITIC PEGMATITES AT STAK NALA, NANGA PARBAT – HARAMOSH MASSIF, NORTHERN PAKISTAN

BRENDAN M. LAURS¹ AND JOHN H. DILLES²*Department of Geosciences, Oregon State University, Corvallis, Oregon 97331, U.S.A.*

YOUSAF WAIRRACH AND ALLAH B. KAUSAR

*Geological Survey of Pakistan, Geoscience Laboratory, P.O. Box 1461, Shahzad Town, Islamabad, Pakistan*LAWRENCE W. SNEE²*U.S. Geological Survey, MS 913, Federal Center, Denver, Colorado 80225, U.S.A.*

ABSTRACT

Miarolitic granitic pegmatites in the Stak valley in the northeast part of the Nanga Parbat – Haramosh Massif, in northern Pakistan, locally contain economic quantities of bi- and tricolored tourmaline. The pegmatites form flat-lying sills that range from less than 1 m to more than 3 m thick and show symmetrical internal zonation. A narrow outer or border zone of medium- to coarse-grained oligoclase – K-feldspar – quartz grades inward to a very coarse-grained wall zone characterized by K-feldspar – oligoclase – quartz – schorl tourmaline. Radiating sprays of schorl and flaring megacrysts of K-feldspar (intermediate microcline) point inward, indicating progressive crystallization toward the core. The core zone consists of variable mixtures of blocky K-feldspar (intermediate microcline), oligoclase, quartz, and sparse schorl or elbaite, with local bodies of sodic aplite and miarolitic cavities or “pockets”. Minor spessartine–almandine garnet and löllingite are disseminated throughout the pegmatite, but were not observed in the pockets. The pockets contain well-formed crystals of albite, quartz, K-feldspar (maximum microcline ± orthoclase overgrowths), schorl–elbaite tourmaline, muscovite or lepidolite, topaz, and small amounts of other minerals. Elbaite is color-zoned from core to rim: green (Fe²⁺- and Mn²⁺-bearing), colorless (Mn²⁺-bearing), and light pink (trace Mn³⁺). Within ~10 cm of the pegmatites, the granitic gneiss wallrock is bleached owing to conversion of biotite to muscovite, with local quartz and albite added. Schorl is disseminated through the altered gneiss, and veins of schorl with bleached selvages locally traverse the wallrock up to 1 m from the pegmatite contact. The schorl veins can be traced into the outer part of the wall zone, which suggests that they formed from aqueous fluids derived during early saturation of the pegmatite-forming leucogranitic magma rich in H₂O, F, B, and Li. Progressive crystallization resulted in a late-stage sodic magma and abundant aqueous fluids. Two late stages of volatile escape are recognized: the first stage caused pressure-quenching of the last magma, which produced aplite and caused albitization (An₃ to An₈) of earlier crystallized K-feldspar and oligoclase. The second stage, released during the rupture of miarolitic cavities, produced platy albite (“cleavelandite,” An₁)

¹ Present address: @ Gemological Institute of America, 5345 Armada Drive, Carlsbad, California 92008, U.S.A.
E-mail address: blaurs@gia.edu

² E-mail addresses: dillesj@bcc.orst.edu, lsnee@usgs.gov

locally associated with F-rich muscovite and elbaite. Albitization is likely due to cooling of alkali-fluoride-dominated fluids at less than 2 kbar pressure. The pegmatites are derived from Himalayan leucogranitic magma emplaced prior to 5 Ma into granulitic gneiss that was at 300° to 550°C and 1.5 to 2 kbar. The pegmatites were emplaced during uplift of the Haramosh Massif, since they cross-cut ductile normal faults but are cut by brittle normal faults. Economically important pink tourmaline mineralization formed in pockets concentrated near the crest of a broad antiform, as a result of trapping of late magmatic aqueous fluids that had become Fe-poor owing to the prior crystallization of schorl.

Keywords: granitic pegmatite, volatile saturation, miarolitic cavity, elbaite tourmaline, hydrothermal alteration, albitization, Stak Nala, Nanga Parbat – Haramosh massif, Pakistan.

SOMMAIRE

Des filons de pegmatite granitique à miaroles dans la vallée de Stak, dans le secteur nord-est du massif de Nanga Parbat – Haramosh, dans le nord du Pakistan, contiennent localement des quantités exploitables de tourmaline bi- ou tri-colorée. Ces pegmatites se présentent sous forme de filons-couches allant de moins de 1 m jusqu'à 3 m en épaisseur, montrant une zonation symétrique interne. Un liseré externe contient l'assemblage oligoclase – feldspath potassique – quartz, à granulométrie moyenne ou grossière. Vers l'intérieur, cette zone devient progressivement la zone de paroi, à granulométrie plus grossière, contenant feldspar potassique – oligoclase – quartz – schorl. Des agencements fibro-radiés de schorl et des mégacristaux en éventail de feldspath potassique (microcline intermédiaire) montrent une orientation centripète, indiquant une cristallisation progressive vers le coeur. Ce coeur contient des proportions variables de feldspath potassique en blocs (microcline intermédiaire), oligoclase, quartz, et schorl ou elbaite plus épars, avec des domaines d'aplite sodique et des miaroles tapissées de cristaux. De faibles quantités de grenat (spessartine–almandin) et de löllingite sont disséminés dans la roche, mais ces minéraux sont absents dans les miaroles, qui contiennent des cristaux bien formés d'albite, quartz, feldspath potassique (microcline complètement ordonné ± surcroissance d'orthose), tourmaline de type schorl–elbaite, muscovite ou lepidolite, topaz, et d'autres minéraux accessoires. L'elbaite est zonée, du coeur vers le centre, de vert (zone à Fe²⁺ et Mn²⁺), à incolore (zone à Mn²⁺), à rose pâle (traces de Mn³⁺). Sur une distance d'environ 15 cm du contact, le gneiss granitique encaissant est lessivé et pâli à cause du remplacement de la biotite par la muscovite, et l'addition locale de quartz et d'albite. Le schorl y est disséminé, et des veines de schorl avec parois pâlies traversent localement l'encaissant jusqu'à 1 m du contact. On peut tracer ces veines de schorl dans la partie externe de la zone de paroi, ce qui fait penser qu'elles se sont formées aux dépens d'une phase fluide aqueuse dérivée à un stade précoce de saturation du magma leucogranitique, enrichi en H₂O, F, B, et Li. Une cristallisation progressive a mené à un magma résiduel sodique et une abondance de fluide aqueux. Nous distinguons deux stades de fuite de la phase fluide. Le premier stade a causé la trempe du magma résiduel, ce qui rend compte de la formation de l'aplite et l'albitisation (de An₃ à An₆) du feldspath potassique et de l'oligoclase déjà cristallisés. Le deuxième, dû à une fuite au cours de la rupture finale des miaroles, a produit l'albite en plaquettes ("cleavelandite", An₁) qu'accompagne localement une muscovite riche en fluor et l'elbaite. L'albitisation serait due au refroidissement de la phase fluide fluorée à une pression inférieure à 2 kbar. Les pegmatites sont dérivées de venues de magma leucogranitiques himalayennes mises en place avant 5 Ma dans des gneiss granulitiques préalablement chauffés entre 300° et 550°C à une pression entre 1.5 et 2 kbar. Les pegmatites ont été mises en place pendant le soulèvement du massif de Haramosh; elles recoupent des failles normales à déformation ductile qui sont recoupées par des failles normales à déformation cassante. Les concentrations économiques de tourmaline rose se sont formées dans des miaroles dont l'accumulation près de la crête d'une vaste antiforme est le résultat du piégeage de la phase fluide orthomagmatique tardive appauvrie en Fe à cause de la cristallisation antérieure du schorl.

Mots-clés: pegmatite granitique, saturation en phase volatile, miarole, elbaite, tourmaline, altération hydrothermale, albitisation, Stak Nala, massif de Nanga Parbat – Haramosh, Pakistan.

INTRODUCTION

Miarolitic granitic pegmatites occur widely in northern Pakistan within the Karakoram mountains. Many of these pegmatites are associated with young leucogranites in the Nanga Parbat – Haramosh area of extremely thick crust and rapid rates of current uplift (e.g., Zeitler 1985). The miarolitic pegmatites are mined for crystals of topaz, beryl (aquamarine), schorl, fluorite, and other minerals (Table 1). At Stak Nala in the northeastern Haramosh massif (Fig. 1), the pegmatites are renowned for well-formed color-zoned tourmaline crystals up to 10 cm in length. The color zoning is typically perpendicular to the *c* axis, ranging from black at the base to green, and locally pink,

colorless, or pale blue at the termination. The tourmaline crystals are valued more as mineral specimens than cut gemstones, owing to abundant fine cracks and inclusions. The tourmaline forms in cavities or "pockets" found locally in the core of the pegmatites, where it is associated with platy albite ("cleavelandite"), quartz, K-feldspar, muscovite, topaz, and several rarer minerals.

In this paper, we present data on the age, geology, internal mineral zonation, and chemical compositions of minerals in the pegmatites and associated metasomatized wallrock. We conclude with a geological and geochemical model to address two fundamental questions: (1) What conditions led to the formation of valuable colored tourmaline, as opposed to the schorl common in most of the pegmatites of the region?

TABLE 1. GEOLOGIC SETTING, AGE, AND MINERAL PRODUCTION OF MIAROLITIC PEGMATITES, NORTHERN PAKISTAN

Location*	Host rocks	Age of pegmatite or associated leucogranite	Principal commodities	Accessory minerals
Dache	Haramosh massif: Iskere gneiss	n.d.	Ap, Aqm, Fl, Qtz, Sps-Alm, Srl, Toz	
Dassu	Asian Plate: Dassu gneiss	n.d.	Aqm, Ap, Fl, Mrg, Qtz, Srl, Sps-Alm, Toz	Bt, Elb, Gsh, Hrd, Lpd, Mic, Phk, Tnt, Ttn, Stl, Vtm
Drot	Haramosh massif: Shengus gneiss, Iskere gneiss	2.8 & 3.3 Ma: Rb-Sr Ms (George <i>et al.</i> 1993) 5 to 8 Ma: U-Pb Zrn (Zeitler & Chamberlain 1991)	Aqm, Ap, Elb, Mrg, Qtz, Sps-Alm, Srl, Toz	Bry, Cst, Col, Gsh, Hlv, Hmb, Hrd, Lpd, Pol, Spd, Tap, Tnt, Ttn
Khaltaro	Haramosh massif: layered gneiss & amphibolite	9.1 Ma: Ar-Ar Ms (Laurs <i>et al.</i> 1996b)	Ap, Aqm, Em, Fl	Srl
Nagar	Asian Plate: Hunza schist	5.6 Ma: K-Ar Ms (Crawford & Searle 1993)	Ap, Aqm, Fl, Srl, Toz	Adl, Axn, Cal
Stak Nala	Haramosh massif: Shengus gneiss	4.6 Ma: Ar-Ar Ms (This study)	Ap, Elb, Fl, Qtz, Srl, Toz	Col, Hmb, Löl, Lpd, Mic, Mrg, Zrn

* See Figure 1 for pegmatite locations.

Note: Mineral commodities from Kazmi *et al.* (1985), Kazmi & O'Donoghue (1990), Laurs *et al.* (1996b), and Smith & Blauwet (1997). Symbols not defined by Kretz (1983): Adl: adularia, Aqm: aquamarine, Axn: axinite, Bry: beryllonite, Col: columbite, Em: emerald, Gsh: goshenite, Ham: hambergite, Hlv: helvite, Hrd: herderite, Löl: löllingite, Mic: microlite, Mrg: morganite, Phk: phenakite, Pol: pollucite, Stl: stellerite, Tap: tapiolite, Tnt: tantalite, Vtm: viitaniemiite.

(2) How is the formation of miarolitic pegmatite linked to tectonic processes in the collision zone between India and Asia?

of thousands. Production has slowed within the last three years, owing to dwindling reserves and the disbanding of GEMCP.

LOCATION AND MINE HISTORY

The pegmatites are located 13 km north of the Indus River on the west side of the Stak valley (Fig. 2), at an elevation of approximately 2800 m. A rough dirt road leads from the Gilgit-Skardu road to Toghla village, and a footpath provides access to the pegmatites about 2 km north and 400 m above the valley floor. Tourmaline was first discovered in the area by local villagers in the early 1980s. Exploration soon afterward by the Gemstone Corporation of Pakistan (GEMCP) revealed abundant tourmaline mineralization at two bodies of pegmatite located about 0.5 km apart, with similar pegmatite bodies extending 3 km south. Most production of tourmaline and associated minerals has come from a single 1-m-thick sill (hereafter called the main mine). Much less tourmaline has been mined from a much thicker (up to ~4 m) pegmatite (hereafter called the south mine) located 500 m south, at the same elevation. We estimate the number of tourmaline crystals mined at Stak Nala since 1984 to be in the tens

SAMPLING AND ANALYTICAL PROCEDURES

Detailed geological mapping (scale 1:240) and sampling were done over a seven-day period in August, 1993. Detailed cross-sectional maps (scale 1:12) were drawn at four well-exposed areas to record mineralogy, texture, and internal zoning of the pegmatites, as well as the adjacent wallrock alteration. Precisely located samples from outcrops and from mine dumps were collected principally from the main mine area.

The $^{40}\text{Ar}/^{39}\text{Ar}$ age spectra were obtained by step-heating pure, hand-picked mineral separates at the U.S. Geological Survey, Denver, Colorado, using methods outlined in Snee *et al.* (1988). Concentrations of major and trace elements in whole-rock samples were measured by X-ray fluorescence at the Islamabad laboratory of the Geological Survey of Pakistan. Chemical compositions of minerals were determined by electron microprobe at Oregon State University (OSU). The structural state of K-feldspar was determined on four samples by powder X-ray diffraction at OSU, using

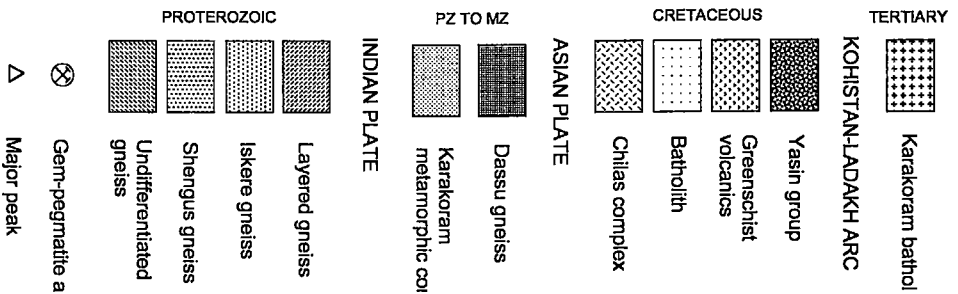
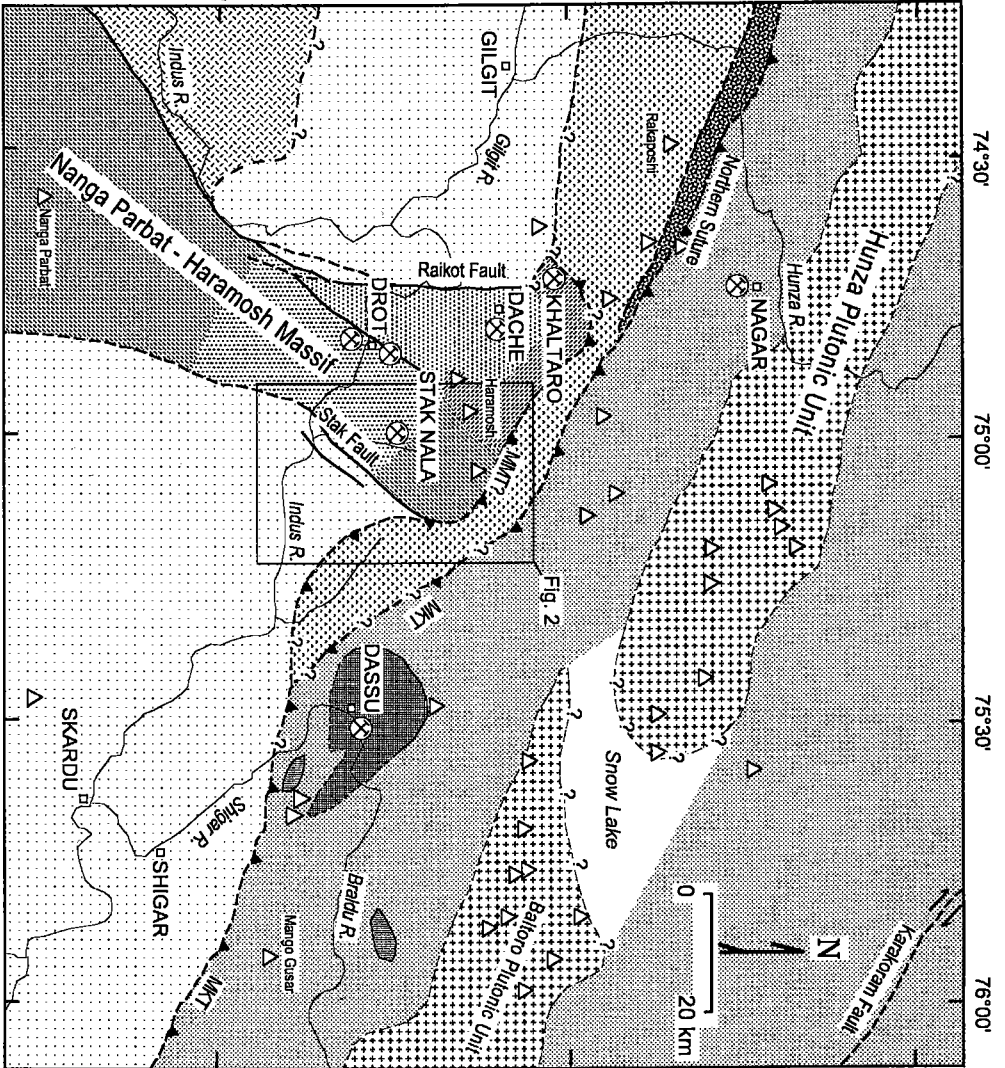


Fig. 1. Regional geological map of the northern Pakistan (after Searle 1991, Pegmatite *et al.* 1993), including part of China (northeast corner of map; border not shown), showing areas with miarolitic pegmatites. See Table 1 for pegmatite ages and mineralogy. Nomenclature of pegmatite districts after Smith & Blauwet (1997). The pegmatite mine at Stak Nala has been called "Isak" by GEMCP; "Nala" refers to a stream or river valley.

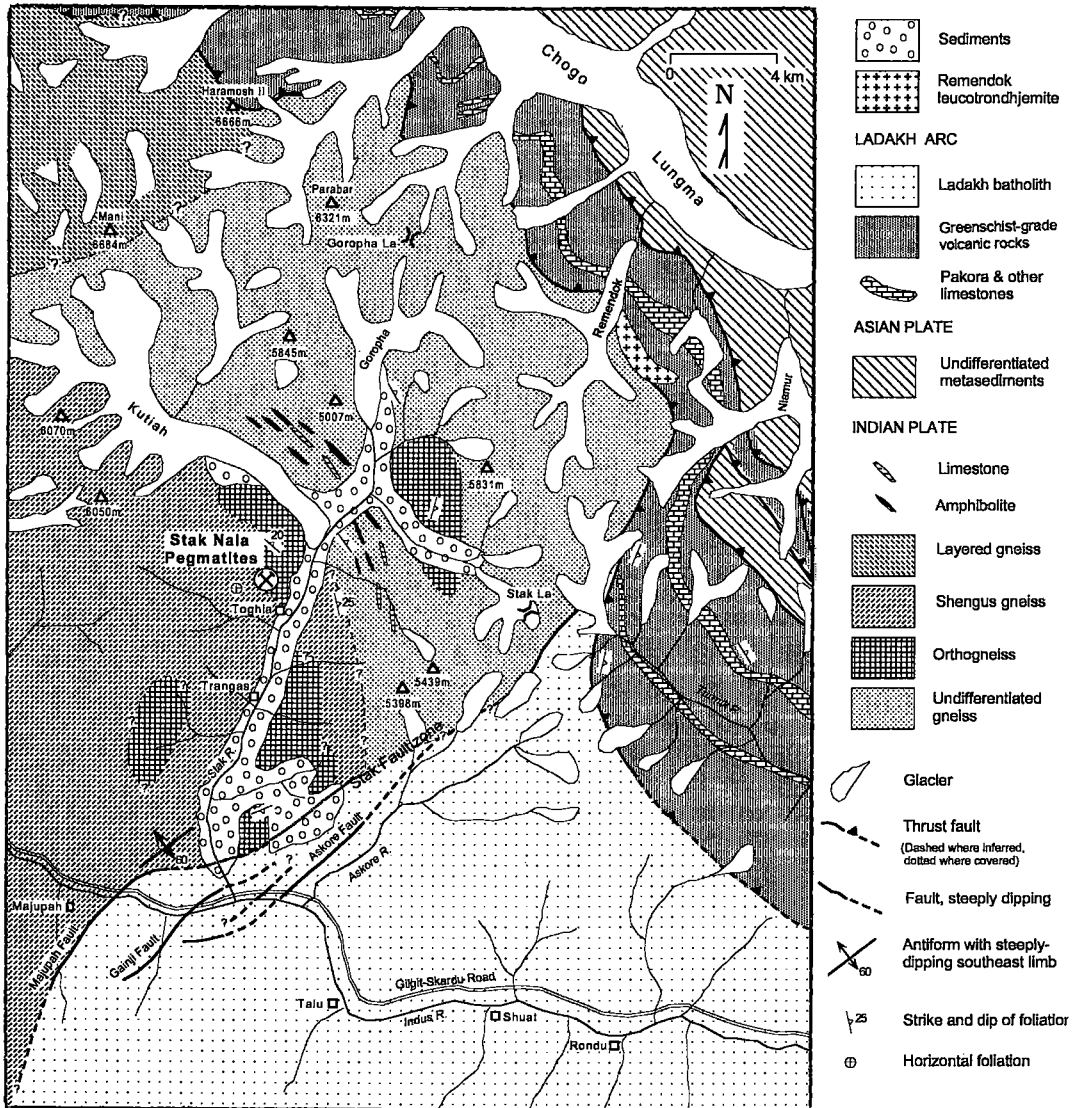


FIG. 2. Geological map of the northeastern portion of the Nanga Parbat - Haramosh massif, including the Stak Nala area (after Zanettin 1964, Verplanck 1986, Pognante *et al.* 1993, Le Fort *et al.* 1995, this study). Haramosh peak (7397 m) is located northwest of Kutiah glacier, slightly outside the map area.

methods described by Ribbe (1983). Boron contents of muscovite were measured by electron microprobe using a PC-3 crystal at Rice University. Mineral abbreviations follow conventions proposed by Kretz (1983). A complete listing of whole-rock compositions and electron-microprobe data is available from the Depository of Unpublished Data, CISTI, National Research Council of Canada, Ottawa, Ontario K1A 0S2.

GEOLOGICAL SETTING

Bodies of miarolitic granitic pegmatite in northern Pakistan are hosted by amphibolite- to granulite-facies schists, gneisses, and amphibolites in a region extending from the Hunza River on the northwest to the Shigar River near Dasso on the southeast (Fig. 1). The pegmatites are exposed in the Indian Plate in the

Haramosh massif at Dache, Drot, Khaltaro, and Stak Nala, and in the Asian Plate near Nagar and Dassu, but not within the Kohistan–Ladakh arc terrane.

The mirolitic pegmatites are invariably young, with cooling ages of less than 10 Ma (Table 1), and are undeformed except near the margins of the Haramosh massif, where they are sheared locally. In general, they form swarms of subparallel, locally anastomosing, discordant dikes and lenses or nearly concordant sills (Kazmi *et al.* 1985, Kazmi & O'Donoghue 1990, Laurs *et al.* 1996a, b). They attain a thickness of up to several meters and are typically traceable for <200 m, although individual dikes >3000 m long have been mapped near Drot (Kazmi & O'Donoghue 1990). The abundance of tourmaline and topaz in the pegmatites (Table 1) indicates that they are B- and F-rich. With the exception of Stak Nala, the pegmatites also are Be-enriched, with abundant aquamarine (*e.g.*, Kazmi *et al.* 1985).

The Stak Nala pegmatites are located in the Nanga Parbat – Haramosh massif (hereafter, Haramosh massif), which forms the northernmost exposure of Indian plate rocks. The massif has been rapidly uplifted and exhumed through the overlying rocks of the Kohistan–Ladakh arc terrane. The Indian Plate rocks consist of Proterozoic (?) biotite-bearing orthogneiss and paragneiss, with subordinate biotite schist, amphibolite, calc-silicate gneiss, and marble (Madin 1986, Madin *et al.* 1989, Treloar *et al.* 1991). In northern Pakistan, Indian Plate rocks are generally in fault contact on the north with the Kohistan–Ladakh arc terrane along the early Cenozoic Main Mantle Thrust, a north-dipping crustal scale suture, which forms a ductile thrust bounding the northern part of the Haramosh massif (Butler *et al.* 1992, Le Fort *et al.* 1995). Near Haramosh, the Indian Plate rocks are also bounded by steeply dipping faults of late Cenozoic – Quaternary age: the Raikot Fault on the west and the Stak Fault on the east (Fig. 1). The steeply east-dipping Raikot Fault is a dextral reverse fault that has accommodated much of the recent uplift of the Haramosh massif (Madin 1986, Madin *et al.* 1989), averaging ~6 mm/year during late Quaternary time (Zeitler 1985, Zeitler *et al.* 1993). Approximately 8 km south of the Stak Nala mine, Verplanck (1986) described the steeply dipping, northeast-striking Stak Fault as an oblique-slip fault juxtaposing the Ladakh arc with the eastern margin of the Indian plate (Figs. 1, 2). Rocks of the Ladakh arc in the area consist of amphibolite and garnet amphibolite cut by garnet–muscovite leucogranite dikes and sills.

The Indian Plate rocks of the Haramosh massif were called the Nanga Parbat Group and broadly subdivided into the Iskere gneiss and the structurally lower Shengus gneiss by Madin (1986). More recently, Butler *et al.* (1992) described a “layered unit” of paragneiss, schist and amphibolite that lies along the northern margin of the Haramosh massif, immediately structurally below the Main Mantle Thrust. The Shengus gneiss

consists principally of layered biotite–muscovite paragneiss with subordinate biotite schist, amphibolite, calc-silicate gneiss, and marble, which are interpreted to be derived from shale, marl, arkosic sandstone, and limestone protoliths, but also includes minor amounts of granitic gneiss (Fig. 2). The Proterozoic-age paragneiss is apparently intruded by or structurally interlayered with the younger granitic gneiss (Madin *et al.* 1989). Zircon from such a granitic gneiss yielded multiple discordant U/Pb ages, interpreted by Zeitler *et al.* (1989) to indicate an early Paleozoic age of crystallization of ~400 to ~500 Ma, with inherited zircon components as old as ~2500 Ma. The Iskere gneiss consists principally of biotite granite and granodiorite orthogneiss. Zeitler *et al.* (1989) obtained a U/Pb zircon age of ~1850 Ma for orthogneiss in the Iskere gneiss.

The northeastern part of the Haramosh massif including Stak Nala is vaguely mapped and described, but consists of both layered paragneiss and orthogneiss (Fig. 2, and below). The gneisses have a granoblastic texture and a mineral assemblage of quartz, K-feldspar, plagioclase, biotite, and garnet characteristic of upper amphibolite to granulite facies. Peak conditions of metamorphism of the layered quartz – plagioclase – biotite – muscovite – garnet – kyanite ± rutile paragneiss at a location about 10 km northeast of the Stak Nala mine were estimated to be 8 to 13 kbar and 650 to 700°C (Pognante *et al.* 1993). Regionally in the Haramosh massif, granulite-facies metamorphism is considered to be of Proterozoic age, whereas younger Tertiary-age metamorphism related to underthrusting of the Indian Plate along the Main Mantle Thrust resulted in lower grades (Treloar *et al.* 1994), typically in the amphibolite facies (*cf.* Laurs *et al.* 1996b).

Postdating the peak of Tertiary metamorphism, uplift of the Haramosh massif was accompanied by emplacement of small, coarse-grained, heterogeneous dikes, sills, and plutons of leucogranite (*e.g.*, George *et al.* 1993, Laurs *et al.* 1996b). These leucogranites have been ascribed to fluid-absent decompression-induced melting of a pelitic source undergoing rapid exhumation (Zeitler & Chamberlain 1991, George *et al.* 1993, Harris *et al.* 1993, Zeitler *et al.* 1993, Treloar *et al.* 1994). Zeitler & Chamberlain (1991) obtained uniformly young U–Pb ages (2.3 to 11 Ma) from the high-U rim of zircon crystals, which they interpreted as crystallization ages; the zircon cores show an inherited component of about 1850 Ma, which is consistent with the age of the Iskere gneiss host-rock.

GEOLOGY AND STRUCTURE OF STAK VALLEY

The Stak valley is principally underlain by light-colored paragneiss and orthogneiss layered on a cm to m scale. These rocks were assigned by Verplanck (1986) to the Shengus gneiss (Fig. 2), a name that we have retained. At the Stak Nala mine, orthogneiss

predominates (Fig. 2). Near and south of the mine, the layered gneisses dip gently ($<10^\circ$). Adjacent to the Stak Fault zone, these gneisses are deformed into a series of folds with gently plunging axes paralleling the fault, with the southeasternmost limb dragged into parallelism with the fault plane (Verplanck 1986). Granodiorite gneiss crops out on both sides of the valley 4 km south of the Stak Nala mine (Zanettin 1964, Fig. 2); garnet, biotite, and 10 to 20 vol.% K-feldspar augen that are 2 cm long are present in eastern exposures.

North and east of the mine, the gently dipping gneissic layering is deflected to a northwest strike and a gentle (20 to 25°) northeast dip. To the northeast of the intersection of the Kutiah glacier with the Stak valley, strongly layered gneisses containing concordant amphibolite and marble bodies predominate and dip gently to moderately northeast. Pognante *et al.* (1993) described a body of orthogneiss in this area, and also noted that the northeast-dipping gneissic layering is deflected toward the Stak Fault at Stak La pass, similar to Verplanck's description to the southeast. Overall, a traverse to the northeast from the Stak Nala mine proceeds up-section in the layered gneisses to the Main Mantle Thrust. On Figure 2, these gneisses are shown as undifferentiated gneisses, which may be equivalent to Shengus gneiss, but are more likely equivalent to the "layered" gneiss unit of Butler *et al.* (1992) lying below the Main Mantle Thrust northwest of Haramosh.

The overall structure of the northeastern portion of the Haramosh massif appears to have two salient features (Fig. 2). First, shallowly dipping gneissic layering is deformed into a moderately northeast-dipping orientation parallel to the overlying Main Mantle Thrust. Second, the Stak Fault zone truncates the gneissic layering of the Haramosh massif, as well as the older fault boundary between the Ladakh batholith and the overlying greenschist-grade volcanic rocks. However, in detail the Stak Fault truncates these features as a series of ductile shears and steep-limbed folds. Thus, as the Haramosh massif gneisses were uplifted along the Stak Fault, they were deformed in ductile fashion.

GEOLOGY OF THE STAK NALA MINE AREA

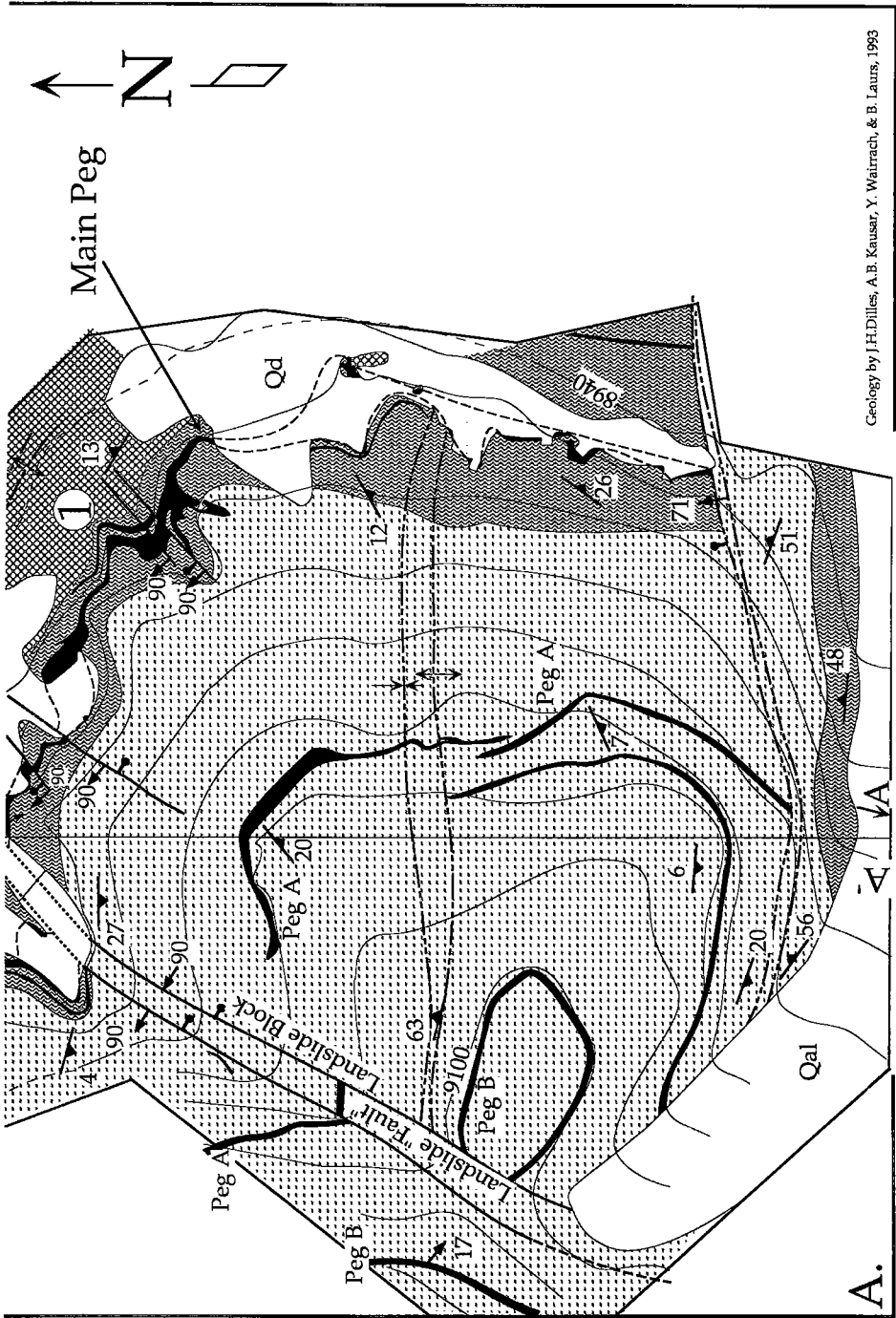
Several varieties of orthogneiss and paragneiss are mapped in the mine area (Figs. 3, 4, 5). The orthogneiss consists of biotite–muscovite flaser granite gneiss, banded leucocratic augen pegmatite gneiss, and biotite granodiorite gneiss (Table 2). The paragneiss consists of biotite – muscovite – garnet quartzofeldspathic gneiss, biotite – muscovite quartzofeldspathic gneiss, and minor dark bands of biotite gneiss. The pegmatites at the main mine area are hosted mainly by the flaser and banded orthogneisses, and at the south mine area by the biotite granodiorite gneiss. At least six sills separated by up to 20 m are exposed within a 100-m section of gneiss in the main mine area, and three sills are exposed in the south mine area.

The dominant $S1$ foliation of the gneisses is flat to gently north- or east-dipping. A stretching lineation marked by feldspar augen and layers of biotite and muscovite trends north to northwest; feldspar augen define kinematic simple shear with top-to-the-north orientation. A series of $F2$ flexural shears deforms the $S1$ fabrics. The axial planes of the $F2$ -flexures strike east–west, dip moderately south, and are strongly asymmetrical: anticlines have gently dipping south limbs and 60° N-dipping north limbs with attenuated and thinned layers (Figs. 3, 4). These anticlines are paired with synclines lying 5 to 10 m to the north. The narrow zone of thinned layers indicates that these flexures are the result of down-to-the-north ductile shearing with normal offset.

The pegmatites form sill-like bodies that cross-cut the $S1$ foliation at a low angle. The contact with the gneisses is sharp, with no evidence for wallrock assimilation. The pegmatites narrow, splay, and pinch where they intersect the $F2$ -flexural shears (Figs. 3, 4), and locally they intrude into the steeply dipping flexures as narrow, <25 -cm-wide dikes. The pegmatites clearly postdate the $F2$ flexures, and locally deform in ductile fashion the gneissic foliation within 0.3 m of their contacts (Fig. 5, location 2; Fig. 6). Brittle, normal faults locally have reactivated the earlier ductile shears, offset the pegmatites, and in places have localized weak hydrothermal alteration, characterized by zones of rock 1 to 5 m wide altered to quartz and sericite, with 1 to 5 vol.% pyrite. The youngest structures are Quaternary, steeply dipping brittle fractures that have accommodated landslide block-slumping along oversteepened slopes into the glaciated Stak valley. These slump-fractures parallel the canyon walls. One has dropped the main mine area down 4.5 m to the southeast, and a second has dropped an area 60 m north down 15 m to the southeast.

ARGON GEOCHRONOLOGY

Age spectra were determined for muscovite from the flaser granite gneiss and lepidolite from a pegmatite pocket at the main mine (Fig. 7). The muscovite yields a $^{40}\text{Ar}/^{39}\text{Ar}$ plateau age of 5.80 ± 0.05 Ma for four steps constituting 57.3% of the ^{39}Ar gas released (Table 3). This date is interpreted as the age of cooling through the 325°C closure temperature for muscovite. The lepidolite yielded a similar $^{40}\text{Ar}/^{39}\text{Ar}$ spectrum, with a plateau age of 4.63 ± 0.12 Ma for six steps constituting 74.7% of the ^{39}Ar gas released (Table 3). The pegmatites could be significantly older than 4.6 Ma, and are clearly older than the 2.3 to 7 Ma crystallization ages interpreted for the pegmatites at Drot, located 17 km west–northwest of Stak Nala (Zeitler & Chamberlain 1991), and the ~ 1 Ma Fingatori leucogranite in the Tato region of Nanga Parbat, ~ 55 km southwest of Stak Nala (Winslow *et al.* 1995). However, the Stak Nala pegmatites are younger than pegmatites at



Geology by J.H.Dilles, A.E. Kauser, Y. Wairach, & B. Laurs, 1993

Fig. 3. A. Geologic map of the main mine area. B. Cross-sectional view of the F2 ductile normal shears cut by pegmatites.

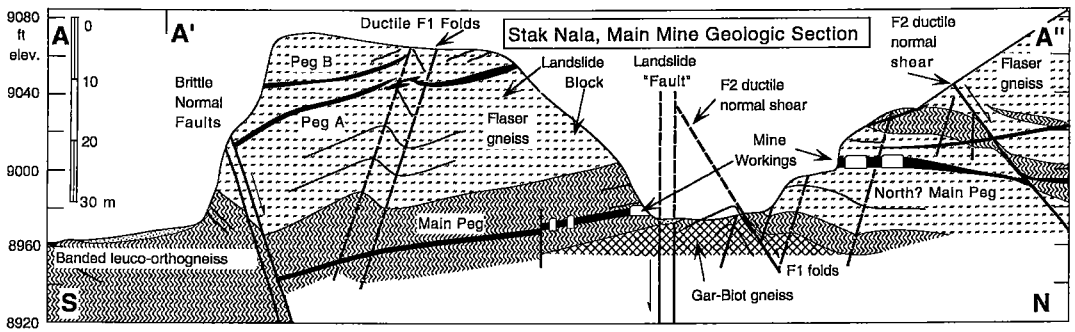


FIG. 4. Geological cross-section of the main mine area.

Khaltaro, located 35 km northwest, with a $^{40}\text{Ar}/^{39}\text{Ar}$ age of 9 Ma on muscovite (Lauris *et al.* 1996b). The 4.6 Ma $^{40}\text{Ar}/^{39}\text{Ar}$ age of the Stak Nala pegmatites is consistent with the southward-younging granite magmatism within the Haramosh massif.

GEOLOGY OF THE PEGMATITES

The granitic pegmatites at Stak Nala are of the complex Li-Cs-Ta type, with characteristics transitional between the elbaite and lepidolite subtypes (*e.g.*, Černý 1991, Novák & Povondra 1995). The pegmatites are mineralogically zoned parallel to the contacts, miarolitic, and consist of coarse-grained K-feldspar, sodic plagioclase, quartz, and schorl, minor muscovite, and traces of spessartine-almandine garnet and löllingite. Locally, the core and pocket zones contain fluorite, colored tourmaline, topaz, lepidolite, apatite, and several rarer minerals (Table 4). Although the pocket mineralization is similar to the pegmatite-aplite bodies in southern California (*cf.* Foord 1976, 1977, Foord *et al.* 1989, 1991a, Jahns & Wright 1951, Stern *et al.* 1986), the internal zonation is quite different: the Stak Nala pegmatites are symmetrically zoned about a centrally disposed core zone, whereas layered pegmatite-aplite bodies in California are asymmetrical, with fine-grained, sodic aplite in the footwall and coarse-grained, graphic K-feldspar-rich, potassic pegmatite in the hanging wall (*e.g.*, Jahns & Tuttle 1963).

The pegmatites at the main mine area form sills that are 0.3 to 1.2 m thick and 30 to at least 120 m long. They show a fairly even thickness along their length, and dip shallowly ($<5^\circ$) southward or are flat-lying except where they deviate crossing F2 flexures. Economically important colored tourmaline occurs only within one of the six pegmatite sills we examined (Fig. 8), although each sill contains pockets. The three pegmatites observed at the south mine form thicker (>1.2 m) sills, of which the largest is the only one mined in the south area (2.1 to 4.6 m thick, >110 m long; Fig. 5). Slivers of wallrock projecting into the

pegmatites are common at both mine areas. Individual sills commonly form a series of sill segments linked to one another by short dike segments near their distal ends (Fig. 9). These linking dikes are typically <1 m long, 10 to 15 cm thick, and contain the same minerals as the sills, but with less pronounced compositional and textural zoning.

Internal zonation in the pegmatite sills: main mine area

On the basis of texture and mineralogy, the Stak Nala pegmatites can be divided into three internal zones, which from the contacts inward are termed the border zone, wall zone, and core zone (Figs. 10, 11, 12). The border and wall zones form laterally continuous envelopes around the core zone. The internal zonation is remarkably persistent along strike, except where perturbed by slivers of wallrock projecting into the pegmatite, or where the pegmatites narrow and core zones are absent or disproportionately thinner. The zones are vertically symmetrical in texture and mineralogy about the central subhorizontal plane of the pegmatite, with minor exceptions: (1) the upper wall zone is slightly thinner than the lower wall zone, (2) schorl is more abundant in the upper wall zone than in the lower wall zone, and (3) cavities or pockets generally form in the upper portion of the core. The following descriptions are generalized for pegmatites at the main mine area.

Extending from the contacts inward up to 10 cm is a *border zone* (Figs. 10, 11) characterized by coarse (<1 to 3 cm) crystals of sodic plagioclase, with subordinate quartz and K-feldspar. However, the modes vary widely, and K-feldspar is locally more abundant. Along the contact, schorl (with or without garnet) commonly forms abundant small (1 to 3 mm) crystals that project into both pegmatite and wallrock. Sodic plagioclase and quartz form irregular intergrowths, and myrmekite is common near the contact between these two minerals. K-feldspar forms elongate wedge-shaped megacrysts that nucleate in the border zone and flare

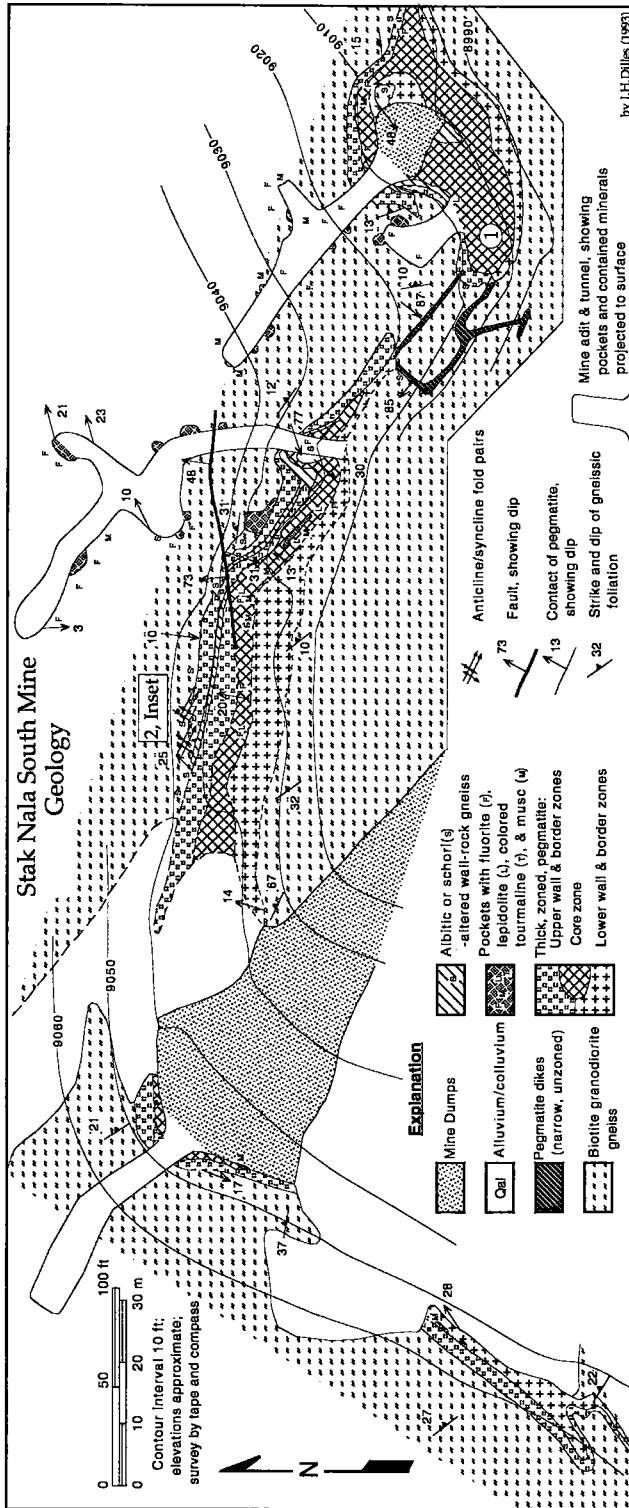


FIG. 5. Geological map of the south mine area.

TABLE 2. BULK COMPOSITION OF HOST GNEISSES, STAK NALA

Description	Flaser	Banded	Biotite	Biotite
Type*	ortho	ortho	para	ortho
Comp'n	granite	granite	? granodiorite	
Mine area	Main	Main	Main	South
SiO ₂ (wt%)	72.22	71.86	64.67	67.85
TiO ₂	0.24	0.38	0.84	0.57
Al ₂ O ₃	14.83	14.41	15.74	14.98
Fe ₂ O ₃	1.67	2.09	7.34	4.49
MnO	0.02	0.03	0.12	0.06
MgO	0.37	0.47	2.32	2.04
CaO	0.86	0.94	1.01	2.52
Na ₂ O	2.60	2.60	2.50	2.83
K ₂ O	6.36	6.55	4.35	4.16
P ₂ O ₅	0.19	0.21	0.14	0.11
LOI	1.38	1.09	1.15	1.19
Total	100.75	100.62	100.18	100.81
Sc (ppm)	<7	<7	14	13
V	<7	11	123	73
Cr	6	87	116	78
Ni	4	7	26	11
Cu	8	6	2	1
Pb	41	n.d.	n.d.	n.d.
Zn	49	65	257	42
Ga	18	19	24	20
As	<2	n.d.	n.d.	n.d.
F	145	n.d.	n.d.	n.d.
B	10	n.d.	n.d.	n.d.
Be	9	n.d.	n.d.	n.d.
Li	21	n.d.	n.d.	n.d.
Rb	279	271	422	221
Cs	41	n.d.	n.d.	n.d.
Sr	94	95	81	175
Ba	435	271	471	606
Ce	73	201	56	110
Nd	36	68	26	39
Y	7	14	32	36
Zr	98	212	220	165
Nb	11	10	22	16
Th	18	75	16	24
U	<7	17	<7	<7

* ortho: orthogneiss, para: paragneiss

Major elements by XRF (Rigaku 3370E instrument) using fused glass disks with 1:5 ratio of rock to Li tetraborate, with errors of ± 1 -2%; trace elements by XRF (± 5 -10%) on pressed pellets. Analyzed by Chemex Labs, Inc. are Li, Be, Cs, Pb, & As by atomic absorption, B by INAA, and F by specific ion electrode; detection limits (ppm): Be: 0.1, Cs: 0.5, As, Pb, and Li: 1, B: 5, and F: 20.

into the wall zone, but lack graphic intergrowths with quartz. Powder X-ray diffraction of one megacrystic sample showed a degree of Si - Al order typical of intermediate microcline. In thin section, the K-feldspar shows subtle cross-hatched twin domains or no twinning. Microperthite and perthite are common; albite lamellae form "beads" and rare "strings" within K-feldspar (*cf.* Deer *et al.* 1992). Interstitial to the K-feldspar, slender needles of schorl locally form conspicuous sprays radiating inward toward the wall zone. Generally, the crystals of schorl are larger and more abundant in the hanging wall. Sparse subhedral (0.5 to 1 mm) spessartine-almandine garnet is commonly associated with schorl. Löllingite forms rare, anhedral tabular-shaped masses up to 1 cm in maximum dimension.

The border zone is texturally gradational into the wall zone, and both zones consist of the same minerals. The wall zone is defined where inwardly flaring K-feldspar megacrysts reach over 3 cm in size. The lack of schorl in the lower wall zone is also useful in distinguishing the border from the wall zone (Figs. 10, 11). The lower wall zone is commonly narrower (ave. 30 cm) than the upper wall zone (45 cm). Inwardly flaring K-feldspar megacrysts originating in the border zone and outer wall zone attain 25 cm in length, and are best developed in the hanging wall. Sodic plagioclase, quartz, and K-feldspar are coarsely intergrown between the megacrysts. In the hanging wall, prismatic crystals of schorl are disseminated and locally form sprays radiating toward the core. The schorl crystals increase in diameter from a few mm to nearly 1 cm as they approach the core zone. Commonly, schorl contains inclusions of skeletal quartz and is fractured perpendicular to the *c* axis; the fractures are filled by quartz or sodic plagioclase. Scattered flakes of muscovite are locally present along the boundary between the wall zone and core zone.

The contact between the wall zone and the centrally disposed core zone varies from gradual to abrupt. The core zone forms up to one-third the pegmatite thickness and is characterized by more complex mineralogy and widely variable grain-size: crystal-lined pockets, small bodies of very fine-grained aplite, and aggregates of lepidolite and "cleavelandite" form locally among very coarse-grained blocky K-feldspar (20 to 30 cm in diameter), with subordinate quartz and sodic plagioclase (Fig. 11). Quartz and sodic plagioclase form monomineralic masses or coarse intergrowths interstitial to K-feldspar. The proportion of K-feldspar to quartz to plagioclase in the core is highly variable, especially between different pegmatite sills. Schorl crystals originating in the wall zone are locally bent or broken in a consistent direction where they enter the core zone, and commonly have a thin (<1 mm) overgrowth of dark green elbaite. Muscovite or lepidolite forms sparse aggregates in feldspathic areas, especially near the pockets. Accessory crystals of

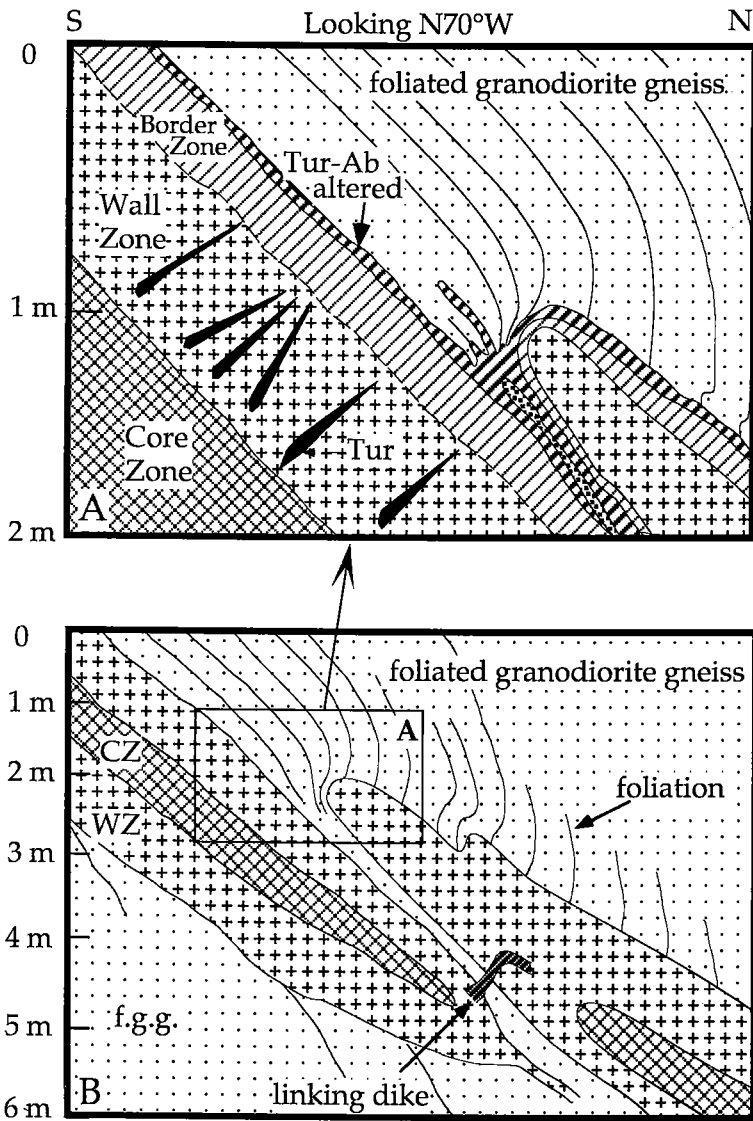


FIG. 6. A. Detail of ductile folding and distribution of wallrock alteration adjacent to pegmatites at the south mine. The stippled pattern within the altered wallrock is a layer of aplitic quartz – sodic plagioclase – schorl. B. Overview of pegmatite–wallrock relations, showing deformation of wallrock foliation around the terminal end of a pegmatite sill.

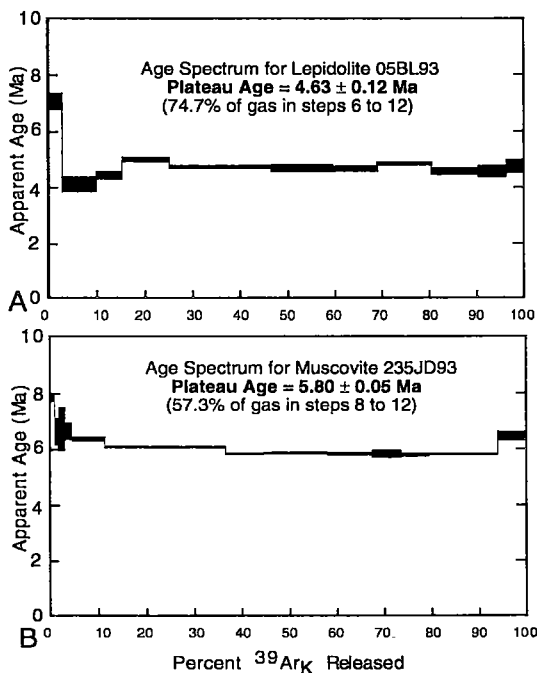


FIG. 7. $^{40}\text{Ar}/^{39}\text{Ar}$ age spectra for (A) lepidolite from a pegmatite pocket, and (B) muscovite from flaser granite gneiss, main mine area.

löllingite, spessartine–almandine garnet, and fluorite are scattered in places through the core zone. Fluorite forms euhedral (1 to 3 cm in diameter) transparent green crystals with abundant fractures. It fluoresces bright yellow under short-wave ultraviolet light, and phosphoresces after exposure to visible and ultraviolet light.

Sporadic bodies of *aplite* form locally in the core zone, especially near the pockets (Figs. 10, 11), and rarely in the wall zone. We interpret these bodies to be pressure-quench *aplite* (e.g., Foord 1976). The *aplite* appears to truncate pegmatite and forms volumetrically small irregular patches or elongate bodies ranging from several millimeters to 20 cm in maximum dimension, which is generally oriented parallel to the contacts of the pegmatite sill, except in rare cases where it forms near wallrock inclusions (Fig. 11). The *aplite* is composed of albite ($< \text{An}_6$), schorl, quartz, and local spessartine–almandine garnet; minor fluorite forms poikilitic masses in places. A very fine-grained (~0.1 mm), equigranular texture predominates, although some bodies contain segregations or fringes of coarser (1–2 mm) grains. Layering is common within the larger bodies of *aplite*, and is imparted by concentrations of schorl or garnet that alternate with albite-rich layers on

TABLE 3. $^{40}\text{Ar}/^{39}\text{Ar}$ DATA FOR MINERAL SEPARATES¹ FROM STAK NALA

Temp (°C)	Radiogenic $^{40}\text{Ar}/^{39}\text{Ar}$	K-derived $^{40}\text{Ar}/^{39}\text{Ar}$	$^{40}\text{Ar}/^{39}\text{Ar}$	Radiogenic yield (%)	Percent ^{39}Ar	Apparent Age and error ⁴ (Ma)
235JD93: MUSCOVITE; HOST-ROCK FLASER GRANITE GNEISS						
Total-gas date: 5.99 ± 0.06 Ma; plateau date: 5.80 ± 0.05 Ma;						
isochron date: 5.84 ± 0.11 Ma (550–1300°C); ($^{40}\text{Ar}/^{36}\text{Ar}$) = 301 ± 5						
J = 0.006635, ± 0.1%; wt., 90.3 mg						
550	0.007	0.011	0.62	2.8	0.1	7 ± 3
650	0.0472	0.0720	0.656	12.7	0.9	7.84 ± 0.15
700	0.0315	0.0570	0.553	9.8	0.7	6.61 ± 0.48
750	0.0572	0.1019	0.562	16.7	1.3	6.71 ± 0.77
800	0.0653	0.1178	0.554	22.9	1.5	6.62 ± 0.30
850	0.2792	0.5272	0.529	18.5	6.9	6.33 ± 0.07
900	0.9784	1.9318	0.506	50.1	25.2	6.05 ± 0.03
950 ^p	0.8011	1.6429	0.488	61.2	21.4	5.83 ± 0.03
1000 ^p	0.3493	0.7192	0.486	44.8	9.4	5.80 ± 0.05
1050 ^p	0.2231	0.4597	0.485	35.9	6.0	5.80 ± 0.13
1100 ^p	0.2210	0.4577	0.483	32.3	6.0	5.77 ± 0.05
1200 ^p	0.5384	1.1120	0.484	50.8	14.5	5.79 ± 0.01
1300	0.2439	0.4512	0.541	49.7	5.9	6.46 ± 0.15
05BL93: LEPIDOLITE; MAIN PEGMATITE						
Total-gas date: 4.68 ± 0.12 Ma; plateau date: 4.63 ± 0.12 Ma;						
isochron date: 4.54 ± 0.11 Ma (550–1300°C); ($^{40}\text{Ar}/^{36}\text{Ar}$) = 299 ± 6						
J = 0.006503, ± 0.1%; wt., 37.8 mg						
550	0.006	0.007	0.87	2.3	0.2	10 ± 10
650	0.0524	0.0874	0.600	9.4	2.7	7.02 ± 0.28
750	0.0779	0.2241	0.347	20.7	7.0	4.07 ± 0.26
800	0.0665	0.1782	0.373	24.9	5.5	4.37 ± 0.13
850	0.1331	0.3158	0.422	31.2	9.8	4.94 ± 0.07
900 ^p	0.2723	0.6850	0.397	46.0	21.3	4.66 ± 0.04
950 ^p	0.1619	0.4104	0.394	50.9	12.8	4.62 ± 0.12
1000 ^p	0.1180	0.3018	0.391	41.2	9.4	4.58 ± 0.08
1050 ^p	0.1513	0.3714	0.407	42.4	11.6	4.77 ± 0.04
1100 ^p	0.1225	0.3187	0.384	37.9	9.9	4.50 ± 0.12
1150 ^p	0.0726	0.1887	0.385	29.9	5.9	4.51 ± 0.20
1300 ^p	0.0501	0.1249	0.401	26.5	3.9	4.70 ± 0.22

¹ Samples were crushed, ground, and sieved and the 80-to-120-mesh-size sieve fractions were passed through a magnetic separator. Concentrates were hand picked to 100% purity, and cleaned in reagent-grade ethanol, acetone, and de-ionized water in an ultrasonic bath. The samples were wrapped in aluminum packages and sealed in silica vials along with monitor minerals prior to irradiation in the TRIGA reactor at the U.S. Geological Survey in Denver, Colorado for 28.75 hours at 1 mcgawatt.

² A Mass Analyzer Products 215 Rare Gas mass spectrometer with a Faraday cup was used to measure argon-isotope abundances. Abundances of ^{40}Ar and ^{39}Ar are reported in volts. Conversion to moles can be made using 9.74×10^{-13} moles argon per volt of signal. Detection limit at the time of this experiment was 2×10^{-17} moles argon. Analytical data for ^{40}Ar and ^{39}Ar are calculated to 5 decimal places; $^{40}\text{Ar}/^{39}\text{Ar}$ is calculated to 3 decimal places. ^{40}Ar , ^{39}Ar , and ^{37}Ar are rounded to significant figures using analytical precisions. Apparent ages and associated errors were calculated from unrounded analytical data and then each rounded using associated errors. All analyses were done in the Argon Laboratory, U.S. Geological Survey, Denver, Colorado. Decay constants are those of Steiger and Jäger (1977), i.e., $\lambda_{^{40}\text{Ar}} = 5.81 \times 10^{-10} \text{ yr}^{-1}$, $\lambda_{^{39}\text{Ar}} = 4.962 \times 10^{-10} \text{ yr}^{-1}$, and $\lambda_{^{37}\text{Ar}} = 5.543 \times 10^{-10} \text{ yr}^{-1}$. The irradiation monitor, hornblende MMBh-1 with percent $\text{K} = 1.555$, $^{40}\text{Ar} = 1.624 \times 10^{-9}$ mole/gm, and K-Ar age = 520.4 Ma (Samson & Alexander 1987), was used to calculate J values for this experiment.

³ $^{40}\text{Ar}/^{39}\text{Ar}$ has been corrected for all interfering isotopes including atmospheric argon. Mass discrimination in our mass spectrometer was determined by measuring the $^{40}\text{Ar}/^{36}\text{Ar}$ ratio of atmospheric argon; our measured value is 298.9 during the period of this experiment; the accepted atmospheric $^{40}\text{Ar}/^{36}\text{Ar}$ ratio is 295.5. Abundances of interfering isotopes of argon from K and Ca were calculated from reactor production ratios determined by irradiating and analyzing pure CaF_2 and K_2SO_4 simultaneously with these samples. The measured production ratios for these samples are ($^{40}\text{Ar}/^{39}\text{Ar}$) $_{\text{K}} = 7.92 \times 10^{-3}$, ($^{38}\text{Ar}/^{39}\text{Ar}$) $_{\text{K}} = 1.309 \times 10^{-2}$, ($^{37}\text{Ar}/^{39}\text{Ar}$) $_{\text{K}} = 1.75 \times 10^{-4}$, ($^{36}\text{Ar}/^{39}\text{Ar}$) $_{\text{Ca}} = 2.68 \times 10^{-4}$, ($^{39}\text{Ar}/^{37}\text{Ar}$) $_{\text{Ca}} = 6.85 \times 10^{-4}$, and ($^{38}\text{Ar}/^{37}\text{Ar}$) $_{\text{Ca}} = 4.40 \times 10^{-5}$. Corrections were also made for additional interfering isotopes of argon produced from irradiation of chlorine using the method of Roddick (1983). The reproducibility of split gas fractions from each monitor (0.05–0.25%, 1 σ) was used to calculate imprecisions in J. J values for each sample were interpolated from adjacent monitors and have similar uncertainties to the monitors. Uncertainties in calculations for the date of individual steps in a spectrum were calculated using modified equations of Dalrymple et al. (1981).

⁴ 1 σ error.

^p Fraction included in plateau date.

The amount of ^{37}Ar during analysis was below background level.

a submillimeter scale, resulting in an overall streaked white and dark gray or red-orange appearance. The layers are oriented roughly parallel to the contacts of the *aplite*, and commonly appear swirled or contorted. The largest masses of *aplite* were seen at the main mine

TABLE 4. MINERALS IN PEGMATITE AND HOST GNEISS, STAK NALA

Mineral or Mineral Group	Pegmatite	Altered Gneiss	Unaltered Gneiss
bertrandite	ER	-	-
beryl	VR	-	-
cassiterite	*	-	-
chalcocopyrite	-	ER	ER
feldspar:			
albite (incl. cleavelandite)	A	-	-
K-feldspar	A	A	A
oligoclase	A	A	A
fluorapatite	R	VR	ER
fluorite	C	VR	-
garnet:			
almandine-grossular-pyrope	-	-	C
almandine-spessartine	C	R	-
hambergite	VR	-	-
ilmenite (manganon)	-	ER	-
löllingite	C	-	-
magnetite	-	VR	VR
manganocolumbite	R	-	-
manganotantalite	*	-	-
mica:			
biotite	-	R	A
borian muscovite	R?	-	-
lepidolite or lithian muscovite	C	-	-
muscovite	C	A	A
microcline	R	-	-
Mn-Fe oxides	R	ER	-
monazite	ER	ER	-
montmorillonite	*	-	-
pyrite	-	VR	VR
quartz	A	A	A
topaz	R	VR	-
tourmaline:			
elbaite	C	VR	-
schorl	A	C	-
zircon	VR	ER	ER
Incompletely characterized minerals:			
Sb-Nb-Ta-W-Pb-Ti-Bi-Sn-As oxide	ER	-	-
Sb-Nb-Ta-W-Ti-Sn-As oxide	ER	-	-
Ti-Nb-Y-U-REE-Ta-Th-W-Fe-Ca oxide (euxenite-polycrase?)	-	ER	-
As-Fe-K oxide (pharmacosiderite?)	ER	-	-
As-Fe-Ca-Ti oxide (cafarsite?)	ER	-	-

A: abundant and widespread, C: common or locally abundant, R: uncommon or rare, VR: very rare, ER: extremely rare, *: reported in Kazmi *et al.* 1985 but not seen by the present authors, -: not seen or reported

at location 2 (Fig. 3). At location 1, in the vicinity of abundant tourmaline mineralization, small sporadic pods ~1 cm in diameter of microcrystalline schorl were noted in the upper wall zone.

Internal zonation in the pegmatite sills: south mine

The south mine pegmatite shows similar internal zoning as the main sill, but on a larger scale, corresponding to its greater thickness (Fig. 12). Compared to pegmatites at the main mine, the following differences

in internal zonation were noted. In terms of *wallrock alteration*, the biotite granodiorite gneiss wallrock is more extensively tourmalinized adjacent to pegmatite. With respect to *internal zonation*, 1) the border zone contains more quartz, spessartine-almandine garnet, and muscovite, but lacks tourmaline, 2) the core zone is thicker in proportion to the rest of the pegmatite (up to 35%), and the lower boundary between the core and wall zone is not well defined, and 3) pockets are consistently located in the upper portion of the core zone, along the contact with the wall zone, and are commonly surrounded by massive quartz that is somewhat smoky. With respect to *mineralogy and texture*, 1) löllingite is very rare in all the zones. 2) K-feldspar megacrysts within the footwall display progressively increasing size (up to ~40 cm) from the border zone toward the core zone. 3) The core zone commonly contains fluorite, blocky K-feldspar megacrysts with patchy green, gray and white coloration, and white euhedral topaz that is locally altered to fine-grained pseudomorphous muscovite. Quartz and apite form abundant and larger masses (<1.5 m long). Irregular aggregates of coarse-grained (up to 1 cm) muscovite and lepidolite are intergrown with schorl and pale pink elbaite, respectively. Finally, 4) albite-enriched zones of hydrothermal replacement (described below) are more abundant, especially in the core.

Hydrothermal assemblages with albite

Albite-bearing mineral assemblages were noted in pegmatites at both mine areas, and formed as a result of metasomatism, as they replace igneous minerals and display vein and pseudomorph textures. The boundaries between albitized and fresh pegmatite are sharp and irregular. Three types of albitic alteration are defined: (1) pseudomorphs of massive albite after K-feldspar and oligoclase, (2) aggregates of "cleavelandite" with mica and elbaite, and (3) blocky albite crystals lining vugs formed by dissolution of quartz.

Pseudomorphs of massive albite after K-feldspar and oligoclase form the most widespread and difficult-to-recognize type of alteration. The massive albite forms in all pegmatite zones extending to the wallrock contacts, but is most common in the core and hanging-wall zones. The alteration is characterized by patchy or complete replacement of K-feldspar and oligoclase by albite, with or without muscovite and traces of fluorite. The albite is identical in appearance to the K-feldspar it replaces; stained rock slabs and electron-microprobe analyses were used to confirm the distribution of albite. Microscopic examination of the albitized areas under crossed polars showed anhedral albite with rare polysynthetic twin planes are that are diffuse or patchy, local veinlets and disseminations of fine-grained muscovite, and rare disseminated fluorite.

Aggregates of "cleavelandite" form cross-cutting

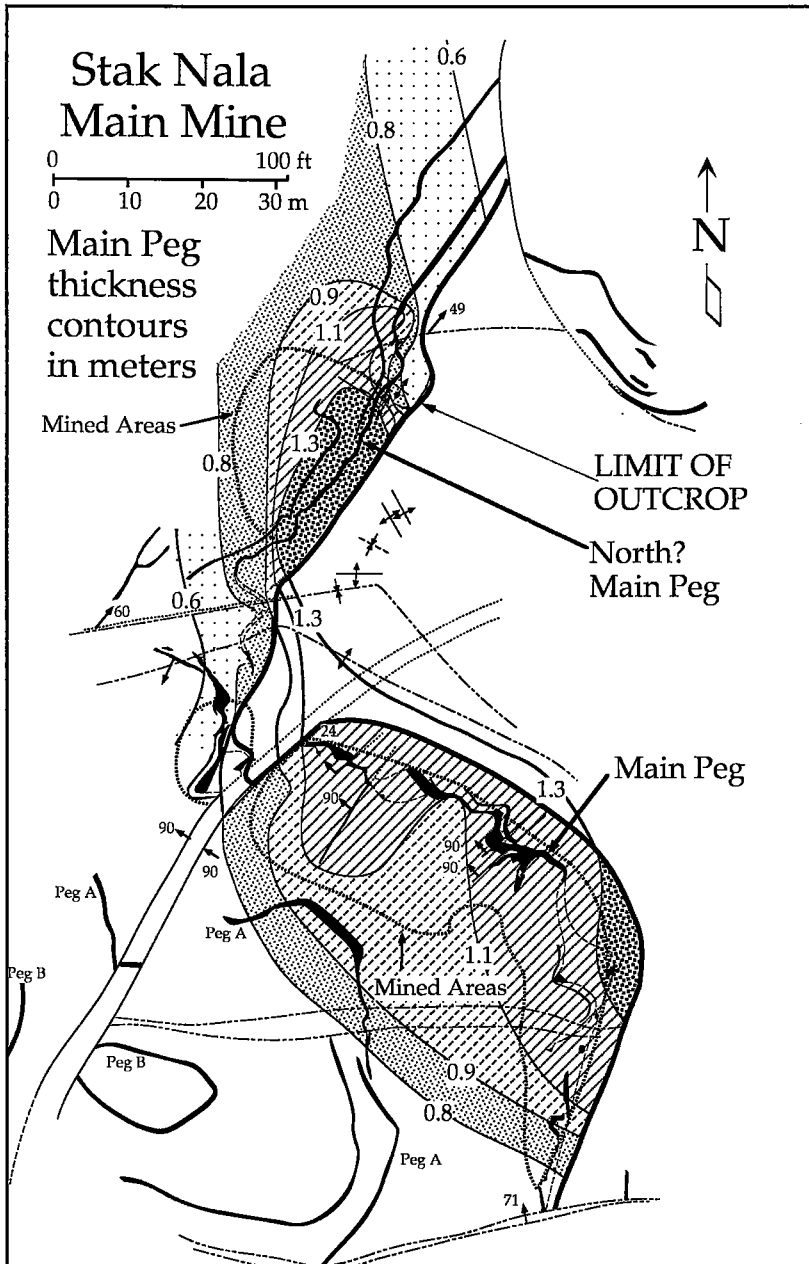


FIG. 8. Map of the Stak Nala main sill, showing contours of pegmatite thickness in meters. Thickness is interpolated between outcrops and exposures within mine tunnels. Heavy dotted line shows extent of mined areas in 1993.

veinlets and irregularly shaped bodies (Fig. 13) up to 20 cm in maximum dimension within the core and intermediate zones, particularly near pockets. The "cleavelandite" is commonly intergrown with muscovite or lepidolite and subordinate dark green

elbaite; traces of topaz, microlite, fluorapatite, and rare beryl and zircon may be present.

Locally in the main mine area (Fig. 3, location 3), the core and upper wall zone of the pegmatite show a vuggy texture caused by dissolution of quartz. The

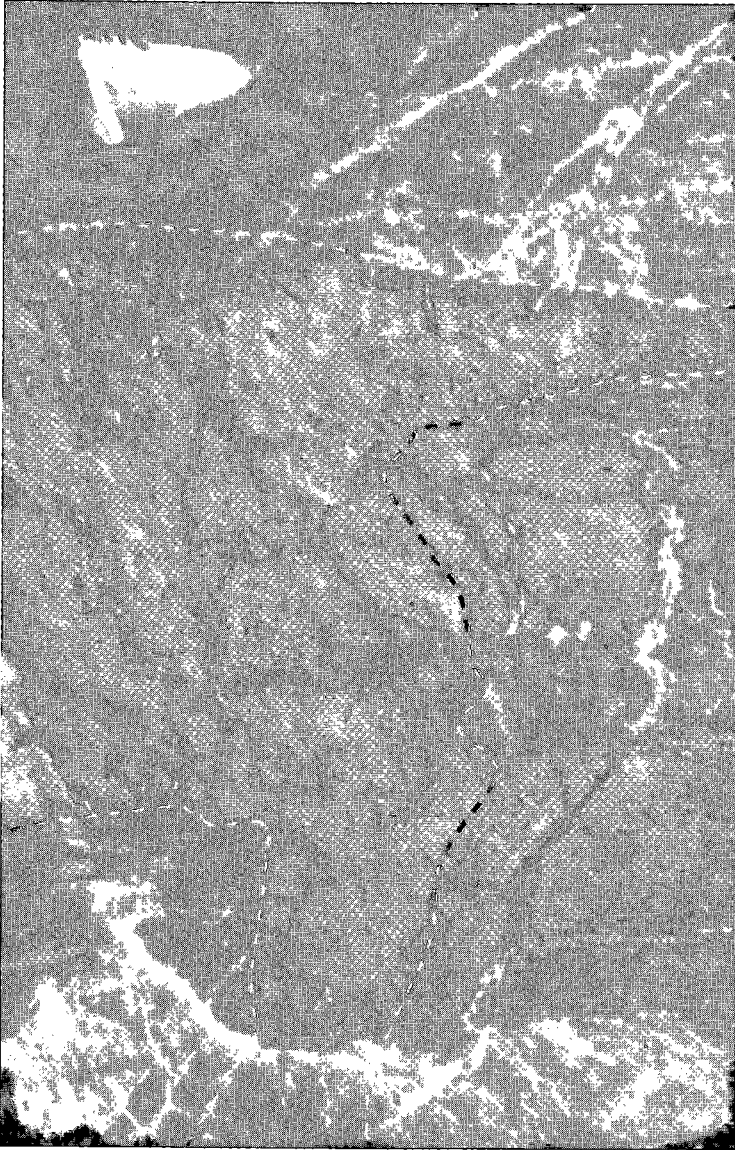


FIG. 9. Photograph of the terminus of a pegmatite sill, and associated wallrock alteration, at the main mine area (pocket knife for scale). A narrow undifferentiated dike links this sill with the main sill (below, off photo). The dashed line marks the contact between pegmatite and altered wallrock. Abundant tourmaline veins cut the flaser granite gneiss wallrock; metasomatism by pegmatite-derived fluids has caused conversion of biotite to muscovite within 10 cm of the pegmatite contact, and the crystallization of schorl locally along foliation.

vugs attain 3 cm in maximum dimension, and correspond in size and distribution to the former location of primary quartz. Primary feldspars in the vuggy rock are replaced by massive albite. Schorl is corroded or partially replaced by muscovite and stained by iron oxides, and coarse crystals of primary muscovite

display embayed and ragged edges, interpreted to reflect partial dissolution. Within the vugs, blocky crystals of albite formed after the period of dissolution. Also present locally are prisms of quartz, needles of green tourmaline, pseudo-hexagonal plates of muscovite, and etched topaz. The vug minerals are lightly coated

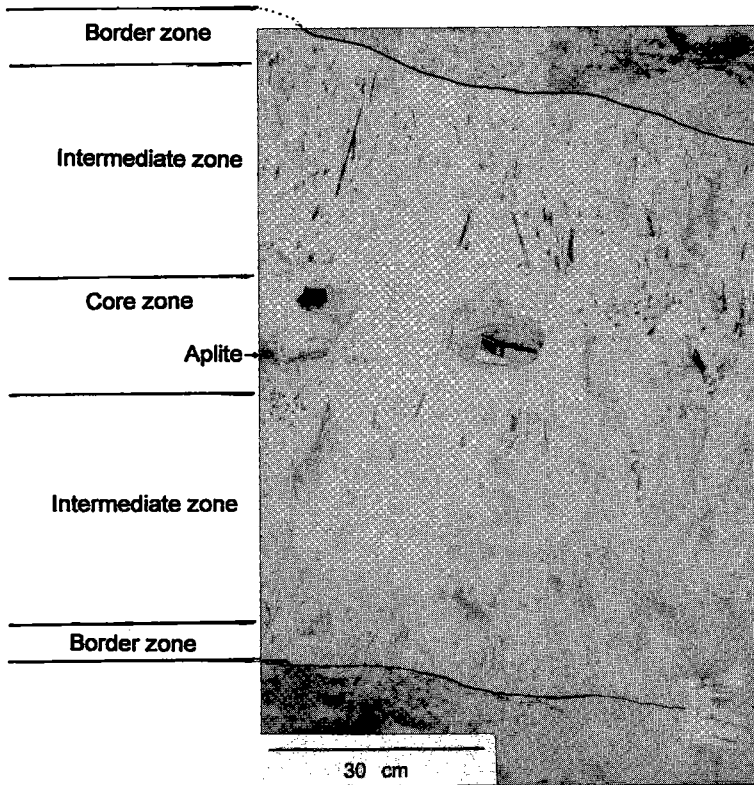


FIG. 10. Photograph of pegmatite sill underground in the north part of the main mine area, in the vicinity of samples collected for microprobe analysis (Fig. 4, location 2). The pegmatite is partially albitized (not visible in photo). Sporadic pockets in the core contained green elbaite and colorless topaz. Two excavated pockets are visible in the core, in the central and left areas of the photograph. The thin, dark gray mass below the left pocket is an aplite body, which is 2 cm thick and visible for ~10 cm in horizontal direction. Light gray mottling is caused by a thin layer of dust on the pegmatite surface.

by flaky aggregates of fine-grained (0.1 mm in diameter) muscovite and by later Mn-Fe oxides.

COLORED TOURMALINE MINERALIZATION

Crystals of green-pink tourmaline have been mined from pockets in the core zone of pegmatite sills at Stak Nala. The economic production comes from a 1.3-m-thick sill at the main mine (Fig. 3, location 1), and minor production also has come from the 3- to 4-m-thick sill at the south mine. At both pegmatites, production is from the thickest part of the sill. Black and green tourmaline are common in pockets from other pegmatites at Stak Nala and from the northern and southern parts of the main mine pegmatite.

At the main mine, the productive zone trends west-northwest along a broad, open, antiformal structure that lies south of and parallels the strike of a

pre-existing *F2* flexural shear in the gneissic wallrock (Fig. 3, location 1). The productive pockets occur where the sill is thicker (>1 m thick; Fig. 8), and within 20 m south of the east-southeast-trending flexural shear, into which the sill splays and pinches. Both to the south and west of the productive zone, the pegmatite is less than 1 m thick, and miners reported fewer pockets and no pink elbaite. To the north of the flexural shear is a probably correlative pegmatite that has had minor production (Fig. 3, location 2); this pegmatite is up to 1.6 m thick, and its zone of maximum thickness trends nearly northwest (Fig. 3, location 2; Fig. 8). Although this pegmatite is in the correct position to be the continuation of the main sill, correlation is uncertain because 5 m of surficial debris covers relations between the pegmatite bodies.

At both the main mine and the south mine, pockets are distributed sporadically through the core zone, but

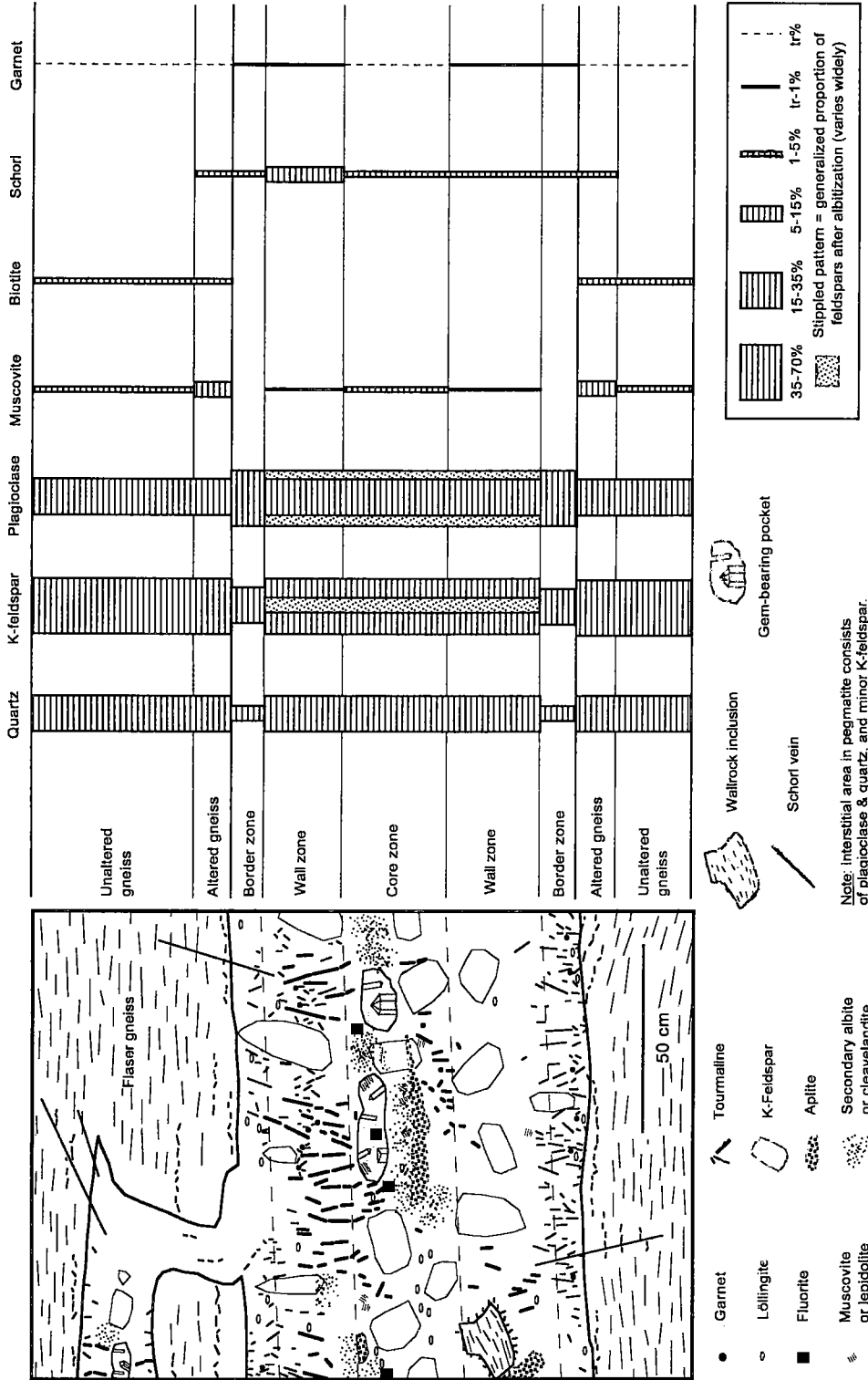


Fig. 11. Internal zonation and modal composition of pegmatite, main mine area. Schematically shown is a small dike linking the main sill to a smaller overlying sill. Modal abundance of quartz, K-feldspar, and plagioclase in the pegmatite core zone varies widely; generalized proportions are shown.

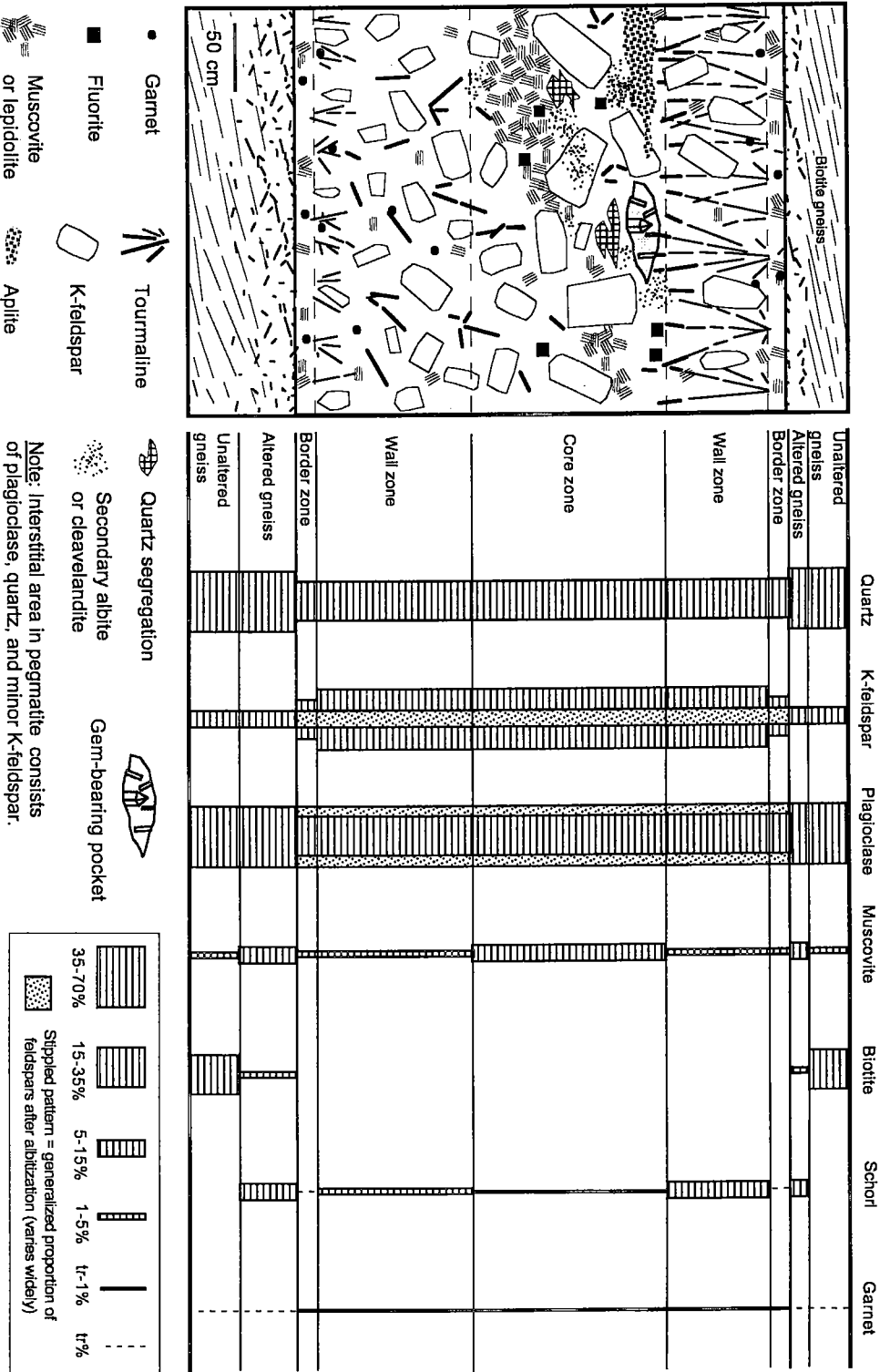


Fig. 12. Internal zonation and modal composition of pegmatite, south mine area. Modal abundance of quartz, K-feldspar, and plagioclase in the pegmatite varies widely, especially in the core zone, generalized proportions are shown.

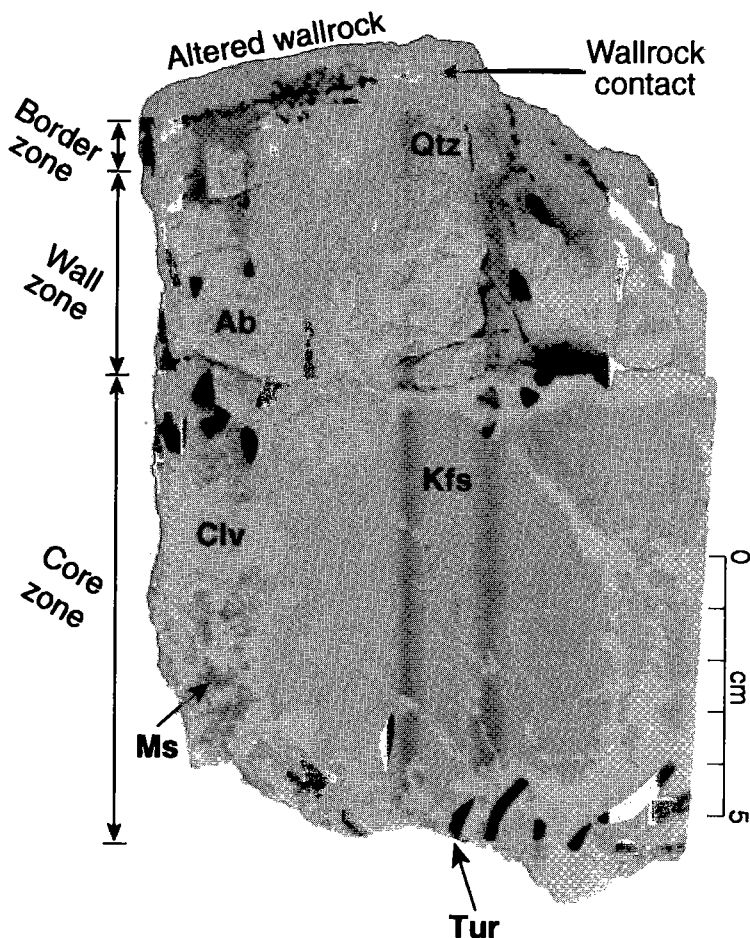


FIG. 13. Photograph of partially albitized pegmatite from the hanging wall and core zone of a 20-cm-thick sill, main mine area. Relict K-feldspar (stained) in the pegmatite core is rimmed and veined by "cleavelandite" (Clv) that locally contains muscovite. Feldspar in wall and border zones is completely replaced by albite.

are most common in the upper part, near the contact with the wall zone. The pockets form oblate to highly irregularly shaped cavities. These are either isolated or interconnected with one another. Individual pockets range in size from small vugs (~1 cm) to large cavities measuring up to 0.5 m in height and 3 m horizontally. The pockets and associated "cleavelandite"-rich replacement zones contain the largest variety of minerals in the pegmatite (Table 4). The most abundant pocket minerals are albite, quartz, K-feldspar, elbaite, muscovite or lepidolite, and fluorite; these project into the pockets from the surrounding pegmatite and also form broken crystals that litter the floor of the pockets. Albite forms wedge-shaped crystals up to several centimeters long, or distinctive "cleavelandite" jackets around elbaite and

quartz crystals (e.g., Fig. 18 in Kazmi *et al.* 1985). Perthitic K-feldspar (maximum microcline) forms blocky crystals (up to 8 cm) that are commonly etched, resulting in a cellular surface texture; a transparent overgrowth of orthoclase over perthite is commonly developed. Well-formed, transparent quartz crystals up to 10 cm in length are commonly intergrown with wedge-shaped albite and "cleavelandite." Some faces on quartz crystals are frosted or pitted; these faces may be overgrown by a thin (<1 mm) layer of clear quartz. Topaz forms transparent colorless to pale brown crystals; according to the miners, single crystals may weigh up to 1 kg. Pseudo-hexagonal crystals of white muscovite or lavender lepidolite (average 0.5 cm) form scattered overgrowths on albite and K-feldspar.

Hambergite occurs rarely; Richards (1996) documented two unusual crystal habits of hambergite on a specimen reportedly from Stak Nala.

Elbaite crystals range from 1 to 10 cm long and up to 1.5 cm in diameter (on average, 4 cm long, 1 cm in diameter), and are typically jacketed by "cleavelandite." They are color-zoned perpendicular to the *c* axis, with black or dark green bases that grade into transparent lighter green flat terminations. Pale pink, colorless, or pale blue elbaite commonly forms an overgrowth on the crystal terminations and on the ends of crystals that were broken off the pocket walls. Therefore, the crystals of elbaite commonly have natural terminations on both ends: on the end that was broken, a pink overgrowth forms a pyramidal termination; on the other end, the flat termination is overgrown by colorless or pale blue elbaite (*e.g.*, Fig. 17 in Kazmi *et al.* 1985). Foord (1976) described such overgrowths in detail from a miarolitic pegmatite–aplite in southern California. Some tourmaline crystals from Stak Nala (especially from the south mine) display concentric zoning, with a black core surrounded by a dark green, pale pink, or colorless rim. Tourmaline crystals within the same pocket may exhibit widely variable proportions of the zones, but have the same pattern of color zonation.

Partially coating all minerals in most pockets is an aggregate of fine-grained (0.0X to 0.X mm) muscovite or borian muscovite that forms a hard granular to porcelaneous layer typically <1 mm thick. A commonly bulbous appearance of these mica aggregates results from drusy overgrowth on microcrystals of elbaite or quartz present on the faces of previously crystallized minerals. Quartz underlying the drusy micas is typically pitted or corroded. Borian muscovite contains 2.0 to 4.5 wt% B₂O₃ in samples from the main mine; no B was detected in drusy mica from the south mine.

WALLROCK ALTERATION

Alteration of the gneissic wallrock adjacent to the pegmatites is characterized by conversion of biotite to muscovite, introduction of disseminated schorl and local veining by schorl, and local alteration to an albite-dominant assemblage. All types of gneiss experience the same kinds of alteration, but to differing degrees: the altered flaser granite gneiss at the main mine area contains less schorl than the biotite-rich granodiorite gneiss at the south mine. Inclusions and slivers of wallrock within pegmatites have experienced the greatest degree of alteration, characterized by up to 50 vol.% schorl with local topaz. Sparse spessartine–almandine is locally present in the wallrock inclusions within 5 mm of the pegmatite contacts.

Biotite has been converted to muscovite within 3 to 7 cm (but locally >15 cm) of the pegmatite contacts, causing a bleached appearance to the altered gneiss (Fig. 9). The bleached zones are equally developed

TABLE 5. BULK COMPOSITION OF ALTERED FLASER GNEISS ADJACENT TO PEGMATITE, STAK NALA MAIN MINE AREA

Dist. to peg.	0-5 cm	25-28 cm	0-10 cm	10-18 cm
Location	HW	HW	FW	FW
Alteration*	bl, Tur	±bl, ±Tur	bl, ±Tur	±bl, ±Tur
Spec. grav.	2.64	2.63	2.66	2.66
SiO ₂ (wt%)	72.69	70.95	72.16	72.05
TiO ₂	0.29	0.19	0.35	0.24
Al ₂ O ₃	14.74	15.63	14.77	15.18
Fe ₂ O ₃	1.95	1.31	2.28	1.57
MnO	0.04	0.02	0.04	0.03
MgO	0.44	0.30	0.51	0.36
CaO	0.85	0.94	1.08	0.99
Na ₂ O	2.43	2.96	2.85	2.64
K ₂ O	5.60	7.04	4.97	6.01
P ₂ O ₅	0.19	0.19	0.19	0.16
LOI	0.66	0.50	0.81	0.81
Total	99.87	100.03	100.01	100.04
V (ppm)	394	<7	<7	<7
Cr	<7	4	8	<7
Ni	4	1	3	1
Cu	42	5	<1	1
Pb	38	45	31	37
Zn	70	41	80	52
Ga	20	18	21	19
As	81	29	92	58
F	970	295	995	365
B	72	30	51	50
Be	10	12	8	5
Li	315	110	257	109
Rb	441	325	386	331
Cs	36	60	28	34
Sr	81	103	85	98
Ba	<24	440	290	348
Ce	22	53	84	39
Nd	<30	<30	35	<30
Y	4	3	6	3
Zr	117	78	140	92
Nb	17	10	19	12
Th	<10	13	28	20

* bl: bleached biotite, Tur: tourmalinized

Sc & U are below detection limit (7 ppm).

Specific gravity of unaltered flaser gneiss is 2.61.

along the hanging-wall and footwall contacts, and contain quartz – sodic plagioclase – tourmaline – muscovite ± K-feldspar ± garnet assemblages. Both biotite and muscovite in the original gneiss are altered

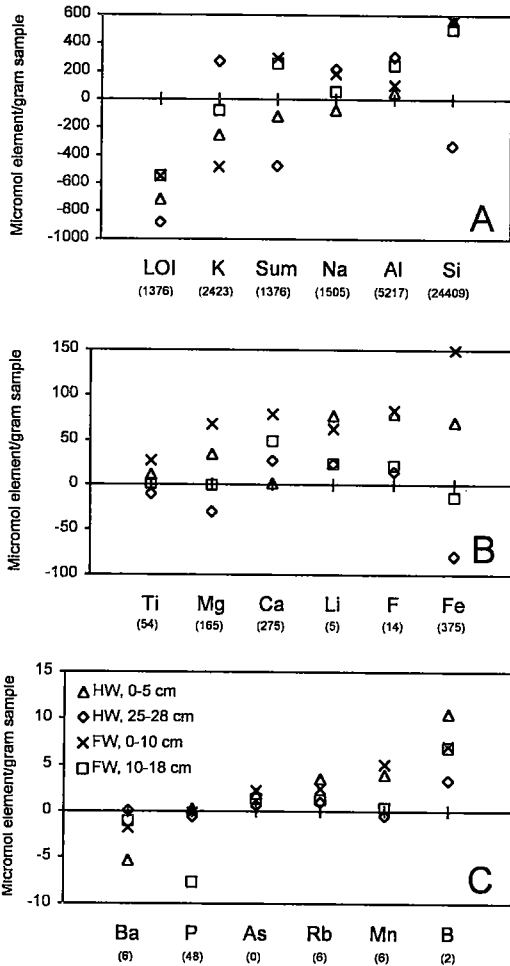


FIG. 14. Gains and losses of selected (A) major, (B) minor, and (C) trace elements in altered flaser granite gneiss adjacent to pegmatite, main mine area. Values are calculated by method of Kretz *et al.* 1989 (after Gresens 1967), in units of micromol of element per gram of sample. The total amount of each element in unaltered gneiss is indicated in parentheses under each element. Visual modifications (conversion of biotite to muscovite and addition of schorl) are generally restricted to proximal samples (Δ and \times). Anomalous behavior of K, Si, Fe, and P in distal samples (\diamond and \square) probably results from pre-metasomatic chemical variations in the gneiss layers.

to a distinctive, bronze-colored muscovite with a coarser grain-size near the pegmatite contact. Scattered relict coarse-grained pods of biotite typically retain their black color within the selvage. Small amounts (<10%) of quartz and traces of apatite are locally added to the bleached zone.

Metasomatic schorl forms 2- to 5-mm-long disseminated prisms within pervasively bleached wallrock, and along locally bleached foliation up to 50 cm from the pegmatite contact. Along the pegmatite contact, randomly oriented crystals of schorl point bidirectionally toward the pegmatite and wallrock. Microscopic examination of the schorl revealed abundant quartz \pm plagioclase inclusions, forming a sieve-like texture. Schorl content is proportional to the original content of mafic minerals in the gneiss, up to 40% by volume.

In the pocket-rich area of the main mine (Fig. 3, location 1), conspicuous schorl-bearing veinlets emanate from the border zone or outer part of the wall zone and cross-cut the wallrock (Fig. 9). The veinlets appear to be more abundant in the hanging-wall gneiss, and typically extend over 1 m from the pegmatite contact. The veinlets are ~1 mm wide and consist of very fine-grained schorl. Less common are thicker (~1 cm) veins containing schorl, quartz, sodic plagioclase, and rare K-feldspar. Both types of veins have narrow bleached selvages that are enriched in quartz and lack biotite and muscovite.

Significant metasomatic albite in wallrock was noted only at the south mine, adjacent to pegmatite that is pervasively albitized. K-feldspar augen within the biotite granodiorite gneiss are converted to untwinned albite and subordinate sericite. Albitization is accompanied locally by late-stage tourmalinization, that is easily differentiated from early-formed tourmalinization described above, on the basis of texture and composition. The late-stage tourmalinization is characterized by elbaite overgrowths and replacements of schorl, both in the pegmatite and in the wallrock within 1 cm of the contact. Rare veinlets of olive green elbaite locally infiltrated the hanging-wall contact.

Whole-rock compositions of metasomatized flaser granite gneiss record addition of Si, Li, F, and B, and removal of H₂O, K, Ba, and possibly Al (Table 5, Fig. 14). Traces of Mn, Rb, Nb, As, Zn, and Zr also were added; Ca, Fe, and Na are locally enriched or depleted in the metasomatized wallrock (depository data).

CHEMICAL COMPOSITION OF PEGMATITE AND APLITE

The bulk composition of the pegmatite is difficult to measure because of the coarse grain-size and inhomogeneous distribution of mineral phases. In order to approximate the bulk composition, a 6-cm-thick linking dike (*e.g.*, Fig. 9) and a 20-cm-thick partially albitized, pocket-bearing pegmatite were analyzed (Table 6). The linking dike consists of evenly distributed, medium-grained (<1 cm) K-feldspar, sodic plagioclase, and quartz, with needles of schorl concentrated in the center and oriented subperpendicular to dike contacts. The linking dike cross-cuts biotite granodiorite gneiss wallrock, which is altered within 20 cm to tourmaline- and muscovite-rich assemblages. The partially albitized pegmatite contains a well-

TABLE 6. BULK COMPOSITION OF PEGMATITE FEEDER DIKE, ALBITIZED PEGMATITE, AND APLITE, STAK NALA

Rock type	pegmatite	pegmatite	aplite
Description	linking dike	albitized	in core zone
Thickness	6 cm	20 cm	5 cm
Mine area	South	Main	Main
Modal data (vol%)*			
K-feldspar	40	20	0
Plagioclase	40	60	63
Quartz	15	5	10
Tourmaline	5	10	5
Other		Ms - 5 Grt - tr	Fl - 2
SiO ₂ (wt%)	72.13	67.94	71.09
TiO ₂	0.02	0.02	0.03
Al ₂ O ₃	15.01	19.07	17.28
Fe ₂ O ₃	0.34	0.86	1.66
MnO	0.02	0.18	0.23
MgO	0.06	0.02	<0.002
CaO	0.66	0.59	1.14
Na ₂ O	3.16	6.15	7.64
K ₂ O	8.09	4.33	0.19
P ₂ O ₅	0.07	0.02	0.03
LOI	1.12	0.86	0.49
Total	100.67	100.04	99.77
Cr (ppm)	<7	<7	20
Ni	2	2	<1
Pb	72	67	25
Zn	16	68	141
Ga	19	50	53
As	20	23	597
F	730	960	4800
B	127	360	512
Be	5	3	3
Li	48	58	30
Rb	606	672	18
Cs	43	<1	<1
Sr	77	11	5
Ba	314	50	<24
Y	1	10	46
Zr	7	5	20
Nb	10	91	42
U	<7	<7	7

* Modal data is estimated visually from hand samples and thin sections.

Elements below detection limit: Ce & Nd (<30 ppm), Th (<10 ppm), Sc & V (<7 ppm), Cu (<1 ppm).

developed internal mineralogical zonation, with a blocky K-feldspar core flanked by finer-grained (1 to 4 cm) assemblages (Fig. 13). The relict K-feldspar in the core is rimmed and veined by assemblages of "cleavelandite" and muscovite. The feldspar in the remainder of the sample is pervasively altered to albite, and the adjacent wallrock of flaser granite gneiss is bleached and contains scattered crystals of schorl.

Some generalizations about elemental gains and losses as a result of albitization can be made from comparison of the linking dike and the albitized pegmatite. However, direct comparisons are unreasonable because the samples are from separate mine areas and have contrasting degrees of internal evolution. Significant amounts of B, F, Li and Rb have likely been lost to the wallrocks, and therefore are not compared. The whole-rock compositions and petrography suggest that albitization has added Al and Nb (in addition to Na), and removed K, Si, and Ba (Table 6).

A sample of aplite also was analyzed for comparison with the pegmatite. The analyzed sample consists of fine-grained (~0.01 mm) subequigranular albite, schorl, and quartz, with local fluorite. Compared to the pegmatite-linking dike, the aplite contains more Na, Al, Fe, Ca, F, As, Zn, Nb, and Y, and less K, Rb, Ba, and Sr. These chemical trends are similar to those measured in the albitized pegmatite. However, the aplite contains distinctly higher levels of F and As, and much lower K, Rb, and Mg/(Mg + Fe) than both pegmatite samples.

MINERAL COMPOSITIONS IN PEGMATITE AND WALLROCK

Plagioclase, garnet, mica, and tourmaline were analyzed with an electron microprobe to evaluate the extent of compositional zoning in individual mineral grains, as well as chemical variation in the pegmatite zones and in the altered wallrock at varying distance from the pegmatite. Samples were selected from the thickest (1.6 m) pegmatite in the main mine area (Fig. 3, location 2). In the area sampled, the K-feldspar is partially albitized in the hanging-wall and core zones, and the core zone contains scattered pockets (up to 30 cm long) lined with crystals of albite, quartz, K-feldspar, muscovite, green elbaite, colorless topaz, and traces of fluorite and apatite. An inclusion of flaser granite gneiss wallrock is present in the lower wall zone. Specimens were collected from each zone of the pegmatite and from the altered wallrock within 25 cm of the hanging-wall and footwall contacts. Limited samples were collected from the south mine: the border zone from the hanging wall and footwall, and altered wallrock within 50 cm of the contacts. Compositions of Nb-Ta oxides, beryl, topaz, and Mn-Fe oxides reported below pertain to scattered samples in both mine areas and are not spatially correlated with the internal zonation of the pegmatite bodies.

Electron-microprobe data are presented schematically according to pegmatite zone and distance

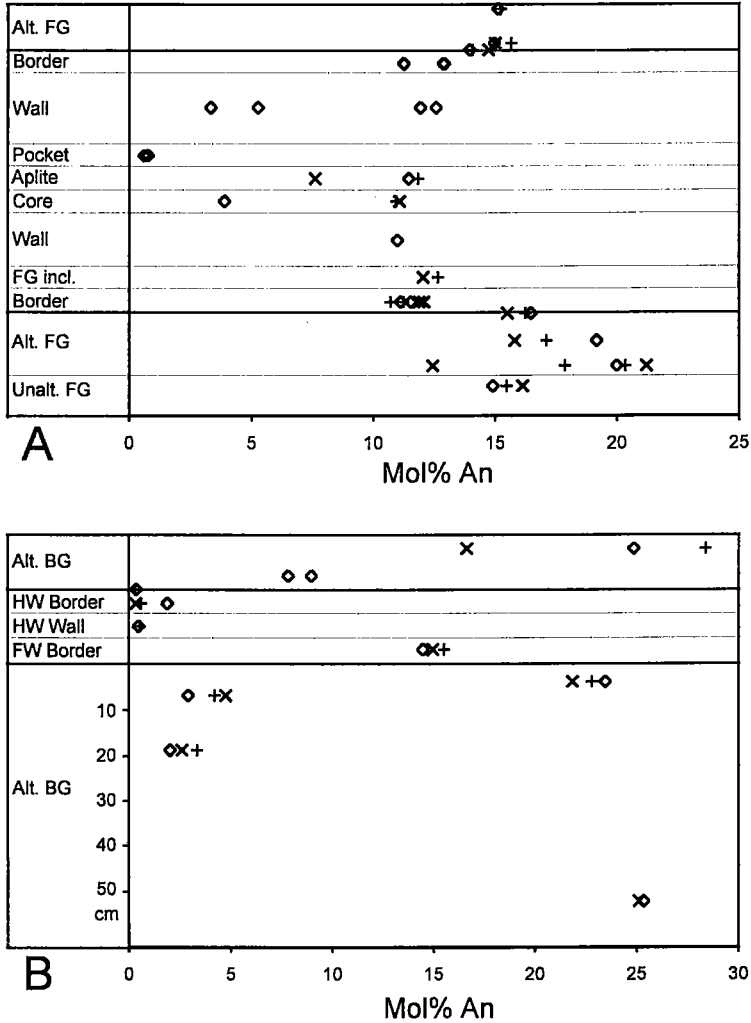


FIG. 15. Plagioclase composition in pegmatite and wallrock; (A) main mine area, and (B) south mine area. Symbols: +: core, \diamond : middle, and \times : rim of individual crystals; BG: biotite granodiorite gneiss, FG: flaser granite gneiss, FW: footwall, HW: hanging wall, incl.: inclusion.

from the pegmatite contacts in Figures 15 to 19. The diagrams show only samples collected from a single location, in order to facilitate comparison of chemical trends between zones. Pocket minerals are an exception to this, however, because these minerals were previously removed during mining and therefore could not be obtained directly from the pockets at the location sampled. Compositions are differentiated from core to rim for plagioclase, garnet, and tourmaline, but not for the micas, which are apparently unzoned. Although

relatively few determinations of mineral composition were made on each mineral from each pegmatite zone, several compositional trends can be recognized.

Plagioclase

Plagioclase from the main sill is oligoclase ($\sim An_{12}$), except for local albite (An_4) in the core zone and upper wall zone (Fig. 15A). Plagioclase within the aplite shows slight normal zoning from core to rim: An_{12} to

An₈. "Cleavelandite" from a pegmatite pocket is pure albite, An_{0.6} to An_{0.8}. Plagioclase composition in both unaltered and metasomatized flaser granite gneiss wallrock is oligoclase (~An₁₅ to An₂₂). Slight Na-enrichment was measured in wallrock plagioclase near the pegmatite contact, especially within the footwall.

Plagioclase in the upper border zone of the south mine pegmatite is albite (An₃ to An₅), in contrast to the oligoclase composition (An₁₅) of the footwall border zone (Fig. 15B). The measured composition of plagioclase in the biotite granodiorite gneiss is ~An₃₀, and in metasomatized gneiss, it ranges from oligoclase (An₂₉) to albite (An₂) with a sporadic distribution. The incidence of albite in the pegmatite and the wallrock coincides with zones of metasomatic albitization, as indicated by the petrographic evidence stated above.

Garnet

Spessartine–almandine is a minor but ubiquitous mineral in the pegmatites, whereas almandine is found in the host gneisses. Within pegmatite, garnet is most abundant (up to 1 vol.%) in the border and wall zones, where it forms scattered red-brown subhedral crystals 1 to 3 mm in diameter that are commonly associated with schorl. Garnet is locally abundant in aplite as fine-grained (0.01 to 0.5 mm) subhedral crystals. It is rare in the core zone, and was not observed in the pockets.

Garnet composition was measured in the core and hanging wall of the main pegmatite, and in the flaser granite gneiss wallrock (Table 7). In the pegmatite, compositions range from Sps₇₄Alm₂₁ in the wall zone to Sps₄₈Alm₄₇ in the core zone; a minor grossular component also is present (Grs₃ to Grs₇; Table 7, Fig. 16). Mn and Fe show perfect inverse correlation in both individual zoned grains and between the pegmatite zones. The values of Mn/(Mn + Fe) generally overlap in all of the pegmatite zones, with slightly higher values measured in the wall zone and lower values in the core zone. Conversely, Mn enrichment is noted from core to rim of individual crystals. Both of these trends are the opposite of compositional trends typically observed in garnet at other granitic pegmatites (e.g., Cerný & Hawthorne 1982). Mg is virtually absent, and the level of Ca is higher than in most other examples of spessartine-rich garnet from granitic pegmatites (e.g., Baldwin & von Knorring 1983, Foord & Kleck 1993, Nakano & Ishikawa 1997).

The garnet from the wallrock is almandine-rich, with less than 13 mol.% each of spessartine, grossular, and pyrope components. In comparison with the pegmatite, garnet from the gneiss thus contains much higher Mg, Ca, and Fe, and less Mn. Within an inclusion of metasomatized flaser granite gneiss wallrock in pegmatite, garnet shows strong rimward enrichment in Mn and depletion in Mg, Ca, and Fe.

Micas

Biotite and muscovite are abundant in the wallrock gneisses, except for the bleached metasomatized zone adjacent to the pegmatites, where relict metamorphic biotite is sparse. Biotite and muscovite compositions were measured in unaltered and metasomatized flaser granite gneiss at the main mine, from the pegmatite contact outward to 25 cm. At the south mine, muscovite compositions were measured in pervasively altered biotite granodiorite gneiss up to 50 cm from the pegmatite contact; no biotite was found in these samples.

The biotite's composition in the unaltered flaser granite gneiss is dominated by the annite component (Table 8). In metasomatized flaser granite gneiss, relict biotite is enriched in Mn, F, and Rb, and depleted in Mg (Fig. 17). F and Rb are strongly correlated and show enrichment up to 25 cm from the contacts, whereas Mn is enriched and Mg is depleted within a few centimeters of the contacts.

Muscovite in altered flaser granite gneiss shows enrichment in Mn and F, but Rb shows little change as the pegmatite contact is approached. Fe is enriched in bronze muscovite along the contacts and extending 3 cm outward, corresponding to the zone of biotite bleaching (Table 8, Fig. 18). In pervasively altered biotite granodiorite gneiss adjacent to the south pegmatite, no biotite was found, and all the muscovite is bronze in color and Fe-rich (Table 8). The FeO content ranges from 3.1 to 15.6 wt%, and the sum of octahedrally coordinated cations ranges from 3.75 to 4.67; these micas are here referred to as muscovite, since the Fe contents and the total amount of octahedrally coordinated cations are too low for biotite. Near the pegmatite contact, this muscovite shows the greatest range in Fe contents; in distal samples, the Fe content is confined to a narrow range (~6 to 7 wt% FeO). The "homogenized" composition of the distal samples may result from their location within a dense network of schorl veins, resulting in more pervasive alteration. The muscovite in the altered gneiss at the south pegmatite is enriched in F (up to 4.3 wt%), and contains elevated concentrations of Rb (up to 0.3 wt%). Low totals of some electron-microprobe analyses suggest that Li also may be present.

In pegmatite, muscovite is sparse in the wall zone and nonexistent in the aplite or the border zone at the main mine. Muscovite and lepidolite are common locally in the core zone, especially near pockets and in replacement zones. Compared to muscovite in the wallrock, muscovite in the pegmatite contains more Al, Na, Mn, F, and Rb, and less Mg and Ti (Table 9, Fig. 18). Lepidolite shows extreme F enrichment (up to 9.5 wt%), and high levels of Rb and Cs (up to 0.94 and 0.79 wt% oxide, respectively). The lavender color of the lepidolite appears to correlate with enriched Mn combined with very low Fe contents.

TABLE 7. REPRESENTATIVE COMPOSITION (ELECTRON MICROPROBE) OF GARNET FROM PEGMATITE AND FLASER GNEISS, STAK NALA MAIN MINE

Description* Position	unaltered FG		UWZ		aplite		core zone	
	core	rim	core	rim	core	rim	core	rim
SiO ₂ (wt%)	38.40	37.52	36.88	37.01	36.09	36.77	36.86	37.32
TiO ₂	0.00	0.00	0.02	0.02	0.10	0.05	0.01	0.01
Al ₂ O ₃	21.91	21.72	20.72	20.29	20.69	21.09	20.28	20.64
FeO	32.10	30.79	13.22	9.47	18.55	13.04	20.49	18.04
MnO	0.96	4.23	27.36	30.99	22.21	27.50	20.20	22.73
MgO	3.11	1.74	0.01	0.00	0.03	0.00	0.02	0.00
CaO	3.84	3.64	1.72	1.72	2.28	1.68	1.58	1.71
Total	100.32	99.64	99.93	99.50	99.95	100.13	99.44	100.45
Cations (24 oxygens)								
Si	6.064	6.032	6.041	6.086	5.944	6.007	6.077	6.079
Al	0.000	0.000	0.000	0.000	0.056	0.000	0.000	0.000
Tet. sum	6.064	6.032	6.041	6.086	6.000	6.007	6.077	6.079
Al	4.080	4.117	4.001	3.934	3.961	4.063	3.943	3.964
Fe	0.000	0.000	0.000	0.063	0.026	0.000	0.056	0.034
Ti	0.001	0.000	0.003	0.002	0.013	0.006	0.001	0.002
Y sum	4.080	4.117	4.004	4.000	4.000	4.069	4.000	4.000
Mg	0.733	0.418	0.003	0.001	0.007	0.001	0.005	0.001
Fe	4.239	4.140	1.811	1.239	2.528	1.781	2.769	2.424
Mn	0.128	0.577	3.795	4.317	3.097	3.805	2.820	3.135
Ca	0.650	0.627	0.302	0.303	0.403	0.293	0.279	0.298
X sum	5.751	5.761	5.911	5.859	6.035	5.880	5.873	5.858
Mg/(Mg+Fe)	0.15	0.09	0.00	0.00	0.00	0.00	0.00	0.00
Mn/(Mn+Fe)	0.03	0.12	0.68	0.78	0.55	0.68	0.50	0.56
sps	2.2	10.0	64.2	73.7	51.3	64.7	48.0	53.5
alm	73.7	71.9	30.6	21.1	41.9	30.3	47.1	41.4
grs	11.3	10.9	5.1	3.6	6.0	5.0	3.3	4.2
adr	0.0	0.0	0.0	1.6	0.7	0.0	1.4	0.8
prp	12.7	7.3	0.1	0.0	0.1	0.0	0.1	0.0

* FG: flaser gneiss wallrock, UWZ: upper wall zone

O.S.U. Cameca SX-50 electron microprobe conditions: wavelength dispersive spectrometers; 15 kV accelerating voltage; 30 nA sample current; 3-5 μ m beam diameter; $\phi(\rho Z)$ data reduction (PAP: Pouchou & Pichoir 1985); standardization at beginning and end for drift correction; detection limits 0.03-0.09 wt% oxide; counting errors (1s) range from ± 0.05 to ± 0.2 wt% oxide. All Fe as FeO.

Compared to muscovite, the borian muscovite coating the pocket minerals is depleted in Fe, Mn, and Na, and is enriched in Rb (Table 9, Fig. 18). The composition of the borian muscovite is similar to boromuscovite from the Little 3 pegmatite in southern California (*e.g.*, Foord *et al.* 1991b) and from a pegmatite in Rečice, Czechoslovakia (*e.g.*, Liang *et al.* 1995). Borian muscovite from Stak Nala shows a positive correlation of B with F, ranging from 2.3 to 4.5 wt% B₂O₃ and 0.8 to 1.6 wt% F. The highest B contents were measured in finer-grained (0.0X mm) samples coating elbaite from the main mine.

Tourmaline

The composition of tourmaline was determined in each zone of the main mine pegmatite and in the adjacent metasomatized wallrock up to 25 cm from the pegmatite contacts; scattered samples from the south mine also were analyzed (Table 10). At the main mine, schorl in the wallrock contains more Mg and Ti, and less Al and Fe, than schorl in the pegmatite (Table 10, Fig. 19). Also, schorl in the wallrock contains slightly more Ca, and slightly less Mn and F, than schorl in the pegmatite. Approaching the pegmatite

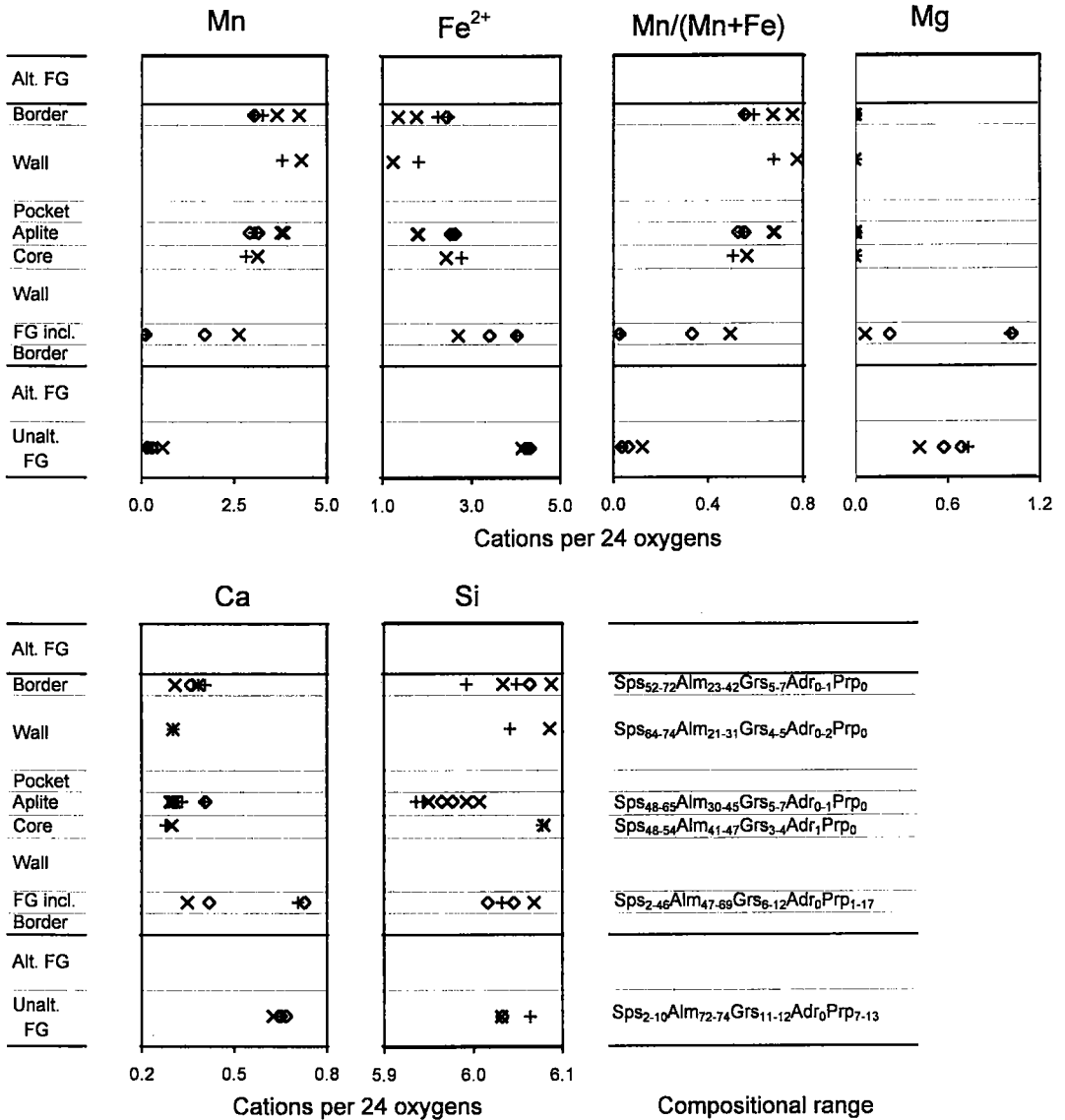


Fig. 16. Garnet composition in pegmatite and flaser granite gneiss, main mine area; symbols as in Figure 15. Fe²⁺ is calculated by difference.

contact, schorl in the wallrock shows progressive enrichment in F, Mn, and Fe, and depletion in Mg and Ti. Within the pegmatite, Mg and Ti are likely derived from the adjacent gneiss, and show enrichment in schorl near the footwall contact and in the lower wall zone near a wallrock inclusion. Otherwise, schorl in the pegmatite shows a fairly constant composition: F is gradually enriched from border to core zone, and the core zone contains slightly more Mn and Al, and less Fe.

Individual crystals of schorl show few consistent compositional trends from core to rim (Fig. 19). Schorl in the altered flaser granite gneiss is unzoned except for

variable Ti. In altered biotite granodiorite gneiss, schorl is distinctly zoned; the level of Fe (and minor Mn) increases, and that of Mg (and minor Si and Ca) decreases from core to rim. Schorl in the pegmatite is not markedly zoned, and shows no systematic correlation of composition from core to rim.

Compared to schorl, elbaite from the pegmatite pockets and hydrothermal replacements is distinctly zoned and contains much less Fe, and more Al, Si, and Li (Fig. 19, Tables 10, 11). Mn, F, and Na/(Na + Ca) are widely variable, e.g., Mn varies from 6.6 wt% MnO to below detection limit (0.07 wt%) in a single crystal of

TABLE 8. AVERAGE COMPOSITION (ELECTRON MICROPROBE) OF MUSCOVITE AND BIOTITE FROM UNALTERED GNEISS AND ALTERED GNEISS ADJACENT TO PEGMATITE, STAK NALA

Mineral Alteration ¹ Location ¹	Main Mine: Flaser Gneiss										South Mine: Biotite Gneiss									
	Ms		Ms		Ms		Ms		Bt		Bt		Bt		Ms		Ms		Ms	
	Tur, bl FW incl.	Tur, bl FW 1cm	±Tur, ±bl FW 14cm	±Tur, ±bl FW 25cm	unaltered FW 1cm	Tur, bl FW 14cm	±Tur, ±bl FW 14cm	±Tur, ±bl FW 25cm	unaltered FW 25cm	Tur, Bl, ±Ab FW 1cm	Tur, Bl, ±Ab FW 1cm	Tur, Bl, ±Ab FW 17cm	Tur, Bl, ±Ab FW 17cm	Tur, Bl, ±Ab FW 17cm	Tur, Bl, ±Ab FW 50cm					
SiO ₂ (wt%)	48.22	47.08	48.93	48.79	48.27	36.53	36.38	36.76	37.07	47.07	39.36	45.84	44.14	47.05						
TiO ₂	0.07	0.67	1.50	1.32	1.34	3.05	3.61	3.12	2.94	0.98	2.58	1.50	1.87	1.20						
Al ₂ O ₃	34.71	30.12	33.24	33.82	32.80	18.38	18.03	18.47	18.56	28.05	18.78	25.95	19.87	24.89						
FeO	2.08	3.60	2.02	1.81	2.10	22.23	22.19	21.95	21.37	3.67	15.61	4.98	10.41	6.25						
MnO	0.11	0.10	0.00	0.00	0.02	0.64	0.32	0.38	0.32	0.10	0.64	0.24	0.37	0.23						
MgO	0.40	1.28	1.12	1.02	0.96	3.42	5.50	5.71	5.28	2.78	6.45	3.95	6.09	4.02						
CaO	0.00	0.00	0.01	0.00	0.00	0.00	0.01	0.01	0.15	0.01	0.00	0.00	0.01	0.00						
Na ₂ O	0.49	0.26	0.36	0.36	0.40	0.11	0.09	0.06	0.50	0.24	0.04	0.16	0.14	0.20						
K ₂ O	10.79	11.04	10.76	10.73	10.88	9.75	9.57	9.60	9.35	10.93	10.36	11.05	10.58	10.67						
BaO	0.00	0.01	0.05	0.06	0.01	0.04	0.04	0.03	0.00	0.07	0.02	0.09	0.01	0.03						
Rb ₂ O	0.12	0.10	0.05	0.07	0.06	0.14	0.09	0.08	0.08	0.22	0.22	0.23	0.29	0.22						
Cs ₂ O	0.01	0.00	0.00	0.00	0.00	0.05	0.02	0.01	0.02	0.03	0.06	0.17	0.24	0.15						
F	0.83	1.62	0.73	0.45	0.30	2.55	1.34	0.90	0.59	2.25	3.08	2.65	4.23	3.09						
Cl	0.02	0.00	0.01	0.01	0.01	0.01	0.06	0.10	0.13	0.01	0.02	0.00	0.01	0.01						
Sum	97.85	95.90	98.79	98.43	97.16	96.91	97.25	97.18	96.36	96.41	97.22	96.83	98.26	97.98						
-O=F, Cl +H ₂ O)*	4.21	3.68	4.30	4.13	4.42	2.74	3.32	3.52	3.64	3.38	2.64	3.15	2.30	2.98						
Total	101.71	98.90	102.78	102.67	101.46	98.57	99.99	100.30	99.73	98.84	98.56	98.86	98.78	99.67						
Cations (22 O equivalents)																				
Si	6.274	6.341	6.307	6.301	6.336	5.550	5.500	5.547	5.619	6.338	5.748	6.239	6.143	6.338						
Al	1.726	1.659	1.693	1.699	1.664	2.450	2.500	2.453	2.381	1.662	2.252	1.761	1.857	1.662						
Tot. sum	8.000	8.000	8.000	8.000	8.000	8.000	8.000	8.000	8.000	8.000	8.000	8.000	8.000	8.000						
Al	3.598	3.123	3.358	3.450	3.412	0.842	0.714	0.833	0.939	2.789	0.981	2.403	1.404	2.290						
Mg	0.078	0.258	0.215	0.196	0.187	0.774	1.240	1.285	1.194	0.559	1.405	0.802	1.264	0.807						
Fe	0.227	0.406	0.218	0.196	0.230	2.824	2.806	2.769	2.712	0.414	1.906	0.567	1.211	0.704						
Ti	0.006	0.068	0.146	0.129	0.132	0.349	0.410	0.354	0.335	0.099	0.286	0.153	0.196	0.122						
Mn	0.012	0.012	0.000	0.000	0.003	0.082	0.041	0.049	0.041	0.012	0.079	0.028	0.044	0.026						
Oct. sum	3.922	3.867	3.936	3.970	3.964	4.870	5.211	5.289	5.221	3.872	4.655	3.954	4.119	3.948						
Ca	0.000	0.000	0.002	0.000	0.000	0.000	0.001	0.002	0.023	0.001	0.000	0.000	0.001	0.001						
Na	0.124	0.069	0.090	0.089	0.102	0.032	0.026	0.018	0.146	0.062	0.010	0.042	0.037	0.051						
K	1.791	1.897	1.770	1.767	1.822	1.889	1.845	1.847	1.811	1.877	1.930	1.918	1.878	1.833						
Ba	0.000	0.001	0.003	0.003	0.000	0.003	0.003	0.002	0.000	0.004	0.001	0.005	0.000	0.001						
Rb	0.010	0.008	0.004	0.006	0.005	0.014	0.008	0.008	0.008	0.019	0.021	0.020	0.026	0.019						
Cs	0.000	0.000	0.000	0.000	0.000	0.003	0.001	0.001	0.001	0.002	0.004	0.010	0.014	0.008						
Int. sum	1.926	1.975	1.868	1.865	1.930	1.941	1.885	1.877	1.989	1.966	1.995	1.958	1.913	1.913						
Sum cations	13.847	13.842	13.804	13.835	13.895	14.811	15.096	15.167	15.210	13.837	14.621	13.949	14.077	13.861						
F	0.342	0.689	0.298	0.183	0.125	1.224	0.638	0.428	0.283	0.960	1.422	1.141	1.861	1.316						
Cl	0.004	0.001	0.001	0.002	0.003	0.003	0.017	0.025	0.033	0.003	0.004	0.001	0.002	0.002						
OH*	3.654	3.310	3.701	3.815	3.872	2.773	3.345	3.547	3.684	3.038	2.574	2.858	2.137	2.681						
Mg/(Mg+Fe)	0.25	0.38	0.50	0.50	0.45	0.22	0.31	0.32	0.31	0.57	0.42	0.59	0.51	0.53						
Mn/(Mn+Fe)	0.05	0.03	0.00	0.00	0.01	0.03	0.01	0.02	0.01	0.03	0.04	0.05	0.03	0.04						
IV(F)	1.0	0.7	1.1	1.3	1.5	0.8	1.3	1.5	1.7	0.7	0.9	0.6	0.6	0.6						
H ₂ O/HF ³	3.7	3.5	3.8	4.0	4.2	3.5	4.0	4.2	4.4	3.4	3.6	3.3	3.3	3.3						

Notes: Compositions averaged from 2 analyses per sample. FW: footwall, incl.: inclusion
¹ Ab: albitized, bl: bleached, Tur: tourmalinized.
² Distance to pegmatite contact.
³ Calculated by the method of Munoiz & Ludington (1977) and Munoiz (1984), assuming an equilibration temperature of 500°C.
 * H₂O is calculated by stoichiometry.

elbaite (Table 11, crystal C). Also present in the pockets and hydrothermal albite-dominant assemblages is tourmaline with similar amounts of Fe and Mn (Table 11, anal. B/4 and D/3). Such compositions transitional between schorl and the hypothetical Mn-rich end-member "tsilaisite" are uncommon (*cf.* Haralampiev 1992).

Several crystals of color-zoned elbaite were analyzed with the electron microprobe to correlate color with chemistry (Table 11, Fig. 20). The zoned crystals have color and compositional boundaries that are both gradual and sharp. The sharp boundaries correspond to overgrowth of late-stage elbaite that is generally colorless. Elbaite overgrowths were analyzed

from the end of broken crystals (Fig. 20B), and also from the prism faces (Fig. 20D). Elements showing significant variation in concentration across the zoned crystals are Mn, Fe, Al, F, Na, Ca and Ti; Mg, K, Cr and Cl are at or below detection limit (0.3 to 0.7 wt% oxide). Dark green or black zones correspond to Fe contents greater than ~0.6 atoms per formula unit (*apfu*, 4.4 wt% FeO). Ti is present in minor concentrations (0.1 to 0.2 wt% TiO₂) in the dark, high-Fe samples, but is below detection limit (0.03 wt%) in the lighter-colored portions. Strong green coloration is present in crystals enriched in Mn combined with subordinate Fe (*e.g.*, Fig. 20C). The colorless overgrowths have variable but low Mn, Ms and Fe contents below detection

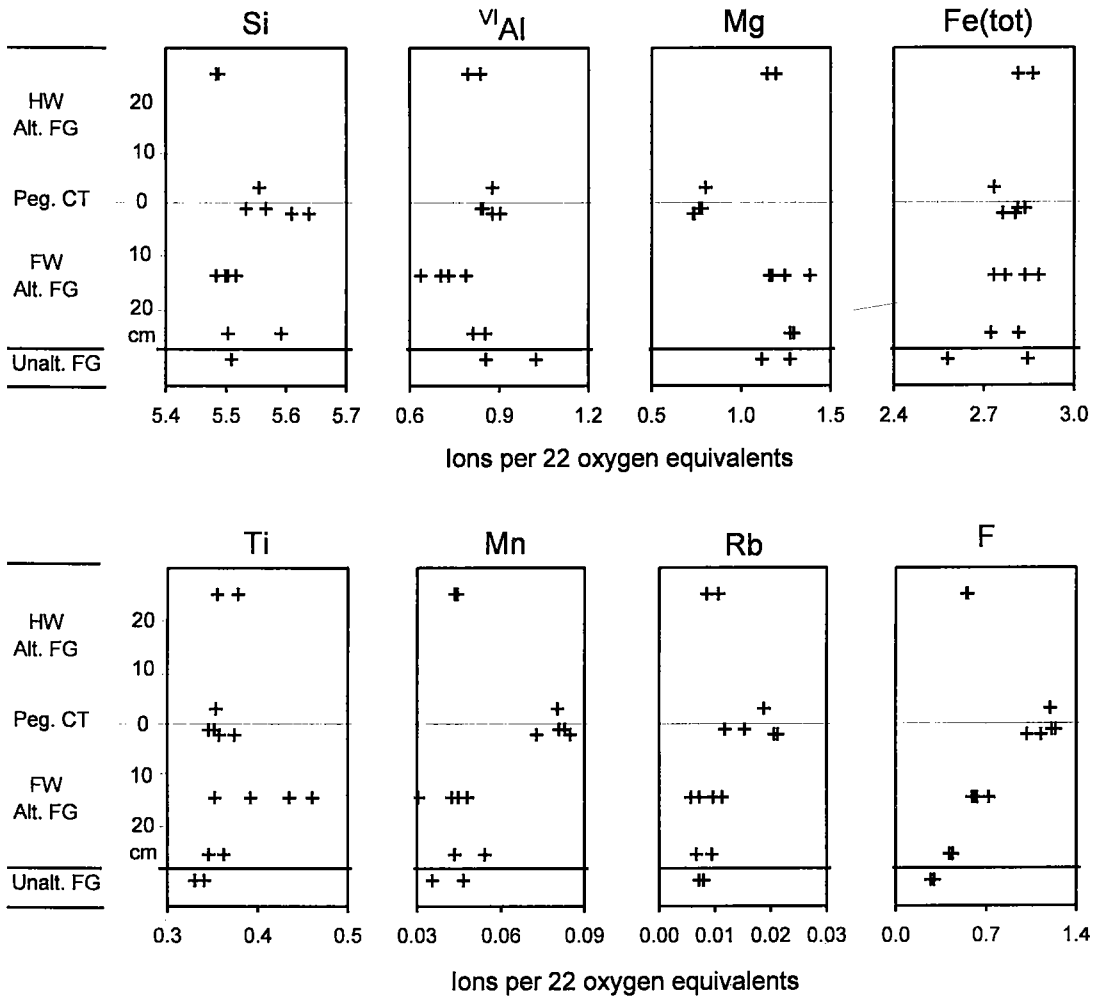


FIG. 17. Biotite composition in unaltered and altered flaser granite gneiss adjacent to pegmatite, main mine area.

limit (0.08 wt% FeO). The level of F and Na generally decreases in the overgrowths, and Al is enriched. Within individual color-zoned crystals, pink and colorless regions show indistinguishable amounts of Mn (0.08 to 0.21 wt% MnO), and Fe contents below the detection limit.

Nb-Ta oxides

Manganocolumbite and microlite form sparsely in the pegmatite pockets and "cleavelandite"-rich replacements. Kazmi *et al.* (1985, Fig. 25) reported manganotantalite up to 5 mm long occurring with dark green elbaite "near Stak Nala." The samples obtained during this study from both the main and south mine areas have Ta/(Ta + Nb) ranging from 0.08 to 0.15, and

therefore are manganocolumbite (Table 12). The manganocolumbite forms dark brown, subhedral to euhedral blocky crystals up to 2 mm in dimension in the pegmatite pockets. Microlite forms smaller crystals (0.5 to 2 mm, 0.5 mm on average) that are transparent amber yellow to rust orange; darker colors correspond to higher Nb content (Table 12). Microlite is rare but widespread within aggregates of "cleavelandite" and lepidolite. Although U was not detected in the microlite, smoky halos were observed near a mineral resembling microlite that forms inclusions in quartz from the pockets.

A quite different Nb-Ta oxide was found in one sample of altered biotite granodiorite gneiss, 7 cm from the upper contact of the south pegmatite. The mineral forms a minute (<0.2 mm) anhedral mass

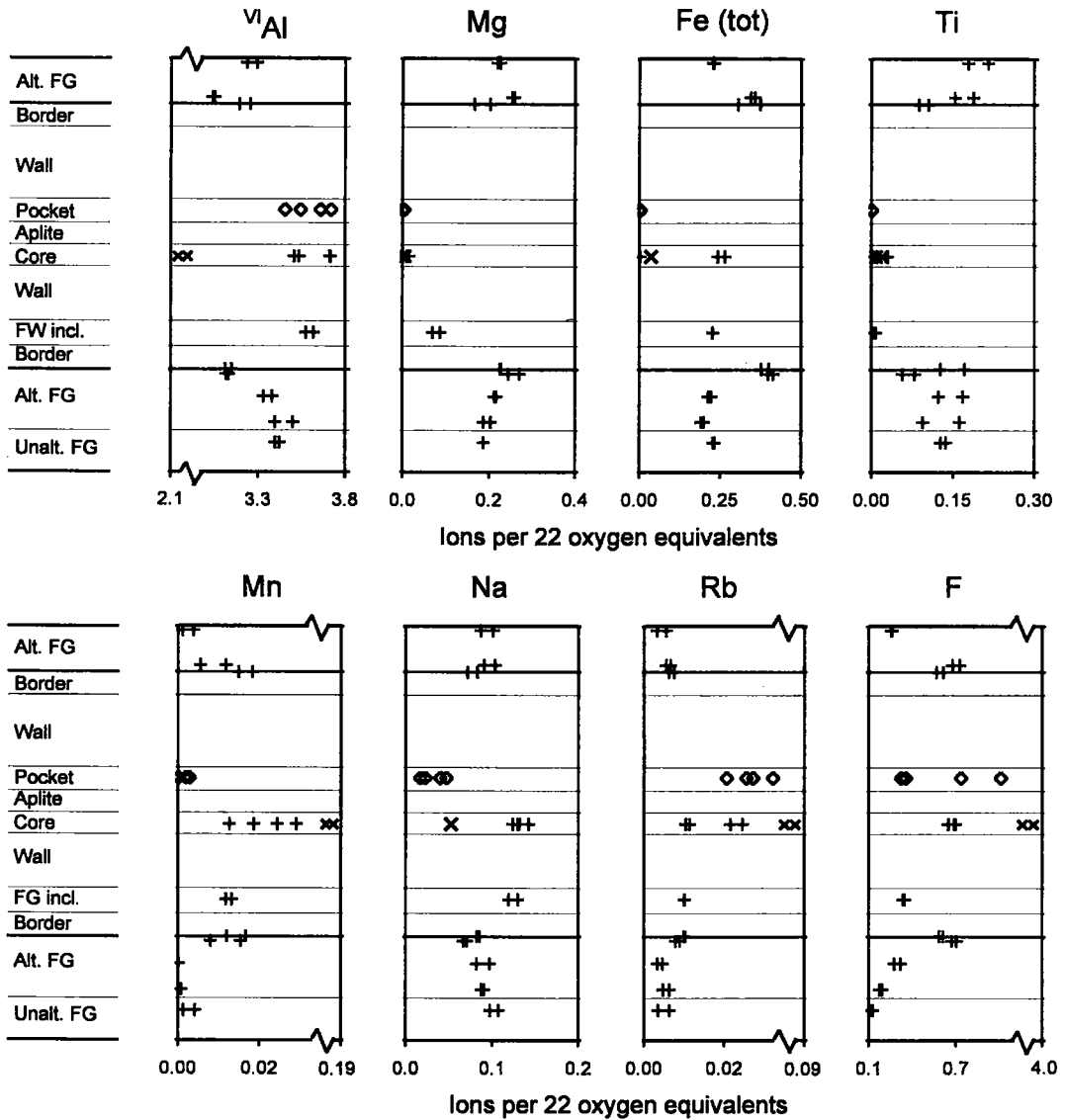


FIG. 18. Compositions of muscovite (+), lepidolite (x), and borian muscovite (◊) in pegmatite and flaser granite gneiss, main mine area.

within a cluster of bleached biotite. Semiquantitative analyses by electron microprobe suggest that the mineral is euxenite, with the composition: $(Ca_{0.01}Fe_{0.01}U_{0.12}Th_{0.05}Y_{0.75}Gd_{0.02}Dy_{0.05}Er_{0.05}Yb_{0.04}Sm_{0.01})_{\Sigma 1.11}(Nb_{0.64}Ta_{0.10}Ti_{1.16}W_{0.03})_{\Sigma 1.93}O_8$. Mn was found to be below detection limit (0.07 wt% oxide). Euxenite is a rare accessory mineral in granitic pegmatites and metasomatized rare-metal granites; it has not been previously reported from altered wallrock adjacent to pegmatites. Euxenite intergrown with bleached biotite was reported in albitized granite from the Transbaikalian region of Russia (Syrtsso *et al.* 1971).

Two unknown Nb-Ta oxides, which are possibly derivatives of stibiotantalite, were discovered on the surface of a colorless crystal of lepidolite from a pegmatite pocket at the main mine. The minerals form minute (<0.5 mm), dark olive green prisms that are intergrown with and overgrown by borian muscovite. Electron-microprobe analyses of the oxides show a Pb-bearing and a Pb-free phase containing major Sb, Nb, Ta, and W, and traces of Ti, Sn, As, and Bi (P. Černý, pers. commun.; this study); traces of B also appear to be present (J. Sisson, pers. commun.). A complete characterization of these minerals is currently under way.

TABLE 9. AVERAGE COMPOSITION (ELECTRON MICROPROBE) OF MUSCOVITE, LEPIDOLITE, AND BORIAN MUSCOVITE FROM PEGMATITE, STAK NALA

Mineral Occurrence Mine area Location	Ms CT South	Ms CT Main	Ms peg South	Ms peg Main	Li?-Ms peg Main	Lpd peg South	Lpd peg Main	Lpd peg South	B-Ms peg Main ¹	BoroMs peg Little ³	BoroMs peg Recize ³
	FW	FW	FW BZ	CZ	CZ	CZ	CZ	CZ	Pocket	Pocket	?
SiO ₂ (wt%)	46.92	47.79	48.59	47.58	46.12	51.50	53.94	56.19	47.47	48.1	48.21
TiO ₂	0.12	1.51	0.03	0.20	0.04	0.05	0.05	0.01	0.01	-	-
Al ₂ O ₃	37.25	31.32	34.91	34.50	36.25	21.82	20.12	21.14	31.87	28.1	29.19
FeO	0.54	3.54	2.09	2.33	0.03	0.15	0.33	0.00	0.02	0.1	0.04
MnO	0.02	0.13	0.09	0.24	0.14	3.37	1.68	0.14	0.01	0.08	-
MgO	0.16	1.16	0.17	0.07	0.00	0.00	0.02	0.00	0.00	0.15	0.03
CaO	0.02	0.00	0.01	0.01	0.00	0.00	0.00	0.00	0.02	0.1	-
Na ₂ O	0.24	0.33	0.16	0.54	0.50	0.16	0.21	0.16	0.07	-	0.06
K ₂ O	11.20	10.58	10.80	10.52	11.14	10.71	10.57	11.04	11.38	11.0	10.93
BaO	0.09	0.04	0.03	0.00	0.00	0.01	0.00	0.00	0.00	-	0.11
Rb ₂ O	0.16	0.12	0.18	0.13	0.27	0.71	0.94	0.62	0.26	0.52	0.03
Cs ₂ O	0.08	0.03	0.08	0.01	0.07	0.74	0.64	0.79	0.02	0.05	0.02
F	0.27	1.44	0.36	1.57	1.67	8.45	9.52	9.26	0.78	0.76	0.11
Cl	0.00	0.00	0.00	0.01	0.00	0.01	0.00	0.01	0.01	-	-
Sum	97.07	98.00	97.50	97.71	96.23	97.69	98.04	99.36	91.93	88.95	88.73
-O=F,Cl	0.11	0.61	0.15	0.66	0.70	3.56	4.01	3.90	0.33	0.32	0.05
+(H ₂ O)*	4.47	3.88	4.43	3.84	3.76	0.50	0.07	0.30	3.99	4.55	4.18
Total	101.42	101.27	101.77	100.89	99.29	94.63	94.10	95.76	95.58	93.18	92.87
Ions (22 O equivalents)											
Si	6.125	6.279	6.335	6.212	6.080	6.850	7.076	7.183	6.527	6.838	6.826
Al	1.875	1.721	1.665	1.788	1.920	1.150	0.924	0.817	1.473	1.162	1.174
Tet. sum	8.000	8.000	8.000	8.000	8.000	8.000	8.000	8.000	8.000	8.000	8.000
Al	3.858	3.131	3.701	3.522	3.714	2.272	2.188	2.368	3.691	3.547	3.699
Mg	0.032	0.227	0.032	0.013	0.000	0.000	0.003	0.000	0.000	0.032	0.006
Fe	0.058	0.389	0.228	0.254	0.003	0.017	0.037	0.000	0.002	0.011	0.005
Ti	0.012	0.149	0.003	0.020	0.004	0.005	0.014	0.001	0.001	-	0.000
Mn	0.002	0.014	0.009	0.027	0.016	0.380	0.187	0.015	0.001	0.010	-
Oct. sum	3.962	3.910	3.973	3.835	3.738	2.674	2.429	2.385	3.696	3.599	3.710
Ca	0.002	0.000	0.002	0.001	0.000	0.001	0.000	0.000	0.003	0.015	-
Na	0.061	0.084	0.040	0.137	0.127	0.041	0.053	0.041	0.020	-	0.016
K	1.864	1.773	1.796	1.752	1.873	1.818	1.769	1.799	1.995	1.995	1.974
Ba	0.005	0.002	0.001	0.000	0.000	0.001	0.000	0.000	0.000	-	0.006
Rb	0.013	0.010	0.015	0.011	0.023	0.061	0.079	0.051	0.023	0.048	0.003
Cs	0.004	0.002	0.005	0.001	0.004	0.042	0.036	0.043	0.001	0.003	0.001
Int. sum	1.950	1.871	1.859	1.902	2.027	1.963	1.937	1.934	2.043	2.061	2.001
Sum cations	13.912	13.780	13.832	13.737	13.765	12.637	12.366	12.319	13.739	13.660	13.710
F	0.111	0.600	0.149	0.650	0.695	3.553	3.949	3.742	0.341	0.342	0.049
Cl	0.000	0.001	0.000	0.002	0.000	0.001	0.000	0.002	0.002	-	-
OH*	3.889	3.399	3.851	3.348	3.305	0.446	0.060	0.257	3.657	3.658	3.951
Mg/(Mg+Fe)	0.35	0.36	0.12	0.04	0.13	0.03	0.08	0.74	0.32	0.75	0.57
Mn/(Mn+Fe)	0.03	0.04	0.04	0.10	0.83	0.96	0.31	0.99	0.29	0.47	0.00
IV(F)	1.5	0.8	1.4	0.6	0.6	n.a.	n.a.	n.a.	0.9	0.9	1.8
fH ₂ O/HF ⁴	4.2	3.5	4.1	3.0	3.0	n.a.	n.a.	n.a.	4.0	4.1	4.9

Notes: Compositions averaged from 2 analyses per sample.

B-Ms: borian muscovite, BoroMs: boromuscovite, Li?-Ms: lithian? muscovite, Lpd: lepidolite, BZ: border zone, CT: contact, CZ: core zone, FW: footwall, peg: pegmatite, -: not detected, --: not determined

¹ Includes 2.6 wt% B₂O₃; analyzed by electron microprobe using PC-3 crystal, 15 kV, 10 nA, 60s count time.; ² Foord *et al.* (1991b); includes 7.0 wt% B₂O₃, 0.05 Li₂O; ³ Liang *et al.* (1995): includes 6.12 wt% B₂O₃, 0.03 Li₂O.

⁴ Calculated by the method of Munoz & Ludington (1977), assuming an equilibration temperature of 400°C for borian muscovite, and 500°C for all others.

* H₂O is calculated by stoichiometry.

TABLE 10. AVERAGE TOURMALINE COMPOSITIONS (ELECTRON MICROPROBE) FROM PEGMATITE AND ALTERED WALLROCKS ADJACENT TO PEGMATITE, STAK NALA

Mine area Variety	Main										South ^{II}				
	Srl alt. FG	Srl alt. FG	Srl CT	Srl peg	Srl alt. BG	Srl alt. BG	Srl CT	Srl peg	Srl peg						
Occurrence	alt. FG	alt. FG	CT	peg	alt. BG	alt. BG	CT	peg	peg						
Location	HW 25cm	HW 3cm	HW	HW BZ	HW WZ	Aplitite	CZ	FW WZ	FW BZ	FW BZ	HW 7cm	HW 2cm	HW	HW BZ	HW BZ
Alteration	≠Tur	Tur, bl	Tur, bl	none	partly Ab	none	Ab	none	none	none	Tur, sbt	Tur, bl; Ab	Tur, bl; Ab	Ab	Ab
Analyses	n=3	n=3	n=3	n=4	n=5	n=5	n=3	n=3	n=3	n=3	n=3	n=3	n=3	blk core	grn o/g
SiO ₂ (wt%)	35.12	34.35	35.12	34.15	33.89	35.04	36.08	35.17	35.32	35.61	34.46	37.57	33.69	36.94	
TiO ₂	1.42	1.01	1.20	0.23	0.27	0.21	0.13	0.85	0.44	1.62	0.78	0.40	0.36	0.09	
Al ₂ O ₃	30.79	31.02	30.86	33.44	33.40	31.86	34.14	31.10	32.18	30.56	31.14	35.68	32.56	36.86	
Cr ₂ O ₃	0.00	0.01	0.02	0.03	0.01	0.01	0.01	0.01	0.00	0.01	0.01	0.00	0.02	0.00	
FeO	11.13	12.40	13.29	15.53	15.91	15.82	11.92	14.98	14.56	11.02	10.58	4.55	16.29	4.88	
MnO	0.07	0.15	0.21	0.55	0.45	0.42	1.09	0.37	0.51	0.08	0.27	0.43	0.61	1.43	
MgO	4.70	3.73	3.01	0.24	0.21	0.26	0.10	1.52	1.28	5.01	5.37	2.75	0.14	0.01	
CaO	0.70	0.68	0.64	0.33	0.36	0.30	0.22	0.48	0.38	0.76	1.00	0.58	0.54	0.75	
Na ₂ O	2.09	2.13	2.13	1.86	1.82	1.92	2.02	2.05	1.95	2.03	2.16	2.44	1.91	2.40	
K ₂ O	0.07	0.07	0.07	0.05	0.06	0.06	0.03	0.07	0.06	0.06	0.05	0.02	0.05	0.03	
F	0.56	1.02	0.92	0.84	0.76	1.09	1.23	0.94	0.97	0.69	1.13	1.62	0.89	1.74	
Cl	0.00	0.00	0.00	0.00	0.00	0.01	0.00	0.01	0.00	0.00	0.00	0.00	0.01	0.00	
Sum	86.67	86.57	87.47	87.26	87.14	86.99	86.98	87.56	87.66	87.45	86.94	86.05	87.06	85.11	
-O=F,Cl	0.24	0.43	0.39	0.35	0.32	0.46	0.52	0.40	0.41	0.29	0.48	0.68	0.38	0.73	
+H ₂ O*	0.10	0.20	0.27	0.24	0.19	0.38	0.71	0.33	0.32	0.05	0.07	1.33	0.23	1.57	
+B ₂ O ₃ **	10.35	10.26	10.33	10.22	10.19	10.19	10.42	10.27	10.33	10.46	10.37	10.75	10.12	10.58	
+H ₂ O*	3.31	3.05	3.13	3.15	3.15	2.99	3.01	3.10	3.10	3.28	3.04	2.94	3.07	2.83	
Total	100.20	99.65	100.82	100.47	100.34	100.09	100.59	100.85	100.99	100.95	99.95	100.38	100.10	99.37	
Ions (31 O equivalents)															
Si	5.896	5.821	5.908	5.807	5.784	5.977	6.020	5.952	5.945	5.920	5.773	6.075	5.785	6.067	
Al	0.104	0.179	0.092	0.193	0.216	0.027	0.000	0.052	0.055	0.080	0.227	0.000	0.215	0.000	
Tet. sum	6.000	6.000	6.000	6.000	6.000	6.003	6.020	6.005	6.000	6.000	6.000	6.075	6.000	6.067	
Al (Z)	5.950	5.963	5.975	6.000	6.000	6.000	6.000	6.000	6.000	5.870	5.884	6.000	6.000	6.000	
Al	0.000	0.012	0.009	0.462	0.454	0.334	0.665	0.110	0.285	0.000	0.000	0.750	0.328	1.079	
Mg	1.177	0.941	0.756	0.062	0.054	0.066	0.024	0.382	0.320	1.242	1.339	0.664	0.037	0.001	
Fe	1.563	1.757	1.870	2.210	2.270	2.257	1.663	2.121	2.051	1.531	1.485	0.615	2.339	0.670	
Ti	0.180	0.129	0.151	0.029	0.034	0.027	0.016	0.108	0.056	0.202	0.098	0.049	0.046	0.011	
Mn	0.010	0.022	0.029	0.079	0.065	0.061	0.155	0.053	0.073	0.011	0.038	0.058	0.089	0.199	
Cr	0.001	0.001	0.003	0.004	0.001	0.002	0.001	0.002	0.000	0.002	0.001	0.001	0.002	0.000	
Li	0.069	0.137	0.182	0.164	0.130	0.263	0.476	0.224	0.215	0.032	0.046	0.863	0.159	1.040	
Y sum	3.000	3.000	3.000	3.000	3.000	3.000	3.000	3.000	3.000	3.020	3.007	3.000	3.000	3.000	
Ca	0.126	0.123	0.115	0.060	0.067	0.054	0.039	0.086	0.068	0.135	0.180	0.100	0.059	0.132	
Na	0.682	0.699	0.695	0.615	0.602	0.636	0.654	0.672	0.637	0.655	0.701	0.764	0.636	0.763	
K	0.015	0.015	0.016	0.010	0.012	0.012	0.007	0.016	0.014	0.013	0.011	0.004	0.010	0.006	
X sum	0.823	0.836	0.825	0.686	0.681	0.703	0.701	0.774	0.719	0.803	0.892	0.869	0.745	0.901	
B	3.000	3.000	3.000	3.000	3.000	3.000	3.000	3.000	3.000	3.000	3.000	3.000	3.000	3.000	
F	0.297	0.547	0.490	0.454	0.408	0.590	0.652	0.505	0.516	0.361	0.598	0.830	0.484	0.903	
Cl	0.001	0.000	0.001	0.001	0.001	0.002	0.001	0.003	0.000	0.001	0.000	0.000	0.002	0.001	
OH	3.703	3.453	3.510	3.557	3.588	3.396	3.348	3.495	3.484	3.639	3.402	3.170	3.516	3.097	
Mg/(Mg+Fe)	0.43	0.35	0.29	0.03	0.02	0.03	0.01	0.15	0.14	0.45	0.47	0.50	0.02	0.00	
Mn/(Mn+Fe)	0.01	0.01	0.02	0.04	0.03	0.03	0.09	0.02	0.03	0.01	0.02	0.09	0.04	0.23	
Na/(Na+Ca)	0.84	0.85	0.86	0.91	0.90	0.92	0.94	0.89	0.90	0.83	0.80	0.88	0.87	0.85	

Note: The last two analyses are representative compositions of the core and rim of a single crystal.

Abbreviations: Ab: albitized, bl: bleached, blk: black, Elb^{II}: secondary elbaite, grn: green, o/g: overgrowth, Srl: schorl, Tur: tourmalized

* Calculated to fill the Y site; ** B calculated assuming 3 B apfu; † calculated assuming 4 (OH+F) apfu

Other minerals

A semiquantitative analysis by electron microprobe of pale pink beryl from a "cleavelandite" replacement at the south mine gave 1.7 wt% Na₂O, 0.51 wt% FeO, 0.15 wt% Rb₂O, 0.05 wt% Cs₂O, and 0.10 wt% F. Manganese, a common chromophore in pink beryl, was not detected. The Na content suggests classification as sodian-lithian beryl, as defined by Černý (1975). The greater abundance of Rb with respect to Cs is unusual in beryl, and may reflect a lack of Cs during late-stage subsolidus alteration. A semiquantitative analysis of

topaz from the south mine gave ~19 wt% F, a value typical for topaz from pegmatites. Zircon from the south mine showed a small U peak in the energy-dispersion spectrum (EDS).

EDS spectra of löllingite from both mine areas show small amounts of S in some samples. The löllingite also contains small blebs of an As-Fe-Ca-Ti mineral (cafarsite?), and microveinlets of an As-Fe-K mineral (pharmacosiderite?).

Mn-Fe oxides that locally form small balls on previously crystallized minerals (including borian muscovite) in vugs and pockets show variable amounts

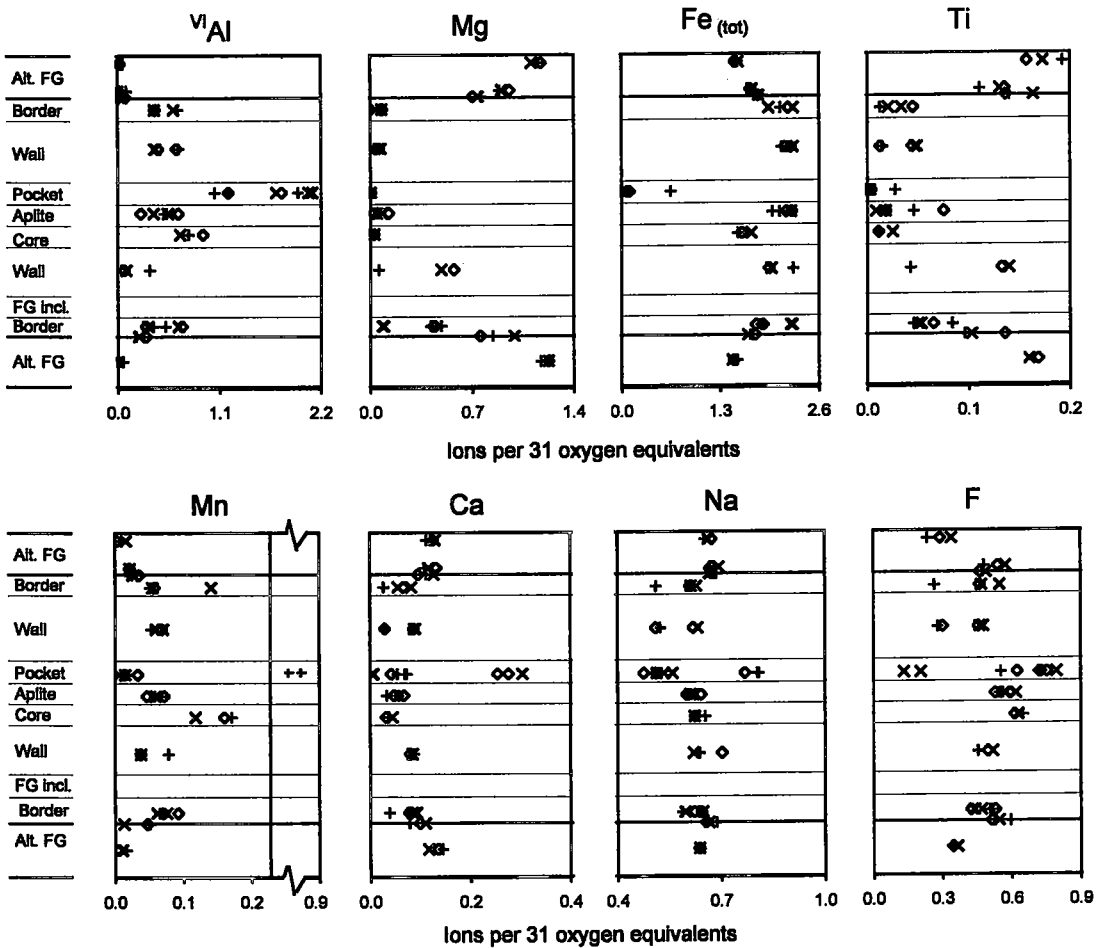


FIG. 19. Tourmaline composition in pegmatite and altered flaser granite gneiss, main mine area; symbols as in Figure 15.

of Fe, Mn, Si, Al, and Na under EDS examination. A Mn-Fe oxide was also observed as inclusions in tourmaline from the upper border - wall zone interface at the south mine. The inclusions form bulbous masses along the sharp boundary between the schorl core and elbaite rim. Concentric cracks are present in the tourmaline around the inclusions, and EDS spectra showed variable Al, Ca, K and Mg (up to 3 wt% oxide), and traces of Sb and Nb. The inclusions appear to result from alteration of a pre-existing mineral such as manganocolumbite.

DISCUSSION

Granitic pegmatites at Stak Nala form flat-lying, symmetrically zoned sills consisting of a coarse-grained border zone that grades into a very coarse-grained wall

zone that surrounds a core dominated by blocky K-feldspar. Inwardly flaring euhedral megacrysts of K-feldspar in the border and wall zones are enclosed by coarse-grained, intergrown, anhedral to subhedral crystals of oligoclase, quartz, and subordinate K-feldspar, and euhedral prismatic schorl that commonly radiates from near the wallrock contact. The core zone is characterized by a wide range of inhomogeneous textures and compositions, and contains sporadic pockets that are mined for multicolored tourmaline. Albitization of the pegmatite bodies is widespread, particularly in areas containing abundant pocket mineralization.

Pegmatite-wallrock interaction

Adjacent to the pegmatite contacts, metasomatism of the host gneisses resulted in a zone of variable width

TABLE 11. REPRESENTATIVE ZONED ELBAITE AND SCHORL-ELBAITE COMPOSITIONS (ELECTRON MICROPROBE) FROM PEGMATITE POCKETS, STAK NALA

Mine area Variety	Main				Main			Main			South		
	Elb v lt gm	Elb cls	Elb v lt pnk	Elb cls	Elb gm	Elb lt pnk	Elb cls	Elb olv gm	Elb gm	Elb cls	Srl-Elb black	Srl-Elb black	Elb cls
Color	base	middle	term	drusy o/g druse	base	term	o/g	base	middle	term o/g	core	middle	rim o/g
Position	A/2	A/5	A/8		B/4	B/1	B/6	C/2	C/4	C/6	D/1	D/3	D/6
Crystal/point ¹													
SiO ₂ (wt%)	37.70	38.11	38.05	36.59	35.67	36.53	37.55	36.38	37.23	38.36	35.23	36.54	37.00
TiO ₂	0.00	0.03	0.02	0.01	0.20	0.02	0.00	0.05	0.03	0.02	0.13	0.15	0.01
Al ₂ O ₃	42.57	41.50	41.74	42.29	38.00	43.22	44.31	37.58	37.44	43.39	36.25	36.40	40.79
Cr ₂ O ₃	0.03	0.05	0.01	0.00	0.00	0.00	0.02	0.01	0.00	0.04	0.03	0.03	0.00
FeO	0.02	0.00	0.02	0.00	4.83	0.02	0.00	0.69	0.79	0.02	7.16	4.38	0.06
MnO	0.13	0.25	0.11	0.08	3.91	0.08	0.04	6.60	6.23	0.05	2.72	3.69	0.56
MgO	0.00	0.00	0.00	0.00	0.00	0.06	0.00	0.00	0.00	0.01	0.00	0.03	0.01
CaO	0.42	1.66	1.83	1.42	0.29	1.37	0.04	0.44	0.25	0.03	0.39	0.35	1.16
Na ₂ O	1.72	1.58	1.71	1.64	2.48	1.69	1.81	2.56	2.48	1.83	2.35	2.67	1.71
K ₂ O	0.01	0.00	0.02	0.00	0.04	0.03	0.01	0.03	0.02	0.02	0.03	0.02	0.01
F	1.12	1.27	1.63	1.37	1.41	1.36	0.43	1.48	1.43	0.37	1.43	1.58	1.34
Cl	0.01	0.01	0.01	0.00	0.00	0.00	0.01	0.00	0.00	0.00	0.00	0.02	0.00
Sum	83.73	84.46	85.17	83.41	86.83	84.40	84.23	85.83	85.90	84.14	85.72	85.86	82.64
-O=F,Cl	0.47	0.54	0.69	0.58	0.60	0.57	0.18	0.62	0.60	0.16	0.60	0.66	0.56
+Li ₂ O*	1.62	1.95	2.00	1.74	1.05	1.80	1.32	1.26	1.38	1.50	0.97	1.29	1.98
+H ₂ O ₃ **	10.98	11.01	11.09	10.88	10.72	11.00	11.07	10.70	10.76	11.07	10.50	10.64	10.76
+H ₂ O [†]	3.25	3.19	3.05	3.10	3.02	3.15	3.61	2.98	3.03	3.64	2.94	2.92	3.08
Total	99.10	100.07	100.63	98.56	101.03	99.77	100.05	100.15	100.45	100.20	99.54	100.05	97.90
Cations (31 O equivalents)													
Si	5.969	6.014	5.964	5.846	5.781	5.775	5.896	5.911	6.017	6.024	5.830	5.967	5.975
Al	0.031	0.000	0.036	0.154	0.225	0.219	0.104	0.089	0.000	0.000	0.170	0.033	0.025
Tet. sum	6.000	6.014	6.000	6.000	6.000	6.000	6.000	6.000	6.017	6.024	6.000	6.000	6.000
Al (Z)	6.000	6.000	6.000	6.000	6.000	6.000	6.000	6.000	6.000	6.000	6.000	6.000	6.000
Al	1.945	1.721	1.714	1.867	1.091	1.823	2.157	1.160	1.133	2.034	0.950	1.008	1.625
Mg	0.001	0.001	0.001	0.001	0.001	0.014	0.001	0.001	0.001	0.002	0.001	0.007	0.001
Fe	0.003	0.001	0.003	0.001	0.660	0.003	0.000	0.095	0.107	0.003	0.999	0.603	0.007
Ti	0.000	0.004	0.003	0.001	0.025	0.003	0.000	0.006	0.003	0.002	0.017	0.019	0.001
Mn	0.018	0.034	0.015	0.010	0.541	0.011	0.006	0.916	0.859	0.007	0.384	0.514	0.076
Cr	0.004	0.006	0.001	0.000	0.000	0.000	0.002	0.002	0.000	0.005	0.003	0.004	0.000
Li	1.028	1.235	1.263	1.120	0.681	1.146	0.834	0.821	0.896	0.947	0.646	0.845	1.289
Y sum	3.000	3.000	3.000	3.000	3.000	3.000	3.000	3.000	3.000	3.000	3.000	3.000	3.000
Ca	0.071	0.282	0.311	0.246	0.050	0.232	0.007	0.077	0.043	0.005	0.070	0.061	0.198
Na	0.533	0.487	0.524	0.514	0.785	0.518	0.557	0.813	0.785	0.561	0.759	0.851	0.531
K	0.001	0.001	0.005	0.001	0.008	0.006	0.002	0.007	0.003	0.004	0.007	0.005	0.001
X sum	0.606	0.771	0.840	0.761	0.843	0.756	0.566	0.896	0.831	0.571	0.836	0.917	0.730
B	3.000	3.000	3.000	3.000	3.000	3.000	3.000	3.000	3.000	3.000	3.000	3.000	3.000
F	0.566	0.640	0.814	0.697	0.731	0.679	0.215	0.766	0.738	0.185	0.753	0.822	0.678
Cl	0.002	0.003	0.002	0.000	0.000	0.001	0.003	0.000	0.001	0.001	0.000	0.006	0.000
OH	3.434	3.360	3.186	3.303	3.269	3.321	3.785	3.234	3.262	3.815	3.247	3.178	3.322
Mg/(Mg+Fe)	0.25	0.48	0.28	0.48	0.00	0.84	0.73	0.01	0.01	0.37	0.00	0.01	0.16
Mn/(Mn+Fe)	0.85	0.98	0.83	0.94	0.45	0.80	0.96	0.91	0.89	0.71	0.28	0.46	0.91
Na/(Na+Ca)	0.88	0.63	0.63	0.68	0.94	0.69	0.99	0.91	0.95	0.99	0.92	0.93	0.73

Abbreviations: lt: light, olv: olive, pnk: pink, term: termination, v: very

¹ Corresponds to letter of crystal and number of analysis graphed in Figure 16.* Calculated to fill the Y site; ** B calculated assuming 3 B apfu; [†] calculated assuming 4 (OH+F) apfu

(typically <10 cm) where biotite was converted to muscovite, and disseminated schorl is present. Within this zone, local narrow (<1 cm) schorl-rich veins have narrow selvages in which both muscovite and biotite have been destroyed, and quartz was added. Compositions of bulk-rock samples and minerals in the altered gneiss reflect the addition of Si, Li, B, As and F, and depletion of K, H₂O, and Ba; locally, addition of Al, Mn, Rb, Nb, As, Zn and Zr, and depletion of Ca, Mg, Na and Ti also are noted. Iron shows significant depletion from altered biotite granodiorite gneiss at the

south mine (depository data). Measured compositions of altered flaser granite gneiss at the main mine do not show iron depletion, but the abundance of Fe-rich schorl in the pegmatite border zone suggests that Fe may have been added there from the flaser granite gneiss by mobilization during hydrothermal alteration. The conversion of biotite to muscovite during wallrock alteration by hydrogen metasomatism provides a mechanism to release Fe. The following two reactions describe the conversion of biotite to muscovite and the addition of schorl to the altered gneiss:

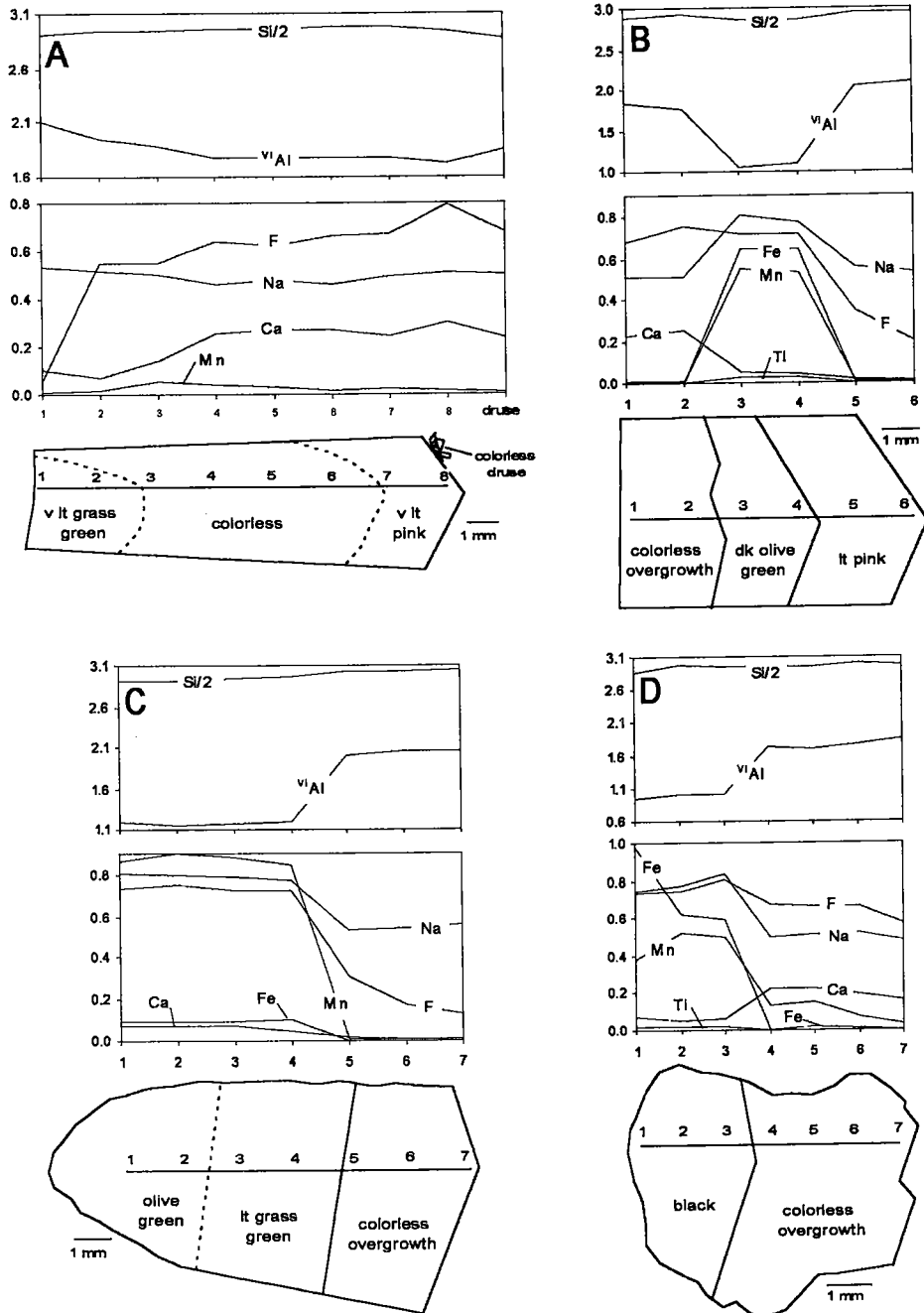
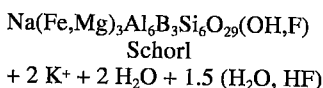
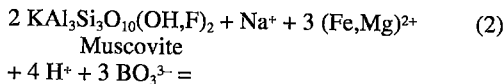
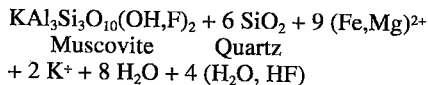


FIG. 20. Composition (ions per 31 oxygen equivalents) of color-zoned elbaite and schorl-elbaite crystals from pegmatite pockets. (A) Pale tricolor elbaite crystal cut parallel to the *c* axis, with drusy overgrowth of fine-grained elbaite and borian muscovite (main mine area); Fe and Ti are below detection limit (0.08 and 0.03 wt% oxide, respectively). (B) Tricolor elbaite crystal cut parallel to the *c* axis (main mine area). (C) Tricolor elbaite crystal cut parallel to the *c* axis, partly Mn-rich (main mine area); Ti is below detection limit. (D) Concentrically zoned schorl-elbaite cut perpendicular to the *c* axis (south mine area).

TABLE 12. REPRESENTATIVE MANGANOCOLUMBITE AND MICROLITE COMPOSITIONS (ELECTRON MICROPROBE), STAK NALA

Mineral Mine area Description Color	Col	Col	Col	Mic	Mic	Mic
	South in Clv dk brn	Main in Clv dk brn	Main in Clv dk brn	South w/ Col org	South w/ Zn ylo	South w/ Zn ylo
Nb ₂ O ₅ (wt%)	68.12	65.88	61.59	37.20	21.51	18.95
Ta ₂ O ₅	10.32	12.33	17.96	38.56	55.63	58.45
Sb ₂ O ₃	0.01	0.00	0.00	0.14	0.18	0.16
WO ₃	1.27	0.96	0.96	1.22	0.50	0.58
Bi ₂ O ₃	0.03	0.10	0.00	0.00	0.00	0.00
TiO ₂	0.93	0.83	0.88	0.10	0.14	0.21
Al ₂ O ₃	0.00	0.01	0.00	0.03	0.03	0.00
CaO	0.03	0.07	0.03	12.26	12.16	11.97
MnO	18.34	16.98	17.57	0.01	0.04	0.03
FeO	1.44	1.95	1.50	0.02	0.00	0.00
Na ₂ O	0.00	0.00	0.00	6.69	5.75	5.87
F	0.00	0.00	0.00	3.95	3.96	3.87
Sum	100.50	99.13	100.50	100.19	99.90	100.09
-O=F	0.00	0.00	0.00	1.66	1.67	1.63
Total	100.50	99.13	100.50	98.53	98.23	98.46
Cations (6 oxygens)						
Nb	1.791	1.769	1.669	1.058	0.665	0.593
Ta	0.163	0.199	0.293	0.659	1.034	1.100
Ti	0.041	0.037	0.039	0.005	0.007	0.011
W	0.019	0.015	0.015	0.020	0.009	0.010
A sum	2.013	2.020	2.017	1.742	1.715	1.715
Sb	0.000	0.000	0.000	0.004	0.005	0.005
Bi	0.000	0.002	0.000	0.000	0.000	0.000
Al	0.000	0.001	0.000	0.002	0.003	0.000
Ca	0.002	0.004	0.002	0.826	0.890	0.887
Mn	0.903	0.855	0.892	0.001	0.002	0.002
Fe	0.070	0.097	0.075	0.001	0.000	0.000
Na	0.000	0.000	0.000	0.816	0.762	0.788
B sum	0.977	0.959	0.970	1.650	1.662	1.682
F	0.000	0.000	0.000	0.786	0.855	0.847
Ta/(Ta+Nb)	0.08	0.10	0.15	0.38	0.61	0.65
Mn/(Mn+Fe)	0.93	0.90	0.92	0.37	0.97	0.96

Abbreviations: brn: brown, Clv: cleavelandite, Col: manganocolumbite, dk: dark, grn: green, Mic: microlite, org: orange, ylo: yellow



The generalized reactions account for added quartz and losses of H₂O and K in the altered gneiss. Some of the Fe and Mg released from biotite is consumed by the crystallization of schorl, both in wallrock and the adjacent pegmatite. The stability of schorl was therefore enhanced by Fe produced by destruction of biotite. The zoned wallrock-alteration selvage adjacent to the narrow schorl-rich veins suggests that schorl crystallized concurrently with the alteration of biotite to muscovite. Thus we infer that volatile saturation occurred early during pegmatite crystallization, and the resultant hydrothermal fluids altered the wallrock to expedite formation of schorl in the outer zones of the pegmatite and in the altered gneiss.

Compositional evolution of pegmatite minerals

The primary plagioclase shows a constant composition (~An₁₂) from the border to the core, whereas metasomatic pseudomorphs are albite (An₃ to An₈), and "cleavelandite" or albite in pockets is end-member albite (An₁). Thus, the plagioclase evolution to massive albite and "cleavelandite" of extremely sodic composition reflects crystallization in a hydrothermal environment at successively lower temperatures, which is typical of pegmatites (*cf.* Černý 1994).

Garnet in the analyzed samples shows anomalous Mn- and Fe-enrichment trends, compared to other granitic pegmatites (*e.g.*, Černý & Hawthorne 1982, Baldwin & von Knorring 1983, Černý *et al.* 1985, Nakano & Ishikawa 1997): increasing Mn/(Mn + Fe) values from core to rim of individual grains, and a lack of Mn enrichment in the core zone. Foord (1976) and Foord & Kleck (1993) documented Fe enrichment (and some cases of Mn enrichment) from core to rim of garnet in miarolitic pegmatite, and noted Mn enrichment spatially within pegmatite during the late stages of crystallization. The perceived low values of Mn/(Mn + Fe) in late-stage garnet at Stak Nala probably are due to the lack of schorl that cocrystallized with garnet in the analyzed sample from the core zone. Because Fe will be preferentially incorporated into schorl over garnet, Mn enrichment is expected in garnet that formed together with schorl (E.E. Foord, pers. commun., 1997).

The evolution from muscovite in altered wallrock to muscovite and lepidolite in the pegmatite core is accompanied by sharp increases in F, Li, Mn, Rb, and Cs, which indicates that these elements were enriched during late stages of crystallization of magma and hydrothermal fluid. In particular, F is extremely enriched in lepidolite (up to 9.5 wt %), which is highly fractionated in terms of Fe/Mn (0.01, molar basis), and moderately fractionated in terms of K/Rb (22) and K/Cs (42) (*cf.* Černý *et al.* 1985). In altered biotite granodiorite gneiss at the south mine, mica compositions are transitional between biotite and

muscovite, and thus may reflect solid solution or interlayered biotite–muscovite intergrowths. On the basis of transmission electron microscopy, Konings *et al.* (1988) attributed similar mica compositions in a rare-metal granite to muscovite–biotite solid solution.

The composition of tourmaline is rather constant in the pegmatite until the onset of elbaite crystallization. The abrupt transition from black schorl to green elbaite within the pockets reflects decreasing Fe and increasing Al, Li and, locally, Mn. Concentrations of Mn, Ca, F, and Na in elbaite vary greatly, and show few consistent trends within individual crystals. Colorless overgrowths of elbaite show sharp compositional changes, with less Mn, Fe, and Na than the substrate elbaite crystals (Figs. 20B, C, D). The Al content is correspondingly greater in the overgrowths, and F and Ca contents are variable. Contrasting elbaite compositional trends were noted by Foord (1976, 1977) at the Himalaya miarolitic pegmatite–aplite in southern California: pink elbaite crystals commonly have green caps enriched in Fe, Mn, and Ca, and depleted in Al. According to Foord (1976, 1977), the green caps formed after rupture of the pockets, which resulted in chemical exchange between the pegmatite pockets and the gabbroic wallrocks. Influx of Fe from the wallrocks is consistent with the green color of the caps (see below). Studies subsequent to 1976 (Foord *et al.* 1986, Laurs & Wise 1991) documented removal of Ca, Mg, and Fe from boron-metasomatized gabbro adjacent to the pegmatite–aplite dike system. At Stak Nala, the colorless elbaite overgrowths do not show enrichment in Fe and Ca, for the following possible reasons: (1) the overgrowths did not result from pocket rupture, or (2) the flaser granite gneiss wallrock at Stak Nala is a poor source of Fe and Ca. The latter explanation is preferred, because several lines of evidence suggest that pocket rupture did indeed occur (see below).

Cause of tourmaline coloration

Iron, Ti, and Mn are common chromophores in tourmaline [see the comprehensive discussion of tourmaline coloration in Dietrich (1985)], and therefore likely account for the black, green, and pink coloration at Stak Nala. Variations in Ca, Na, Al, and F apparently do not contribute to tourmaline coloration, so will not be considered further. Compositional ranges of Fe, Mn, and Ti given below are derived from all analyses obtained (data depository), and therefore do not precisely match the data shown in Tables 10 and 11.

The black color has commonly been ascribed to Fe (Ward 1931, Dietrich 1985). At Stak Nala, black tourmaline contains >5 wt% FeO and the highest amounts of Ti (0.10 to 1.14 wt% TiO₂). The green color in tourmaline has been widely attributed to charge transfer involving Fe (Faye *et al.* 1974, Leckebusch 1978, Smith 1978, Mattson & Rossman 1987); Fe is always present in strongly green-colored elbaite from

Stak Nala (0.68 to 4.83 wt% FeO). Green crystals enriched in Mn (4.0 wt% MnO) combined with relatively high Ti (0.2 wt% TiO₂) [e.g., Table 11, anal. B/4] may derive their color from Mn²⁺–Ti⁴⁺ charge transfer (e.g., Rossman & Mattson 1986). The pink color in tourmaline is widely ascribed to Mn³⁺ (e.g., Slivko 1961, Manning 1969, 1973, Leckebusch 1978), or Mn²⁺ → Mn³⁺ transition (Manning 1969, Leckebusch 1978, Reinitz & Rossman 1988). At Stak Nala, pink elbaite is pale in color, and contains very little Mn (0.08 to 0.21 wt% MnO), Fe (0 to 0.02 wt% FeO), and Ti (0 to 0.02 wt% TiO₂). For comparison, compositions of pink to red elbaite from granitic pegmatites reported in the literature (Staatz *et al.* 1955, Slivko 1961, Donnay & Barton 1972, Foord 1976, 1977, Leckebusch 1978, Sahama *et al.* 1979, Deer *et al.* 1997,) contain 0.18 to 2.08 wt% MnO, 0 to 0.23 wt% FeO, and 0 to 0.05 wt% TiO₂. The lower Mn content of elbaite at Stak Nala is consistent with its pale pink coloration. Some crystals contain more Mn where they are colorless than where they are light pink (e.g., Table 11, anal. A/5 versus A/8). Since Mn³⁺ causes pink coloration (e.g., Leckebusch 1978), the colorless portion must contain only Mn²⁺.

Petrogenesis of the pegmatites

Evidence for sidewall crystallization. Several lines of textural and compositional evidence suggest that crystallization of the pegmatites proceeded from the walls inward: (1) the gradual increase in grain size toward the core, (2) the distribution of minerals in zones parallel to the walls and nearly symmetrical about a centrally disposed horizontal plane, (3) the directional growth of radiating aggregates of schorl and the inwardly flaring K-feldspar megacrysts from the border zone toward the core (comb texture), (4) the evolution of mineral compositions within the pegmatite, and (5) the formation of crystal-lined pockets enriched in incompatible elements in the core zone. These characteristics are similar to observations at other cases of granitic pegmatite where sidewall crystallization is inferred (*cf.* Jahns 1953, Herrera 1968, Foord 1976).

Significance of the lack of graphic quartz – K-feldspar intergrowth. A graphic quartz – feldspar intergrowth is common in many varieties of granitic pegmatite (*cf.* Jahns & Burnham 1969, Černý 1991), but is absent at Stak Nala. Formation of the graphic texture is contingent upon an appropriately high degree of undercooling, thus limiting the intergrowth almost exclusively to pegmatites. Fenn (1986) emphasized that the growth rate of feldspar must be high relative to the diffusivity of SiO₂ in silicate melt to form the graphic texture. Within the relatively narrow (~1 m) miarolitic pegmatite–aplite dikes in southern California, perthite megacrysts contain graphic quartz in their outer

portions (near the wallrock contact), but not in the pegmatite core (e.g., Jahns & Burnham 1969, Fig 5B; Foord 1976, Foord *et al.* 1989). Foord *et al.* (1989) attributed the lack of a graphic texture to decreasing growth-rate of alkali feldspar in the pegmatite core. The rate of growth is expected to decrease in the core, because of lower degrees of undercooling (e.g., Fenn 1977). At Stak Nala, the lack of any graphic quartz – K-feldspar intergrowth suggests that the pegmatites were less strongly undercooled than pegmatites with graphic intergrowths. The wallrocks were evidently quite hot when the pegmatites were emplaced, which is indicated by (1) the $^{40}\text{Ar}/^{39}\text{Ar}$ data presented herein, which require emplacement of the pegmatites when the wallrocks were at temperatures $>300^\circ\text{C}$ (see below), and (2) local ductile deformation of the wallrock by the pegmatites (Fig. 6), suggesting that the wallrock temperatures were 300 to $<550^\circ\text{C}$. The high heat content of the wallrock gneisses is consistent with the elevated geotherm in the Haramosh massif (Craw *et al.* 1994, Winslow *et al.* 1994).

Timing of vapor saturation. The timing of vapor saturation of the pegmatite-forming magma in published models of pegmatite crystallization ranges from early to late during crystallization. Wallrock alteration adjacent to pegmatites provides evidence for the timing of vapor saturation because it is produced by infiltrating fluids derived by exsolution during vapor saturation of the pegmatite-forming magma (e.g., Morgan & London 1987, London 1990). D. London (in Foord *et al.* 1991a) suggested that sporadic presence of tourmaline in gabbroic wallrock adjacent to the miarolitic Himalaya pegmatite–aplite in southern California indicates that vapor saturation occurred at very late stages, since the tourmaline is spatially related to rupture of elbaite-bearing pockets. At Stak Nala, schorl addition to the wallrock is not controlled by the location of pockets, and the schorl apparently formed during early stages of pegmatite crystallization (discussed above). Veins of schorl at the main mine (Fig. 3, location 2; Fig. 9) provide evidence for early saturation in magmatic vapor because they originate within the border zone or outer wall zone, and traverse outward into wallrocks. These relations suggest that vapor saturation and expulsion of B-rich aqueous fluids occurred, at the latest, after crystallization of the border zone.

Overview of existing models for pegmatite genesis

The classic Jahns & Burnham (1969) model, refined by Jahns (1982) and Burnham & Nekvasil (1986), evokes vapor saturation and separation of an aqueous fluid phase from the crystallizing aluminosilicate melt to explain the textural and compositional evolution of granitic pegmatites: granitic or aplitic textures represent silicate melt crystallizing without vapor,

whereas giant pegmatite minerals such as K-feldspar megacrysts crystallize in the presence of low-viscosity aqueous fluid. London *et al.* (1989) and London (1990, 1991) proposed a much different model, in which rare-element pegmatites do not become vapor-saturated until they are largely crystalline; the pegmatitic textures and zonation result from undercooling of the melt, which causes disequilibrium crystallization, with metastable persistence of melt. Undercooling decreases the potential of forming crystal nuclei (e.g., Fenn 1977, 1986, Swanson & Fenn 1986), as do network-modifying melt components such as H_2O , B, P, and F or some combination of these (e.g., London 1987).

The Stak Nala pegmatites are inferred to have become vapor-saturated very early during crystallization, and therefore are expected to show several features of the Jahns–Burnham model. In many pegmatites modeled by Jahns & Burnham (1969), there is a marked asymmetry about the central core zone, in which the footwall is characterized by a Na-rich, layered albite–quartz aplite, whereas the hanging wall is characterized by a K-rich, perthite-dominated, giant-textured pegmatite. Although pegmatites at Stak Nala lack Na–K stratification and layered footwall aplite, they do show giant texture, inhomogeneous composition, widespread mineral replacements, and evidence for early alteration of wallrock; all these features were ascribed to vapor-saturated crystallization by Jahns & Burnham (1969).

Although London's model emphasizes vapor-undersaturated conditions, several points pertaining to the effects of increasing volatiles clearly apply to the F- and B-rich pegmatites at Stak Nala. In particular, London (1986a) proposed that in miarolitic pegmatites, vapor saturation and resulting formation of pockets are promoted by the removal of B from the pegmatitic system. Experimental studies (Pichavant 1981, 1983a, Holtz *et al.* 1993, London 1987) have demonstrated that H_2O solubility in the melt is significantly enhanced in the presence of B. Therefore, crystallization of tourmaline within the pegmatite may trigger vapor saturation and the exsolution of H_2O ; if the H_2O does not escape into the wallrock, then formation of gem pockets may result (London 1986a). Experimental studies (*cf.* London 1987) suggest that in the presence of volatiles such as B and F, compositions of residual melts will be driven towards alkaline, Na-rich compositions enriched in incompatible elements. Late-stage crystallization and metasomatism at Stak Nala are characterized by formation of minerals enriched in Na, Al, F, B, Mn, and Li in the pockets, and by widespread albitization of pegmatite (see below).

Model for crystallization of the Stak Nala pegmatites

Geochemically evolved, volatile-rich pegmatite-forming magma of low viscosity intruded subhorizontal fractures as a series of sills that are

locally interconnected. Each sill subsequently crystallized from the walls inward, under restricted-system conditions. Thus, the pegmatites were closed to further magmatic injection, but open to interaction with the wallrock *via* an exsolved aqueous fluid phase that evolved shortly after crystallization began. Escape of fluids during initial consolidation caused alteration of wallrock biotite to muscovite and schorl, accompanied by veins of schorl traversing the wallrock-pegmatite contact.

Fluid exsolution and formation of pockets. Crystallization of dominantly anhydrous assemblages (Fig. 21) in the outer pegmatite zones resulted in progressive saturation in a volatile phase. Ascent of low-density aqueous fluid containing B may account for the concentration of schorl in the upper part of the pegmatite. Where the rate of volatile production exceeded the rate of volatile escape from the pegmatite system, the percentage of volatiles would have gradually increased in the core zone. The increased proportions of volatiles may have led to coalescence of initially widely separated, small bubbles into a few large pockets of aqueous fluid, trapped beneath the crystal-melt interface. During early stages of

coalescence of bubbles, overpressured pockets of fluid likely could not be contained, and when rupturing occurred, volatile loss from melt caused formation of pressure-quenched albite-rich aplite and subsequent albitization of feldspars (see below). Continued collection of aqueous fluid contained by the almost completely solidified pegmatite produced the late-stage crystal-lined pockets.

The pockets form in the central portions of the pegmatites from silicate-rich aqueous fluid (*cf.* Jahns & Burnham 1969, Jahns 1982, London 1986a) after the silicate melt is consumed. Miaroles did not form in the outer zones of the pegmatite because exsolved aqueous fluids had not yet coalesced, or because they escaped as quickly as they were generated. The rise of less-dense aqueous fluids within the core is shown by the common presence of pockets in the upper part of the core zone. The mineral assemblage in the pockets (Fig. 21) indicates that the silicate-rich aqueous fluid must have contained Al, Na, K, Ca, B, Li, F, Mn, with local Be and Nb. The availability of Ca at late stages to form minor fluorite and traces of apatite may be due to sequestering of some Ca in the melt as fluoride complexes, as suggested by Weidner & Martin (1987) for a leucogranite containing primary fluorite.

Mineral or Mineral Group	Primary Pegmatite Crystallization	Initial Pocket Crystallization	Late-Stage Pocket & Repl. Zones
K-feldspar (microcline)	—	—	—
oligoclase	—	—	—
quartz	—	—	—
schorl	—	—	—
spessartine-almandine	—	—	—
löllingite	—	—	—
muscovite	—	—	—
fluorite	—	—	—
monazite	—	—	—
albite (incl. "cleavelandite")	—	—	—
elbaite	—	—	—
lepidolite or lithian muscovite	—	—	—
topaz	—	—	—
fluorapatite	—	—	—
beryl	—	—	—
manganocolumbite	—	—	—
K-feldspar (orthoclase)	—	—	—
microlite	—	—	—
zircon	—	—	—
hambergite	—	—	—
bertrandite	—	—	—
borian muscovite	—	—	—
Mn-Fe oxides	—	—	—

FIG. 21. Paragenetic diagram for crystallization of the Stak Nala pegmatites.

Alternatively, Ca could be derived from albitization of plagioclase (*cf.* Manning & Exley 1984).

Increasing vapor pressure is thought to cause rupture of the pockets during late stages of development (Foord 1976, Jahns 1982, Foord *et al.* 1991a). Foord *et al.* (1989, 1991a) noted that pocket rupture is important for the removal of residual fluids that would otherwise cause etching or alteration of pocket minerals to micas and clays; pocket minerals at Stak Nala show very little to moderate etching (most pronounced on topaz and microcline), and have not experienced alteration. Bent and broken crystals, mineral shards, and mineral overgrowths within the pockets also provide evidence for pocket rupture at Stak Nala. The elbaite overgrowths presumably formed after pocket rupture, and contain sharp boundaries in color and composition that reflect loss of Fe, Mn, Na, and F (Fig. 20). The loss of volatile-rich fluids from the late-rupturing pockets may be closely associated with the formation of hydrothermal "cleavelandite" (An_1), which represents a younger and lower-temperature hydrothermal alteration than the massive albite (An_3 to An_8) described above. Microcrystalline muscovite or borian muscovite is the final mineral to crystallize from the aqueous fluids after pocket rupture. Conditions of boromuscovite deposition in pockets at the Little 3 pegmatite in southern California are inferred to have been 350 to 400°C and 1 to 2 kbar (Foord *et al.* 1991b); these conditions are reasonable for crystallization of borian muscovite at Stak Nala.

Formation of aplite. The small bodies of albite – schorl – garnet – quartz aplite at Stak Nala are remarkably similar to late-stage aplite described by Foord (1976) from the miarolitic Himalaya pegmatite–aplite dike in southern California. Foord (1976) ascribed the aplite to a "pressure quench" as a consequence of pocket rupture. Similar late-stage, rare-metal-enriched albitites have also been attributed to a "boron quench," that occurs when the fluxing alkali borate component is removed from late-stage melts by crystallization of tourmaline, resulting in a rise in solidus temperature (London 1986b, 1987, 1990). At Stak Nala, the bodies of aplite formed without spatial regard to schorl-rich areas. The aplite probably formed by pressure-quenching, when rupturing of early-formed pockets of fluid caused quenching of the residual Na-rich melt produced by fractional crystallization of the F-, B-, and Li-rich silicate melt (*e.g.*, London 1987). The aqueous fluoride-enriched fluid released at that point caused local massive replacement of K-feldspar and oligoclase by hydrothermal albite (An_3 to An_8) (see below).

Late-stage albitization and mineral dissolution. Widespread but sporadic replacement of K-feldspar and oligoclase by albite may be attributed to infiltration and cooling of a F-bearing aqueous fluid evolved during

final stages of pegmatite consolidation (*cf.* Doherty 1990). Fluorine abundance in late-stage fluid at Stak Nala is indicated by the presence of fluorite and relatively high F contents in muscovite, elbaite, and microcline that formed in albitized pegmatite. Using the method of Munoz & Ludington (1977) and Munoz & Swenson (1981), calculated values of $\log [f(H_2O)/f(HF)]$ at 500°C for secondary muscovite hosted by albitized K-feldspar range from 3.4 to 3.8, and the fluorine intercept ranges from 0.6 to 1.1; these values overlap with values obtained for F-rich porphyry molybdenum deposits (*cf.* Munoz 1984). The calculated $\log [f(HF)/f(HCl)]$ of biotite in the altered wallrock near the pegmatites ranges from 0.4 to 0.9 at 500°C, suggesting that the pegmatite-derived fluids were enriched in F compared to Cl.

Simple cooling of alkali-chloride-bearing fluid in equilibrium with albite and K-feldspar will cause increasing a_{Na^+}/a_{K^+} of the fluid, which is maintained by replacement of albite by K-feldspar (Orville 1963, Fournier 1976, Lagache 1984). However, cooling of alkali-fluoride-bearing fluid at pressures below 2 kbar should promote albitization (*cf.* Barton & Frantz 1983, Pichavant 1983b, Doherty 1990). Sodium metasomatism will be augmented by the late-stage enrichment of F, B, and P in the melt, which shifts the granite minimum toward albite composition, and will thus yield a magmatic aqueous fluid with a higher Na/K (*e.g.*, Manning 1981, London 1987).

A vuggy texture caused by quartz dissolution accompanies albitization at one location of the main mine (Fig. 3, location 2), and has been documented in other miarolitic pegmatites (Balitskiy 1966, Foord *et al.* 1989) and in rare-metal granites (*e.g.*, Charoy & Pollard 1989). The solubility of quartz (and, in some cases, feldspar) is significantly enhanced in neutral to weakly alkaline fluids containing alkali chlorides, fluorides, or carbonates (Balitskiy 1966, Anderson & Burnham 1967, Rykl & Štemprok 1988). Cooling of the fluid phase could have caused quartz dissolution; Fournier (1986) demonstrated that the retrograde solubility of quartz shifts to higher temperatures and pressures with added NaCl. The dissolution of quartz was followed by its local precipitation as euhedral crystals in the vugs at lower temperatures, accompanied by blocky crystals of albite.

Implications for tourmaline mineralization

Miarolitic pegmatites with pocket mineralization that closely resembles that seen at Stak Nala are present in southern California, within dikes consisting of layered pegmatite–aplite (*e.g.*, Foord 1976, 1977, Foord *et al.* 1989, 1991a, Jahns & Wright 1951, Stern *et al.* 1986). This study documents miarolitic pegmatites that lack the asymmetrical K–Na zoned pegmatite–aplite association, and show instead symmetrical internal zonation. Other miarolitic

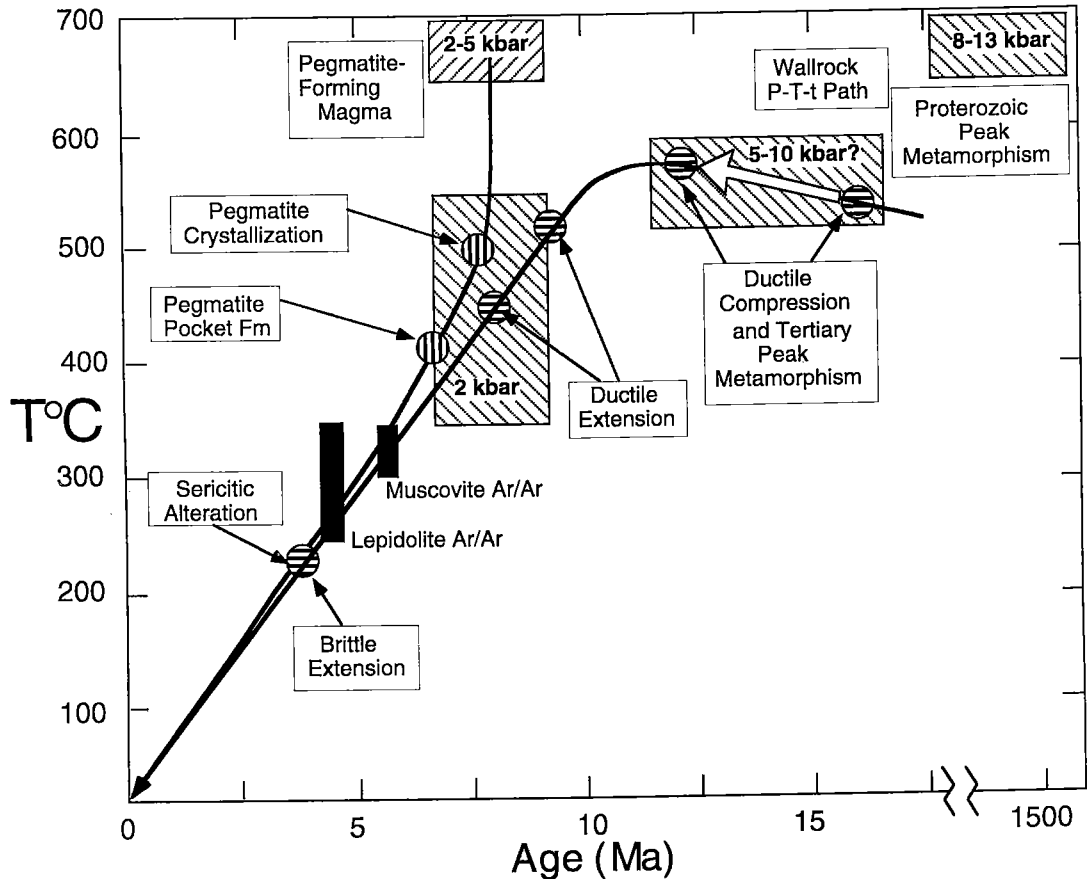


FIG. 22. Stak Nala pressure - temperature - time diagram showing converging paths of wallrock (horizontally ruled circles) and pegmatite (vertically ruled circles). See text for discussion.

pegmatites in Pakistan at Khaltaro (*e.g.*, Laurs *et al.* 1996b) and Shengus (unpubl. data of B.M. Laurs & J.H. Dilles) similarly lack footwall aplite and show symmetrical internal zonation.

Economically important pink tourmaline mineralization formed at Stak Nala partly because Fe (and Ti) were depleted in melt prior to crystallization of the pockets, principally through crystallization of abundant schorl in the outer zones of the pegmatite. Thus, the occurrence of pink tourmaline at Stak Nala is favored by the abundance of B available at early stages for the crystallization of schorl. Relatively high amounts of As likewise caused removal of Fe by promoting the crystallization of löllingite.

The accumulation of abundant volatiles in pockets, with associated pink tourmaline mineralization in the productive area of the main sill, was enhanced by structural trapping of volatiles. The pocket mineralization is preferentially located in the crest of an open

antiform, bounded by a steeply dipping shear to the north. In our opinion, magmatic aqueous fluid migrated upward (north) along the gently south-dipping sill, and accumulated in the antiformal crest.

Most of the pegmatites at Stak Nala area have been little explored, and have significant potential to produce more colored tourmaline, except for the main mine pegmatite, which is largely mined out. The thicker south pegmatite has not been well explored, and contains more abundant Li mineralization (lepidolite). Other pegmatites in the region also may contain gem-bearing pockets.

Links between pegmatites and Himalayan tectonism

The Stak Nala pegmatites are integrally related to the processes of Himalayan orogenesis (Fig. 22). Indian Plate rocks were underthrust beneath the Kohistan-Ladakh arc and Asian Plate rocks beginning

in the Paleocene (Figs. 1, 2). Subsequently within the Haramosh massif, the overthickened crustal wedge began to thin by faulting and experienced rapid uplift, cooling, and erosion beginning at ~10 Ma before present (e.g., Zeitler 1985), and earlier in the Khaltaro region (Laurs *et al.* 1996b). The rapid uplift led to local fluid-absent, decompression-induced melting due to biotite breakdown to produce low-temperature, volatile-rich leucogranite melts (Zeitler & Chamberlain 1991).

Field relations from the Stak Nala area prove that leucogranitic magma was emplaced as pegmatite sills during uplift and extension of the Haramosh massif. Batches of pegmatite-forming magma were generated below the current level of exposure, which contains no evidence for anatexis. The sills are emplaced along the gently dipping foliation, and cross-cut open, northwest-trending compressional folds that likely formed during the last stages of Tertiary convergence of the Indian and Asian plates. The foliation and these compressive folds are cut by ductile shears with normal, down-to-north displacement that strike west-northwest and dip steeply north (Figs. 3, 4). The pegmatites cut the ductile *F2* normal shears (Fig. 3A) and hence must have been emplaced after the beginning of normal faulting.

The gneisses apparently deformed by tensile fracturing, indicating brittle (<550°C) behavior of the feldspar-dominated rock, to allow emplacement of the pegmatite sills. However, the ductile *F2* shears and deflected foliation near the ends of pegmatite sills (Fig. 6) indicate ductile behavior of quartz (>300°C). Thus, pegmatites were emplaced when wallrocks were between ~550 and 300°C and at pressures of ~1.5 to 2 kbar on the basis of miarolitic cavities and the inferred phase-equilibria for hydrothermal albitization. These temperature estimates are consistent with the elevated geotherm in the Haramosh massif (Craw *et al.* 1994, Winslow *et al.* 1994), and with the ⁴⁰Ar/³⁹Ar data, which yielded nearly identical 5 Ma ages for lepidolite in pegmatite and muscovite in the wallrock gneiss. The ³⁹Ar closure temperature of lepidolite is not well established, but is estimated to be not more than ~70°C lower than muscovite (closure temperature ~325°C). If the lepidolite ³⁹Ar closure temperature is about 50°C lower than muscovite, then the two ages represent identical cooling paths through slightly different isotherms. Therefore, the pegmatites were emplaced at >5 Ma into gneisses that were >300°C, and both gneiss and pegmatite cooled through the 300°C isotherm synchronously. Brittle faults with similar orientations reactivated the *F2* structures and cut the pegmatites, and indicate continued uplift in the brittle regime. Southeast of Stak Nala, the Tertiary-age Stak Fault was reactivated as a ductile reverse fault with late-stage brittle behavior, presumably with similar timing to the normal faults at the Stak Nala mine.

The orientation of ductile and brittle normal faults at Stak Nala suggests a general mechanism for uplift of

the Haramosh massif along a series of north-dipping normal faults paralleling the Main Mantle Thrust bounding the Indian and Asian plates immediately north of Stak Nala. During early Cenozoic convergence, the plate boundary was a thrust, but during relaxation in the late Cenozoic, isostatic rebound, and uplift of the Haramosh massif to the south the Main Mantle Thrust, the movement likely changed to a normal sense as in the case of the ductile *F2* normal faults at the Stak Nala mine. Normal movement along faults in the northern end of the Haramosh massif up to the Main Mantle Thrust must have commenced prior to 11 Ma, on the basis of ⁴⁰Ar/³⁹Ar data from the Khaltaro area (Laurs *et al.* 1996b), and has continued since 5 Ma in the Stak Nala area.

ACKNOWLEDGEMENTS

The Geological Survey of Pakistan (GSP) provided valuable logistical support in the field and use of laboratory facilities. We are grateful to Ali H. Kazmi (GSP), Nasir Ali Bhatti (GEMCP), and Robert D. Lawrence (OSU) for their assistance with Pakistan field studies. This study was funded in part by the OSU Department of Geosciences Ore Geology Fund. Electron-microprobe analyses were supported by the OSU College of Science and College of Oceanic and Atmospheric Sciences, assisted by Roger Nielsen. We thank Virginia Sisson (Rice University) for providing electron-microprobe analyses of borian muscovite and of the unknown Nb-Ta oxide minerals, and Petr Černý (University of Manitoba) for further analyses and evaluation of these unknowns. Frank Hawthorne and Julie Selway (both at University of Manitoba) provided electron-microprobe analyses of some Stak Nala tourmaline samples that were also analyzed in this study, for purposes of data comparison and evaluation. Reed Glasman (OSU) assisted with X-ray diffraction of the K-feldspar. The late Eugene E. Foord (USGS, Denver) identified a sample of bertrandite, provided a helpful review of this manuscript, and is acknowledged for stimulating discussions about pegmatite mineralogy and genesis. We also thank R.F. Martin and W.B. Simmons for their constructive reviews. David Reinert (OSU) photographed specimens and prepared Figs. 9, 10, and 13, and the interlibrary loan staff at OSU's Valley Library is thanked for their untiring assistance.

REFERENCES

- ANDERSON, G.M. & BURNHAM, C.W. (1967): Reactions of quartz and corundum with aqueous chloride and carbonate solutions at high temperatures and pressures. *Am. J. Sci.* **265**, 12-27.
- BALDWIN, J.R. & VON KNORRING, O. (1983): Compositional range of Mn-garnet in zoned granitic pegmatites. *Can. Mineral.* **21**, 683-688.

- BALITSKIY, V.S. (1966): Alteration of granite and pegmatite under the influence of alkaline silica-containing hydrothermal solutions at high pressure. *Dokl. Acad. Sci. U.S.S.R., Earth Sci. Sect.* **171**, 222-225.
- BARTON, M.D. & FRANTZ, J.D. (1983): Exchange equilibria of alkali feldspars with fluorine-bearing fluids. *Carnegie Inst. Washington, Year Book* **82**, 377-381.
- BURNHAM, C.W. & NEKVASIL, H. (1986): Equilibrium properties of granite pegmatite magmas. *Am. Mineral.* **71**, 239-263.
- BUTLER, R.W.H., GEORGE, M., HARRIS, N.B.W., JONES, C., PRIOR, D.J., TRELOAR, P.J. & WHEELER, J. (1992): Geology of the northern part of the Nanga Parbat massif, northern Pakistan, and its implications for Himalayan tectonics. *J. Geol. Soc. London* **149**, 557-567.
- ČERNÝ, P. (1975): Alkali variations in pegmatitic beryl and their petrogenetic implications. *Neues Jahrb. Mineral., Abh.* **123**, 198-212.
- _____ (1991): Rare-element granitic pegmatites. I. Anatomy and internal evolution of pegmatite deposits. *Geosci. Canada* **18**(2), 49-67.
- _____ (1994): Evolution of feldspars in granitic pegmatites. In *Feldspars and Their Reactions* (I. Parsons, ed.). *NATO Adv. Study Inst. Ser., Ser. C* **421**, 501-540. Kluwer, The Netherlands.
- _____ & HAWTHORNE, F.C. (1982): Selected peraluminous minerals. In *Granitic Pegmatites in Science and Industry* (P. Černý, ed.). *Mineral. Assoc. Can., Short-Course Handbook* **8**, 163-186.
- _____, MEINTZER, R.E. & ANDERSON, A.J. (1985): Extreme fractionation in rare-element granitic pegmatites: selected examples of data and mechanisms. *Can. Mineral.* **23**, 381-421.
- CHAROY, B. & POLLARD, P.J. (1989): Albite-rich, silica-depleted metasomatic rocks at Emuford, northeast Queensland: mineralogical, geochemical, and fluid inclusion constraints on hydrothermal evolution and tin mineralization. *Econ. Geol.* **84**, 1850-1874.
- CRAW, D., KOONS, P.O., WINSLOW, D., CHAMBERLAIN, C.P. & ZEITLER, P. (1994): Boiling fluids in a region of rapid uplift, Nanga Parbat massif, Pakistan. *Earth Planet. Sci. Lett.* **128**, 169-182.
- CRAWFORD, M.B. & SEARLE, M.P. (1993): Collision-related granitoid magmatism and crustal structure of the Hunza Karakoram, North Pakistan. In *Himalayan Tectonics* (P.J. Treloar & M.P. Searle, eds.). *Geol. Soc., Spec. Publ.* **74**, 53-68.
- DALRYMPLE, G.B., ALEXANDER, E.C., JR., LANPHERE, M.A. & KRAKER, G.P. (1981): Irradiation of samples for $^{40}\text{Ar}/^{39}\text{Ar}$ dating using the Geological Survey TRIGA reactor. *U.S. Geol. Surv., Prof. Pap.* **1176**.
- DEER, W.A., HOWIE, R.A. & ZUSSMAN, J. (1992): *An Introduction to the Rock-Forming Minerals* (2nd ed.). Longman, London, U.K.
- _____, _____ & _____ (1997): *Rock-Forming Minerals. 1B. Disilicates and Ring Silicates*. The Geological Society, London, U.K.
- DIETRICH, R.V. (1985): *The Tourmaline Group*. Van Nostrand Reinhold, New York, N.Y.
- DOHERTY, S.B. (1990): *An Experimental Investigation of Supercritical Alkali Halide - Mineral Exchange Equilibria*. M.S. thesis, Univ. of California, Los Angeles, California.
- DONNAY, G. & BARTON, R., JR. (1972): Refinement of the crystal structure of elbaite and the mechanism of tourmaline solid solution. *Tschermaks Mineral. Petrogr. Mitt.* **18**, 273-286.
- FAYE, G.H., MANNING, P.G., GOSSELIN, J.R. & TREMBLAY, R.J. (1974): The optical absorption spectra of tourmaline; importance of charge-transfer processes. *Can. Mineral.* **12**, 370-380.
- FENN, P.M. (1977): The nucleation and growth of alkali feldspars from hydrous melts. *Can. Mineral.* **15**, 135-161.
- _____ (1986): On the origin of graphic granite. *Am. Mineral.* **71**, 325-330.
- FOORD, E.E. (1976): *Mineralogy and Petrogenesis of Layered Pegmatite-Aplite Dikes in the Mesa Grande District, San Diego County, California*. Ph.D. dissertation, Stanford University, Stanford, California.
- _____ (1977): The Himalaya dike system, Mesa Grande district, San Diego County, California. *Mineral. Rec.* **8**, 461-474.
- _____ & KLECK, W.D. (1993): Garnets in the gem-bearing pegmatite dikes of San Diego County, California. *Mineral. Rec.* **24**, 66-67.
- _____, LONDON, D., KAMPF, A.R., SHIGLEY, J.E. & SNEE, L.W. (1991a): Gem-bearing pegmatites of San Diego County, California. In *Geological Excursions in Southern California and Mexico* (M.J. Walawender & B.B. Hanan, eds.). *Geol. Soc. Am., Annual Meeting, Guidebook* **9**.
- _____, MARTIN, R.F., FITZPATRICK, J.J., TAGGART, J.E. & CROCK, J.G. (1991b): Boromuscovite, a new member of the mica group, from the Little Three mine pegmatite, Ramona district, San Diego County, California. *Am. Mineral.* **76**, 1998-2002.
- _____, SPAULDING, L.B., JR., MASON, R.A. & MARTIN, R.F. (1989): Mineralogy and paragenesis of the Little Three pegmatites, Ramona district, San Diego County, California. *Mineral. Rec.* **20**, 101-127.
- _____, STARKEY, H.C. & TAGGART, J.E., JR. (1986): Mineralogy and paragenesis of "pocket" clays and associated minerals in complex granitic pegmatites, San Diego County, California. *Am. Mineral.* **71**, 428-439.

- FOURNIER, R.O. (1976): Exchange of Na⁺ and K⁺ between water vapor and feldspar phases at high temperature and low pressure. *Geochim. Cosmochim. Acta* **40**, 1553-1561.
- _____ (1986): The behavior of silica in hydrothermal solutions. In *Geology and Geochemistry of Epithermal Systems* (B.R. Berger & P.M. Bethke, eds.). *Rev. Econ. Geol.* **2**, 45-61.
- GEORGE, M.T., HARRIS, N.B.W. & BUTLER, R.W.H. (1993): The tectonic implications of contrasting granite magmatism between the Kohistan island arc and the Nanga Parbat - Haramosh massif, Pakistan Himalaya. In *Himalayan Tectonics* (P.J. Treloar & M.P. Searle, eds.). *Geol. Soc., Spec. Publ.* **74**, 173-191.
- GRESENS, R.L. (1967): Composition-volume relationships of metasomatism. *Chem. Geol.* **2**, 47-65.
- HARALAMPIEV, A.G. (1992): Relations between Fe and Mn in tourmalines from the Latinka pegmatite vein, Rhodope Mountain, south Bulgaria. *Geol. Soc. Am., Abstr. Programs* **24**, A259.
- HARRIS, N.B.W., INGER, S. & MASSEY, J. (1993): The role of fluids in the formation of High Himalayan leucogranites. In *Himalayan Tectonics* (P.J. Treloar & M.P. Searle, eds.). *Geol. Soc., Spec. Publ.* **74**, 391-400.
- HERRERA, A.O. (1968): Geochemical evolution of zoned pegmatites of Argentina. *Econ. Geol.* **63**, 13-29.
- HOLTZ, F., DINGWELL, D.B. & BEHRENS, H. (1993): Effects of F, B₂O₃, and P₂O₅ on the solubility of water in haplogranite melts compared to natural silicate melts. *Contrib. Mineral. Petrol.* **113**, 492-501.
- JAHNS, R.H. (1953): The genesis of pegmatites. I. Occurrence and origin of giant crystals. *Am. Mineral.* **38**, 563-598.
- _____ (1982): Internal evolution of pegmatite bodies. In *Granitic Pegmatites in Science and Industry* (P. Černý, ed.). *Mineral. Assoc. Can., Short-Course Handbook* **8**, 293-328.
- _____ & BURNHAM, C.W. (1969): Experimental studies of pegmatite genesis. I. A model for the derivation and crystallization of granitic pegmatites. *Econ. Geol.* **64**, 843-864.
- _____ & TUTTLE, O.F. (1963): Layered pegmatite-aplite intrusives. *Mineral. Soc. Am., Spec. Pap.* **1**, 78-92.
- _____ & WRIGHT, L.A. (1951): Gem- and lithium-bearing pegmatites of the Pala district, San Diego County, California. *Calif. Div. Mines, Spec. Rep.* **7-A**.
- KAZMI, A.H. & O'DONOGHUE, M. (1990): *Gemstones of Pakistan: Geology and Gemmology*. Gemstone Corporation of Pakistan, Peshawar, Pakistan.
- _____, PETERS, J.J. & OBODDA, H.P. (1985): Gem pegmatites of the Shingus-Dusso area, Gilgit, Pakistan. *Mineral. Rec.* **16**, 393-411.
- KONINGS, R.J.M., BOLAND, J.N., VRIEND, S.P. & JANSEN, J.B.H. (1988): Chemistry of biotites and muscovites in the Abas granite, northern Portugal. *Am. Mineral.* **73**, 754-765.
- KRETZ, R. (1983): Symbols for rock-forming minerals. *Am. Mineral.* **68**, 277-279.
- _____, HARTREE, R. & JONES, P. (1989): Metasomatic crystallization of muscovite in granite and tourmaline in schist related to pegmatite emplacement near Yellowknife, Canada. *Contrib. Mineral. Petrol.* **102**, 191-204.
- LAGACHE, M. (1984): The exchange equilibrium distribution of alkali and alkaline-earth elements between feldspars and hydrothermal solutions. In *Feldspars and Feldspathoids* (W.L. Brown, ed.). *NATO Adv. Study Inst., Ser. C* **137**, 247-279. Kluwer, The Netherlands.
- LAURS, B.M., DILLES, J.H. & SNEE, L.W. (1996a): Geologic origin of gem-bearing pegmatites, Stak Nala, Haramosh massif, Pakistan. *11th Himalaya-Karakoram-Tibet Workshop (Flagstaff, Arizona)*, 83.
- _____, _____ & _____ (1996b): Emerald mineralization and metasomatism of amphibolite, Khaltaro granitic pegmatite - hydrothermal vein system, Haramosh mountains, northern Pakistan. *Can. Mineral.* **34**, 1253-1286.
- _____ & WISE, W.S. (1991): The metasomatic effects of the emplacement and crystallization of the Himalaya pegmatite - aplite dike on gabbro-norite wallrock, San Diego County, California. *Discovery: University of California, Santa Barbara, Journal of Undergraduate Research* **14**, 100-138.
- LECKEBUSCH, R. (1978): Chemical composition and colour of tourmalines from Darre Pêch (Nuristan, Afghanistan). *Neues Jahrb. Mineral., Abh.* **133**, 53-70.
- LE FORT, P., LEMENNICIER, Y., LOMBARDO, B., PECHER, A., PERTUSATI, P., POGNANTE, U. & ROLFO, F. (1995): Preliminary geological map and description of the Himalaya-Karakoram junction in Chogo Lungma to Turmik area (Balistan, northern Pakistan). *J. Nepal Geol. Soc.* **11**, 17-38.
- LIANG, JIAN-JIE, HAWTHORNE, F.C., NOVÁK, M., ČERNÝ, P. & OTTOLINI, L. (1995): Crystal-structure refinement of boromuscovite polytypes using a coupled Rietveld - static-structure energy-minimization method. *Can. Mineral.* **33**, 859-865.
- LONDON, D. (1986a): Formation of tourmaline-rich gem pockets in miarolitic pegmatites. *Am. Mineral.* **71**, 396-405.
- _____ (1986b): Magmatic-hydrothermal transition in the Tanco rare-element pegmatite: evidence from fluid inclusions and phase equilibrium experiments. *Am. Mineral.* **71**, 376-395.
- _____ (1987): Internal differentiation of rare-element pegmatites: effects of boron, phosphorus, and fluorine. *Geochim. Cosmochim. Acta* **51**, 403-420.

- _____ (1990): Internal differentiation of rare-element pegmatites; a synthesis of recent research. In *Ore-Bearing Granite Systems; Petrogenesis and Mineralizing Processes* (H.J. Stein & J.L. Hannah, eds.). *Geol. Soc. Am., Spec. Pap.* **246**, 35-50.
- _____ (1991): A dynamic chemical model for pegmatite crystallization. *Geol. Soc. Am., Abstr. Programs* **23**(4), 43.
- _____, MORGAN, G.B., VI & HERVIG, R.L. (1989): Vapor-undersaturated experiments with macusanite glass + H₂O at 200 MPa, and the internal differentiation of granitic pegmatites. *Contrib. Mineral. Petrol.* **102**, 1-17.
- MADIN, I.P. (1986): *Structure and Neotectonics of the Northwestern Nanga Parbat – Haramosh Massif*. M.S. thesis, Oregon State Univ., Corvallis, Oregon.
- _____, LAWRENCE, R.D. & UR-REHMAN, S. (1989): The northwestern Nanga Parbat – Haramosh massif: evidence for crustal uplift at the northwestern corner of the Indian craton. In *Tectonics of the Western Himalayas* (L.L. Malinconico & R.J. Lillie, eds.). *Geol. Soc. Am., Spec. Pap.* **232**, 169-182.
- MANNING, D.A.C. (1981): The effect of fluorine on liquidus phase relationships in the system Qz–Ab–Or with excess water at 1 kb. *Contrib. Mineral. Petrol.* **76**, 206-215.
- _____ & EXLEY, C.S. (1984): The origins of late-stage rocks in the St Austell granite – a re-interpretation. *J. Geol. Soc. London* **141**, 581-591.
- MANNING, P.G. (1969): An optical absorption study of the origin of color and pleochroism of pink and brown tourmalines. *Can. Mineral.* **9**, 678-690.
- _____ (1973): Effect of second-nearest-neighbor interaction on Mn³⁺ absorption in pink and black tourmalines. *Can. Mineral.* **11**, 971-977.
- MATTSON, S.M. & ROSSMAN, G.R. (1987): Fe²⁺–Fe³⁺ interactions in tourmaline. *Phys. Chem. Minerals* **14**, 163-171.
- MORGAN, G.B., VI & LONDON, D. (1987): Alteration of amphibolitic wallrocks around the Tanco rare-element pegmatite, Bernic Lake, Manitoba. *Am. Mineral.* **72**, 1097-1121.
- MUNOZ, J.L. (1984): F–OH and Cl–OH exchange in micas with applications to hydrothermal ore deposits. In *Micas* (S.W. Bailey, ed.). *Rev. Mineral.* **13**, 469-493.
- _____ & LUDINGTON, S.D. (1977): Fluoride–hydroxyl exchange in synthetic muscovite and its application to muscovite–biotite assemblages. *Am. Mineral.* **62**, 304-308.
- _____ & SWENSON, A. (1981): Chloride–hydroxyl exchange in biotite and estimation of relative HCl/HF activities in hydrothermal fluids. *Econ. Geol.* **76**, 2212-2221.
- NAKANO, T. & ISHIKAWA, Y. (1997): Chemical zoning of pegmatite garnets from the Ishikawa and Yamanoo areas, northeastern Japan. *Geochem. J.* **31**, 105-118.
- NOVÁK, M. & POVONDRA, P. (1995): Elbaite pegmatites in the Moldanubicum: a new subtype of the rare-element class. *Mineral. Petrol.* **55**, 159-176.
- ORVILLE, P.M. (1963): Alkali ion exchange between vapor and feldspar phases. *Am. J. Sci.* **261**, 201-237.
- PICHAVENT, M. (1981): An experimental study of the effect of boron on a water-saturated haplogranite at 1 kbar pressure: geological applications. *Contrib. Mineral. Petrol.* **76**, 430-439.
- _____ (1983a): Melt–fluid interaction deduced from studies of silicate–B₂O₃–H₂O systems at 1 kbar. *Bull. Minéral.* **106**, 201-211.
- _____ (1983b): (Na, K) exchange between alkali feldspars and aqueous solutions containing borate and fluoride anions; experimental results at P = 1 kbar. *Third NATO Adv. Study Inst. on Feldspars, Feldspathoids, and their Parageneses, Program Abstr.*, 102.
- POGNANTE, U., BENNA, P. & LE FORT, P. (1993): High-pressure metamorphism in the High Himalayan Crystallines of the Stak Valley, northeastern Nanga Parbat – Haramosh syntaxis, Pakistan Himalaya. In *Himalayan Tectonics* (P.J. Treloar & M.P. Searle, eds.). *Geol. Soc., Spec. Publ.* **74**, 161-172.
- POUCHOU, J.-L. & PICOIR, F. (1985): 'PAP' ϕ (ρZ) procedure for improved quantitative microanalysis. *Microbeam Analysis*. San Francisco Press, San Francisco, California (104-106).
- REINITZ, I.M. & ROSSMAN, G.R. (1988): Role of natural radiation in tourmaline coloration. *Am. Mineral.* **73**, 822-825.
- RIBBE, P.H. (1983): *Feldspar Mineralogy* (2nd ed.). *Rev. Mineral.* **2**.
- RICHARDS, R.P. (1996): Twinned hambergite from the Gilgit district, northern Pakistan. *Can. Mineral.* **34**, 615-621.
- RODDICK, J.C. (1983): High precision intercalibration of ⁴⁰Ar–³⁹Ar standards. *Geochim. Cosmochim. Acta* **47**, 887-898.
- ROSSMAN, G.R. & MATTSON, S.M. (1986): Yellow, Mn-rich elbaite with Mn–Ti intervalence charge transfer. *Am. Mineral.* **71**, 599-602.
- RYKL, D. & ŠTEMPROK, M. (1988): Hydrothermal reaction of water and of some inorganic solutions with the Cínovec granite at 300 and 400°C and 50 MPa pressure: an experimental study. *Proc. 7th Quad. IAGOD Symp.*, 437-447.
- SAHAMA, T.G., VON KNORRING, O. & TÖRNROOS, R. (1979): On tourmaline. *Lithos* **12**, 109-114.

- SAMSON, S.D. & ALEXANDER, E.C., JR. (1987): Calibration of the interlaboratory ^{40}Ar - ^{39}Ar dating standard, MMhb-1. *Chem. Geol.* **66**, 27-34.
- SEARLE, M.P. (1991): *Geology and Tectonics of the Karakoram Mountains*. John Wiley & Sons, Chichester, U.K.
- SLIVKO, M.M. (1961): Manganese tourmalines. *Int. Geol. Rev.* **3**(1), 195-201.
- SMITH, G. (1978): Evidence for absorption by exchange-coupled Fe^{2+} - Fe^{3+} pairs in the near infra-red spectra of minerals. *Phys. Chem. Minerals* **3**, 375-383.
- SMITH, W. & BLAUWET, D. (1997): A guide to mineral localities of the Northern Areas, Pakistan. *Mineral. Rec.* **28**, 183-200.
- SNEE, L.W., SUTTER, J.F. & KELLY, W.C. (1988): Thermochronology of economic mineral deposits - Dating the stages of mineralization at Panasqueira, Portugal, by high-precision $^{40}\text{Ar}/^{39}\text{Ar}$ age-spectrum techniques on muscovite. *Econ. Geol.* **83**, 335-354.
- STAATZ, M.H., MURATA, K.J. & GLASS, J.J. (1955): Variation of composition and physical properties of tourmaline with its position in the pegmatite. *Am. Mineral.* **40**, 789-804.
- STEIGER, R.H. & JÄGER, E. (1977): Subcommittee on geochronology: convention on the use of decay constants in geo- and cosmo-chronology. *Earth Planet. Sci. Lett.* **36**, 359-362.
- STERN, L.A., BROWN, G.E., JR., BIRD, D.K., JAHNS, R.H., FOORD, E.E., SHIGLEY, J.E. & SPAULDING, L.B., JR. (1986): Mineralogy and geochemical evolution of the Little Three pegmatite-aplite layered intrusive, Ramona, California. *Am. Mineral.* **71**, 406-427.
- SWANSON, S.E. & FENN, P.M. (1986): Quartz crystallization in igneous rocks. *Am. Mineral.* **71**, 331-342.
- SYRITSO, L.F., ZALASHKOVA, N.YE., ZORINA, M.L. & SOKOLOVA, YE.P. (1971): Micas in metasomatically altered granites of the acid series. *Int. Geol. Rev.* **13**(5), 717-729.
- TRELOAR, P.J., POTTS, G.J., WHEELER, J. & REX, D.C. (1991): Structural evolution and asymmetric uplift of the Nanga Parbat syntaxis, Pakistan Himalaya. *Geol. Rundsch.* **80**, 411-428.
- _____, WHEELER, J. & POTTS, G.J. (1994): Metamorphism and melting within the Nanga Parbat syntaxis, Pakistan Himalaya. *Mineral. Mag.* **58A**, 910-911.
- VERPLANCK, P.L. (1986): *A Field and Geochemical Study of the Boundary Between the Nanga Parbat - Haramosh Massif and the Ladakh Arc Terrane, Northern Pakistan*. M.S. thesis, Oregon State Univ., Corvallis, Oregon.
- WARD, G.W. (1931): A chemical and optical study of the black tourmalines. *Am. Mineral.* **16**, 145-190.
- WEIDNER, J.R. & MARTIN, R.F. (1987): Phase equilibria of a fluorine-rich leucogranite from the St. Austell pluton, Cornwall. *Geochim. Cosmochim. Acta* **51**, 1591-1597.
- WINSLOW, D.M., CHAMBERLAIN, C.P. & ZEITLER, P.K. (1995): Metamorphism and melting of the lithosphere due to rapid denudation, Nanga Parbat massif Himalaya. *J. Geol.* **103**, 395-409.
- _____, ZEITLER, P.K., CHAMBERLAIN, C.P. & HOLLISTER, L.S. (1994): Direct evidence for a steep geotherm under conditions of rapid denudation, western Himalaya, Pakistan. *Geology* **22**, 1075-1078.
- ZANETTIN, B. (1964): Geology and petrology of Haramosh - Mango Guser area. *Italian Expeditions to the Karakoram (K²) and Hindu Kush, Scientific Reports. III. Geology - Petrology, Vol. 1*. E.J. Brill, Leiden, The Netherlands.
- ZEITLER, P.K. (1985): Cooling history of the NW Himalaya, Pakistan. *Tectonics* **4**, 127-151.
- _____, & CHAMBERLAIN, C.P. (1991): Petrogenetic and tectonic significance of young leucogranites from the northwestern Himalaya, Pakistan. *Tectonics* **10**, 729-741.
- _____, & SMITH, H.A. (1993): Synchronous anatexis, metamorphism, and rapid denudation at Nanga Parbat (Pakistan Himalaya). *Geology* **21**, 347-350.
- _____, SUTTER, J.F., WILLIAMS, I.S., ZARTMAN, R. & TAHIRKHELI, R.A.K. (1989): Geochronology and temperature history of the Nanga Parbat - Haramosh massif, Pakistan. In *Tectonics of the Western Himalayas* (L.L. Malinconico & R.J. Lillie, eds.). *Geol. Soc. Am., Spec. Pap.* **232**, 1-22.

Received May 1, 1997, revised manuscript accepted December 15, 1997.